

**Development of a Peripheral Nerve Specific Extracellular Matrix-based Hydrogel and its  
Use in Augmenting Peripheral Nerve Injury and Repair**

by

Travis Austin Prest

Bachelor of Science, Slippery Rock University, 2011

Master of Science, University of Pittsburgh, 2015

Submitted to the Graduate Faculty of  
Swanson School of Engineering in partial fulfillment  
of the requirements for the degree of  
Doctor of Philosophy

University of Pittsburgh

2019

UNIVERSITY OF PITTSBURGH  
SWANSON SCHOOL OF ENGINEERING

This dissertation was presented

by

Travis Austin Prest

It was defended on

October 30, 2018

and approved by

Donald Crammond, Ph.D., Associate Professor, Department of Neurological Surgery

Xinyan Tracy Cui, Ph.D., Professor, Department of Bioengineering

Kacey Marra, Professor, Ph.D., Department of Plastic Surgery, Department of Bioengineering

Michel Modo, Ph.D., Professor, Department of Radiology, Department of Bioengineering

Dissertation Director: Bryan Brown, Ph.D., Assistant Professor, Department of

Bioengineering

Copyright © by Travis A Prest

2019

# **Development of a Peripheral Nerve Specific Extracellular Matrix-based Hydrogel and its Use in Augmenting Peripheral Nerve Injury and Repair**

Travis A Prest, Ph.D.

University of Pittsburgh, 2019

Peripheral nerve injury commonly results in loss of neuromuscular function, often resulting in significant impact upon both quality of life and cost of care for patients. One promising target for improving patient outcomes is the use of a peripheral nerve specific extracellular matrix hydrogel (PNM) as an injectable, regenerative support. It has been long understood that the extracellular matrix (ECM) not only provides structural support but also regulates cell growth, survival, maturation, differentiation, and development of resident cells. The objective of this dissertation was to develop and characterize a decellularized peripheral nerve hydrogel, investigate its effect on key properties of peripheral nerve regeneration, and finally assess its ability to enhance return to function in several peripheral nerve injury models. We found that PNM provides a tissue-specific microenvironment which is conducive to nerve repair, including: nerve specific growth factors that are chemotactic signals for Schwann cells, promote neurite outgrowth, as well as factors that modulate the macrophage inflammatory response to injury. When employed as a lumen filler for conduit repair of peripheral nerve defects, a switch in the ratio of M1:M2 phenotype macrophages was observed, a phenomenon associated with improved nerve growth and promotion of Schwann cell migration across a gap defect. This was associated with improved function over time in non-critical common peroneal and sciatic nerve defects. Furthermore, we provided proof-of-concept for the use of PNM in treating nerve crush injuries. The injection of the PNM hydrogel directly into the nerve injury was found to be safe with no impact on downstream function. The

application of PNM to the crush injury resulted in enhanced return to function and a more robust axon regrowth across the injury.

In conclusion, we developed an injectable material that provides a regeneration promoting, tissue-specific microenvironment at the site of injury. The material has shown the ability to promote recruitment of alternately activated, M2 macrophages, enhance Schwann cell migration, and axon extension. Finally, the use of PNM has enhanced recovery and return to function in numerous peripheral nerve injury models. PNM shows promise in augmenting current surgical practices for peripheral nerve injury and repair and has the potential to significantly improve quality of life for affected patients.

**Table of Contents**

**1.0 Introduction .....1**

**1.1 Peripheral Nervous System .....1**

**1.1.1 Anatomy and Physiology .....1**

**1.1.2 Peripheral Nerve Injury .....5**

**1.2 Clinical Repair of Nerve Injuries and Current Research .....10**

**1.2.1 Significance .....10**

**1.2.2 Clinical Approaches .....11**

**1.2.3 Current Research .....17**

**1.3 Extracellular Matrix .....20**

**1.4 ECM Scaffolds in Soft Tissue Repair .....21**

**1.5 Specific Aims of Dissertation .....25**

**1.5.1 Specific Aim 1: Characterize a PNM Hydrogel and Determine if PNM Hydrogels Provide a Preferred Microenvironment for Peripheral Nerve Repair as Compared to Non-Nerve-specific ECM (SIS and UBM) Hydrogels .....26**

**1.5.2 Specific Aim 2: Determine if PNM Generates Enhanced Recovery Via Mechanisms Beyond Simple Structural Support by Assessing PNM’s Effect on the Regenerative Response in a Peripheral Nerve Defect Injury Model .....27**

1.5.3	Specific Aim 3: Determine the Translational Potential of PNM by Investigating Functional Recovery Outcomes After a Critical Length Sciatic Nerve Defect Injury.....	28
2.0	Development and Characterization of a PNM Scaffold and Hydrogel for Peripheral Nerve Repair .....	29
2.1	Introduction.....	29
2.2	Methods .....	44
2.2.1	Preparation of Peripheral Nerve ECM .....	44
2.2.2	Formation of Hydrogel from Enzymatic Degradation Products.....	47
2.2.3	Confirmation of Decellularization.....	47
2.2.4	Assessment of Extracellular Matrix Ultrastructure and Components .....	48
2.2.5	Mechanical and Morphologic Aspects of the Resultant Hydrogels.....	50
2.3	Results.....	50
2.3.1	Confirmation of Decellularization.....	50
2.3.2	Maintenance of Extracellular Matrix Ultrastructure and Components...	56
2.3.3	Canine Sciatic Nerve Decellularization .....	58
2.3.4	Maintenance of Extracellular Matrix Ultrastructure and Components...	65
2.3.5	Assessment of Mechanical and Morphometric Characteristics of Resultant PNM Hydrogel.....	65
2.3.6	Defining Best Practices for Injectable Hydrogel.....	69
2.4	Discussion .....	72
3.0	PNM hydrogel Enhances Recovery Through Increase in Axon Extension, Schwann Cell Recruitment, and Phenotypic Changes in Macrophages .....	76

<b>3.1</b>	<b>Introduction.....</b>	<b>76</b>
<b>3.2</b>	<b>Methods .....</b>	<b>80</b>
<b>3.2.1</b>	<b>Evaluation of Effects of Enzymatic Degradation Products Upon Neurite Outgrowth .....</b>	<b>80</b>
<b>3.2.2</b>	<b>Evaluation of Enzymatic Degradation Products of Porcine PNM Upon Schwann Cell Migration .....</b>	<b>81</b>
<b>3.2.3</b>	<b>Assessment of Macrophage Phenotype in Vitro Using a NanoString's nCounter Technology .....</b>	<b>82</b>
<b>3.2.4</b>	<b>Assessment of Macrophage Response and Schwann Cell Migration in an Animal Model of Sciatic Nerve Defect Injury .....</b>	<b>83</b>
<b>3.2.5</b>	<b>Immunolabeling and Quantitative Analysis .....</b>	<b>84</b>
<b>3.3</b>	<b>Results.....</b>	<b>86</b>
<b>3.3.1</b>	<b>Bioactivity of Degradation Products .....</b>	<b>86</b>
<b>3.3.2</b>	<b>Assessment of Macrophage Phenotype .....</b>	<b>91</b>
<b>3.3.3</b>	<b>In Vivo Test of Macrophage and Schwann Cell Response to PNM Hydrogel .....</b>	<b>93</b>
<b>3.4</b>	<b>Discussion .....</b>	<b>96</b>
<b>4.0</b>	<b>PNM Can be Utilized in Both Crush and Nerve Defect Injuries to Increase Axon Growth and Functional Recovery .....</b>	<b>99</b>
<b>4.1</b>	<b>Introduction.....</b>	<b>99</b>
<b>4.2</b>	<b>Methods .....</b>	<b>103</b>
<b>4.2.1</b>	<b>Pilot Study of Critical-length Gap Defect of Rat Sciatic Nerve Surgical Procedure.....</b>	<b>104</b>

4.2.2	Pilot Non-critical Gap Defect of Rat Common Peroneal Nerve Surgical Procedure.....	105
4.2.3	Surgical Model of a 1cm Gap Defect Injury of Rat Sciatic Nerve .....	105
4.2.4	Surgical Model of Sciatic Nerve Crush Injury .....	106
4.2.5	Large Animal Model of Recurrent Laryngeal Nerve Reconstruction ....	108
4.2.6	Common Peroneal Functional Index and Sciatic Functional Index .....	111
4.2.7	Kinematics Collection and Analysis .....	113
4.2.8	Nociception Testing with Von Frey Fibers.....	116
4.2.9	Electrophysiologic Analysis of Evoked CMAP .....	116
4.2.10	Staining of NF200 to Analysis Axon Growth Across Injury .....	117
4.2.11	Histologic Analysis of Downstream Muscles.....	118
4.3	Results.....	120
4.3.1	Improvement of Function with a Sciatic Nerve Defect Model .....	120
4.3.2	Improvement of Function with a Common Peroneal Defect.....	122
4.3.3	Assessment of Functional Recovery in a Rodent Sciatic Nerve Gap Defect Model .....	124
4.3.4	Assessing Functional Recovery in a Rat Model of Sciatic Nerve Crush .	133
4.3.5	Electrophysiology of Downstream Muscle .....	140
4.3.6	Sex Base Variance in Compound Motor Action Potential Measures of Recovery .....	142
4.3.7	Restoration of Nerve Function Following Reconstruction of the RLn in Canine Model .....	143
4.4	Discussion .....	147

<b>5.0</b>	<b>PNM Increases the Effectiveness of an Engineered Nerve Guidance Conduit Containing Cell-secreted Neurotrophic Factors.....</b>	<b>157</b>
<b>5.1</b>	<b>Introduction.....</b>	<b>157</b>
<b>5.2</b>	<b>Materials and Methods .....</b>	<b>159</b>
<b>5.2.1</b>	<b>Fabrication of Cell-seeded PCL/GelMA Nerve Conduits .....</b>	<b>159</b>
<b>5.2.2</b>	<b>ECM Hydrogel Preparation .....</b>	<b>160</b>
<b>5.2.3</b>	<b>Scaffold Implantation .....</b>	<b>160</b>
<b>5.2.4</b>	<b>Explanation and Immunohistochemical Analysis.....</b>	<b>162</b>
<b>5.2.5</b>	<b>Rat Sciatic Functional Index Testing .....</b>	<b>162</b>
<b>5.2.6</b>	<b>Statistical Analysis .....</b>	<b>163</b>
<b>5.2.7</b>	<b>Immunohistochemistry of Nerve Conduit Sections and Analysis .....</b>	<b>163</b>
<b>5.3</b>	<b>Results.....</b>	<b>164</b>
<b>5.3.1</b>	<b>Multilayered Nanofibrous Nerve Conduits Possess Suitable Physical Properties for <i>in Vivo</i> Implantation.....</b>	<b>164</b>
<b>5.3.2</b>	<b>Conduits with Wall-encapsulated Cells Improve Peripheral Nerve Regeneration.....</b>	<b>166</b>
<b>5.4</b>	<b>Discussion .....</b>	<b>172</b>
<b>6.0</b>	<b>Overall Summary and Conclusions .....</b>	<b>174</b>
	<b>Appendix A. Abbreviations Used .....</b>	<b>179</b>
	<b>Appendix B. Programing Code.....</b>	<b>181</b>
<b>B.1</b>	<b>Matlab Code .....</b>	<b>181</b>
<b>B.1.1</b>	<b>MatLab Code Used to Process SFI from Photographs of Ink Footprint Impressions.....</b>	<b>181</b>

<b>B.1.2 MS Amplitude from CMAP Analysis</b>	<b>RMS Amplitude from CMAP</b>
<b>Analysis.....</b>	<b>183</b>
<b>Bibliography .....</b>	<b>185</b>

## List of Tables

Table 1: Nerve fiber types and properties .....	4
Table 2: Partial list of available nerves for autograft repairs .....	13
Table 3: Clinically available nerve repair products and alternatives to the nerve autograft .....	16
Table 4: Review of current research on lumen fillers for nerve conduits .....	18
Table 5: Partial list of commercially available extracellular matrix-based scaffolds .....	22
Table 6: Summary of decellularization agents and techniques .....	31
Table 7: Partial list of decellularization methods for peripheral nervous system.....	34
Table 8: List of antibodies used .....	85
Table 9: Diagram of Pre-clinical studies and experiments used.....	103

## List of Figures

Figure 1: Relative expected outcome of peripheral nerve injury based on severity of injury .....	6
Figure 2: Depiction of nerve structure and repair. ....	8
Figure 3: Confirmation of decellularization for an equine sciatic nerve.....	51
Figure 4: Confirmation of decellularization of a canine sciatic nerve .....	53
Figure 5: Conformation of decellularization of a porcine sciatic nerve.....	54
Figure 6: Composition analysis of equine sciatic nerve.....	57
Figure 7: Characterization of remaining content within canine sciatic nerve after decellularization .....	60
Figure 8: Structural ECM components of porcine sciatic nerve.....	63
Figure 9: Bioactive components in porcine PNM .....	64
Figure 10: Mechanical and morphometric properties of canine PNM hydrogel.....	67
Figure 11: Varying salt concentration changes mechanical properties of porcine PNM hydrogel .....	68
Figure 12: Porcine PNM hydrogel shows a maximal storage modulus .....	69
Figure 13: Testing different protocols for <i>in vivo</i> injection of PNM hydrogel into a silicone conduit .....	71
Figure 14: PNM digestion products promote neurite outgrowth and can be formed into a stable hydrogel .....	88
Figure 15: Porcine PNM effect on primary spinal cord neurite outgrowth.....	89
Figure 16: Porcine PNM effect on Schwann cell migration in vitro .....	91

Figure 17: A nanostring assay for gene expression using mouse bone marrow derived macrophages looking at macrophage phenotype promoted by the nerve specific extracellular matrix. .....	92
Figure 18: Representative longitudinal sections of regenerative nerve bridge stained for M1 and M2 macrophage markers.....	94
Figure 19: Macrophage recruitment and Schwann cell migration into nerve bridge .....	95
Figure 20: Representative surgical images of sciatic nerve defect model .....	106
Figure 21: Representative surgical images of sciatic nerve crush model .....	107
Figure 22: Anatomy of the recurrent laryngeal nerve.....	109
Figure 23: SFI measurements in a rat model of sciatic nerve defect injury.....	113
Figure 24: Representative still of kinematic analysis videos from TSE Motorater.....	115
Figure 25: Representation of SFI walking track analysis using inked paw prints.....	121
Figure 26: SFI for PNM in a pilot rat critical length sciatic nerve defect.....	122
Figure 27: Common Peroneal Nerve Functional Index (PFI) .....	123
Figure 28: Functional metrics for a rat model of sciatic nerve defect .....	125
Figure 29: Assessment of SFI and ankle angle at 4 and 24 weeks .....	127
Figure 30: Representative compound motor action potential traces of the sciatic nerve measured at the tibialis anterior .....	129
Figure 31: Compound motor action potential of the sciatic nerve at the tibialis anterior muscle .....	130
Figure 32: Axon count across sciatic nerve defect injury .....	132
Figure 33: Safety of PNM hydrogel injection into nervous tissue .....	134
Figure 34: Intraneural injection of PNM as a treatment for peripheral nerve injury .....	136

Figure 35: Axon growth across injury in sciatic nerve crush injury ..... 138

Figure 36: Atrophy of gastrocnemius muscle after sciatic nerve crush injury ..... 139

Figure 37: Electrophysiology of tibialis anterior muscle after sciatic nerve crush injury ..... 141

Figure 38: Sex base variance in compound motor action potential measures of recovery ..... 143

Figure 39: Functional recovery of RLn in a canine model..... 146

Figure 40: Equations for calculating Sciatic Functional Index ..... 148

Figure 41: Diagram of groups used to test engineered conduit with PNM as lumen filler ..... 161

Figure 42: Implant and explant of nerve conduits ..... 165

Figure 43: Masson Trichrome staining of 6 week nerve conduit explants. (Top, Bottom) ..... 168

Figure 44: Combination of centrally located wall-encapsulated ASCs and PNM improve functional  
return ..... 169

Figure 45: Conduits with centrally located wall-encapsulated ASCs improve axon myelination  
..... 171

Figure 46: Graphical abstract of the use of PNM in augmenting peripheral nerve injury response  
..... 175

## **1.0 Introduction**

### **1.1 Peripheral Nervous System**

#### **1.1.1 Anatomy and Physiology**

The peripheral nervous system encompasses all nerves outside of the central nervous system (CNS), including cranial nerves, spinal roots, and all other nerves of the extremities. The peripheral nervous system contains three types of cells: neuronal cells, glial cells, and stromal cells. The peripheral nervous system is also comprised of a combination of motor, sensory and autonomic neurons. Efferent neurons (motor and autonomic) deliver signals from the CNS to effectors, such as the musculature. Afferent neurons (sensory) relay sensory information back to the brain or interneurons in the spinal cord, generating a reflex response [1, 2].

The sensory division of the peripheral nervous system is made up of specialized sensory receptors that collect a variety of stimuli information and relay it back to central nervous system. Sensory neurons are made up of a receptor, an axon back to the cell body that resides in the dorsal ganglia of the spinal cord, and an axon that communicates the signal to the CNS. Sensory receptors can be classified by the type of stimulus, their location in the body and their structural complexity. Classifications for receptors based on stimulus type include mechanoreceptors, thermoreceptors, photoreceptors, chemoreceptors, and nociceptors (pain receptors). Three receptor classes are

recognized according to either their location or the location of the activating stimulus: exteroceptors (external stimuli), interoceptors (internal stimuli), proprioceptors (internal stimuli on body movement.) Sensory receptors can also be divided by structure broadly into unencapsulated (free nerve endings, Merkel discs, hair follicle receptors) and encapsulated (Meissner's and Pacinian corpuscles, Ruffini endings, muscle spindles, Golgi tendon organs, and joint kinesthetic receptor) [1, 2].

Somatic motor neurons originate in the central nervous system and project their axons to skeletal muscles. Three types of motor neurons exist: alpha ( $\alpha$ ), beta ( $\beta$ ), and gamma ( $\gamma$ ) neurons. Alpha neurons stimulate skeletal muscle to cause contraction and movement. Beta and gamma neurons have supporting roles of adjusting the sensitivity of muscle spindles, a specialized sensory receptor in muscles that allow for the detection of proprioception and limb movement speed. The autonomic nervous system unconsciously controls internal systems such as heart rate, digestion, respiratory rate, pupillary response, among others [1, 2].

Nerve tissue is highly responsive to stimuli. When adequately stimulated, an action potential is generated, an electrical impulse that is conducted along the length of its axon. This is either a sensory response generated by a receptor or a motor response from the CNS. This response is always the same regardless of the source or type of stimulus. Generation of the action potential involve three main changes in the membrane permeability resulting in the depolarization of the axon membrane. These changes involve the transient increase in  $\text{Na}^+$  permeability, followed by restoration of  $\text{Na}^+$  impermeability and then a short duration increase in  $\text{K}^+$  permeability. If the initial stimulus surpasses a threshold, these changes is propagated along the axon's entire length [1, 2].

The main glial cell within the peripheral nervous system is the Schwann cell. It plays an important role in the maintenance and function of peripheral nerves. Schwann cells ensheath nerves in a layer of myelin and provide trophic support. Myelin aids in the conduction velocity of action potentials by limiting the sites of ionic transfer along the axon to only nodes of Ranvier [1, 2]. The nodes of Ranvier being gaps in the myelin sheath between adjacent Schwann cells. This results in a faster action potential propagation down the axon. The most heavily myelinated fibers are large motor neurons (Type A $\alpha$ ), next followed by afferent muscle spindles (Type A $\beta$ ). Nerve conduction velocities in Type A $\alpha$  and A $\beta$  are approximately 30-120 m/s. In contrast, unmyelinated neurons (Type C), including sensory and sympathetic neurons conduct action potentials at approximately 1-2 m/s [3]. Nerve types are described in Table 1. Schwann cells synthesize and release a wide range of growth factors, such as neurotrophins, neuroregulatory cytokines, TGF- $\beta$ s, glial cell line-derived neurotrophic factor (GDNF), epidermal growth factors (EGFs), and platelet-derived growth factor (PDGF) [4]. Peripheral nerve injury stimulates distinct changes in growth factor expression including increased production of nerve growth factor (NGF), brain-derived neurotrophic factor (BDNF) and neurotrophin-4 and decreased expression of neurotrophin-3 [4].

Other non-neuronal cells and connective tissues surrounding the neuronal axons provide a complex stromal tissue and extracellular matrix. Surrounding individual axons is the endoneurium. Axons are bundled into fascicles by a dense connective tissue layer called the perineurium. Finally, the outermost layer of the nerve surrounding the nerve trunk is the epineurium. Micro-vessels exist in all layers providing blood supply to neuronal and non-neuronal cell populations. Injury to the various layers of this structure define the degree of injury and are the major determinate to recovery potential.

**Table 1: Nerve fiber types and properties**

Modified from: Berde CB & Strichartz GR. *Local Anesthetics. Miller: Miller's Anesthesia, 7<sup>th</sup> ed. Lars (eds) Eriksson I, Fleisher LA, Wiener-Kronish JP, Young WL. 2009. And Menorca, R. M., Fussell, T. S., & Elfar, J. C. (2013). Nerve physiology: mechanisms of injury and recovery. Hand clinics, 29(3), 317-30.[5]*

<b>Fiber Class</b>	<b>Diameter (mm)</b>	<b>Conduction Velocity (m/s)</b>	<b>Myelin</b>	<b>Location</b>	<b>Function</b>
<b>A<math>\alpha</math></b>	6-22	30-120	+	Efferent to muscles	Motor control
<b>A<math>\beta</math></b>	6-22	30-120	+	Afferent from skin and joints	Tactile, proprioception
<b>A<math>\delta</math></b>	1-4	5-30	+	Afferent sensory nerves	Pain, cold, temperature, touch
<b>B</b>	1-3	3-15	+	Preganglionic sympathetic	Various autonomic functions
<b>sC</b>	0.3-1.3	0.7-1.3	-	Postganglionic sympathetic	Various autonomic functions
<b>dC</b>	0.4-1.2	0.1-2.0	-	Afferent sensory nerves	Various autonomic functions, pain, warm, temperature, touch

### **1.1.2 Peripheral Nerve Injury**

Every nerve can be injured by blunt or sharp trauma, and the resultant injury can be partial or complete, transient or permanent (Figure 1). Peripheral nerve injury exists on a spectrum and can be graded from 1<sup>st</sup> - 5<sup>th</sup> using the Sunderland grading system [6]. In a Sunderland type 1 injury, local myelin is disrupted but the axons are preserved, and no degeneration occurs. This injury type, also referred to as neuropraxia is not marked by any real pathological changes and is instead a block in conduction alone without any need for significant regeneration. Beyond neuropraxia, the axon continuity is disrupted, and prognosis depends on how much of the nerve structure is damaged: only the axons (2<sup>nd</sup> degree), endoneurium (3<sup>rd</sup> degree), perineurium (4<sup>th</sup> degree), or complete transection (5<sup>th</sup> degree). In all of these cases, the nerves must undergo two major processes before regeneration can occur: neuronal survival and reaction, and Wallerian degeneration ( 2) [7, 8].

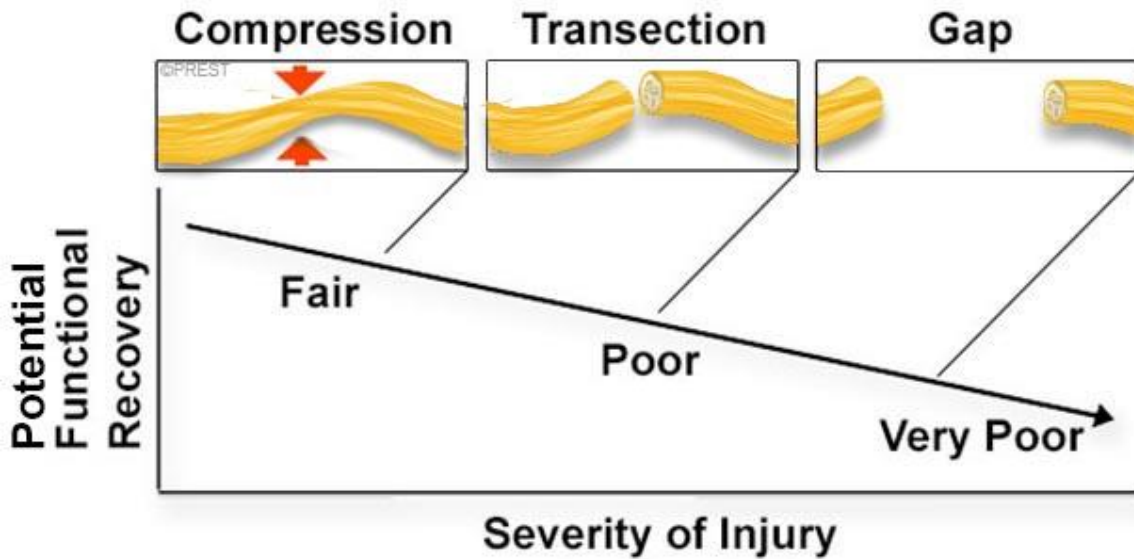


**Figure 1: Relative expected outcome of peripheral nerve injury based on severity of injury**

These two processes provide the peripheral nervous system with a superior regenerative potential compared to injuries of the central nervous system and ultimately stems from the supportive environment generated after nerve injury [9]. Neuronal cell bodies of the PNS within the CNS and dorsal root ganglion (DRG) possess the ability to shift from a transmitting state to a pro-repair phenotype to regrow after injury. This neuronal reaction represents the metabolic changes necessary for regeneration and axonal elongation. Underlying this process are prominent changes in gene expression, which lead to a decrease in the synthesis of neurotransmission-related products and an increased synthesis of growth-associated proteins and structural components of the membrane. This process is triggered and maintained by signals integrated at

the injury site/growth cone[10]. In contrast, where the environment inhibits recovery after CNS injury, the PNS has complex mechanisms that support regeneration at the site of injury [11-15].

Axonotmesis and neurotmesis injuries to the peripheral nervous system elicit a response from multiple cell types both at the site of injury and distally to support regenerating axons towards their original targets [16, 17]. Denervated axons distal to the injury are degraded by local Schwann cells followed by the infiltration of macrophages in a process known as Wallerian degeneration [18]. Myelin sheaths are also degraded as they contain regeneration-inhibitory factors, mainly myelin-associated glycoprotein. This process creates a microenvironment distal to the injury site that is favorable for the axonal regrowth of surviving neurons [16, 19, 20]. This process begins within 2 days of the injury, lasting approximately 2 weeks [20]; however, the macrophage population does not peak until 2-3 weeks post-injury. The presence of macrophages plays an additional role of supporting Schwann cells, fibroblasts and promoting angiogenesis through the release of cytokines and mitogenic signals [7, 16, 21, 22]. Triggered by inflammatory macrophages during the first few days after injury, Schwann cells de-differentiate and take on a repair-supportive phenotype [7, 9, 13]. Beyond phagocytosing myelin and axonal debris, these de-differentiated Schwann cells proliferate and secrete neurotrophic factors, including NGF and BDNF to support axon regeneration [7, 9, 23] [7, 9, 13]. Ultimately, the de-differentiated Schwann cells migrate along new, axially aligned vasculature promoted by macrophages guiding axons towards their distal targets [7, 16, 21, 22].

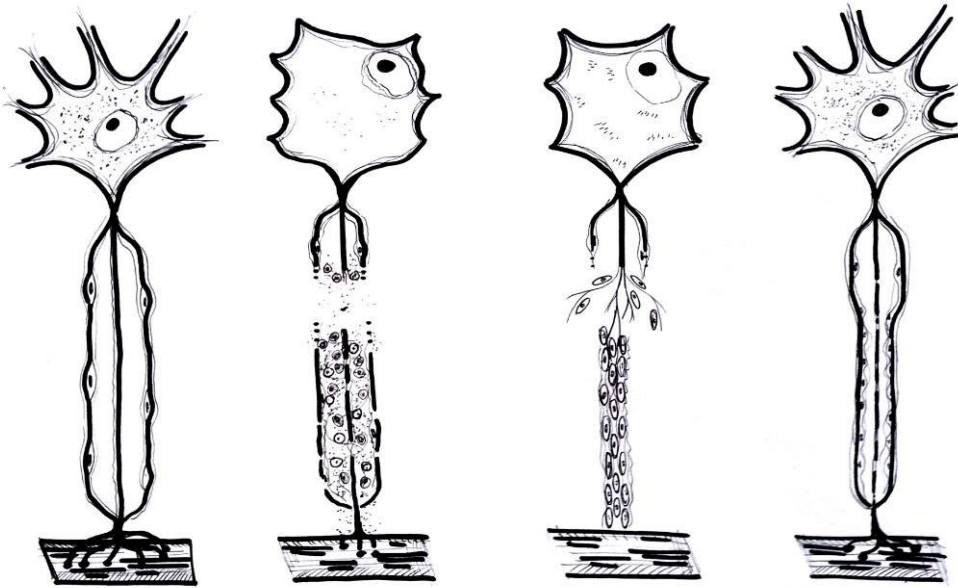


**Figure 2: Depiction of nerve structure and repair.**

Nerves undergo neuronal survival at the cell body and Wallerian degeneration at the injury site and distally immediately after injury. Schwann cells dedifferentiate, proliferate, and line up to form bands of Büngner. Axon sprouts produce a growth cone that follow signals produced by Schwann cells. After the axon has reached its target, Schwann cells mature and begin to remyelinate the axon.

Despite these mechanisms for PNS regeneration, actual patient outcomes after peripheral nerve injury remain varied, with factors such as severity and location of the injury impacting functional outcomes. Mild axonotmesis injuries recover better than more severe axonotmesis and neurotmesis injuries [14] These injuries are subject to misalignment of motor and sensory nerves as they regrow randomly towards distal targets [24, 25]. Large distances from injury to the end

organ also plays a large role in poor outcomes [14, 26]. The rate of axon growth is limited to around 1mm/day [8, 24]. However, phenotypic changes favoring repair in neurons and Schwann cells are not static and decline with prolonged axotomization and denervation [13, 26].

Functional recovery is rare if reinnervation is not established within a window of 12-18 months, largely due to atrophy of the target muscle and neuromuscular junctions [8].

Blunt force trauma usually results in neurapraxia or minor axonotmesis injuries, Sunderland's first and second-degree injuries [5]. These types of injuries often fully recover in most patients. In cases of minor neurapraxia injuries, full recovery occurs within days, but for more severe neurapraxia or axonotmesis injuries recovery can take weeks to months. Sharp trauma such as glass or knife lacerations are common causes of significant, traumatic nerve injury. Thin shards of glass and knife blades can penetrate deeply while leaving a minor skin laceration and can involve vascular and/or tendon lacerations. These factors can lead to undetected nerve lacerations unless a thorough examination is done. Even when the neurotmesis is found and repaired, these nerve injuries often have disappointing outcomes in adults especially in terms of recovering fine sensory function [27, 28].

Entrapment neuropathies are a type of chronic compression or crush injury that present commonly in six different peripheral nerves. The median nerve can be compressed at the wrist and is called carpal tunnel syndrome. This is the most prevalent entrapment neuropathy effecting 3-6% of the adult population to some degree, with 118,000 procedures performed annually [29]. Carpal tunnel syndrome presents as numbness or tingling involving one or more of the first four digits. It also appears as weakness and atrophy of the thenar muscles, particularly abductor pollicis brevis [30]. The ulnar and radial nerves can also be entrapped causing significant deficits. The ulnar nerve can be compressed in the cubital tunnel at the elbow causing paresthesias and pain in

the fifth digit and the medial half of the fourth, as well as difficulty spreading the fingers. Compression of the radial nerve results in wrist drop and sensory loss of the dorsal aspect of the hand [30]. Presentation of radial nerve compression can be caused at multiple points along the upper extremity, including at the level of the axilla (“Saturday night palsy”), the spinal groove, or in the forearm (posterior interosseous neuropathy.) Lower extremity neuropathies include meralgia paresthetica, femoral neuropathy, and peroneal neuropathy. Meralgia paresthetica stems from an entrapment of the lateral femoral cutaneous nerve near the inguinal ligament and causes a burning sensation and variable loss of sensation over the anterolateral thigh [30]. Femoral neuropathy causes overall leg weakness, especially when attempting to stand or walk and are usually caused by trauma from surgery, stretch injury, diabetes mellitus, and other inflammatory processes. Entrapment of the peroneal nerve between the neck of the fibula and the insertion of the peroneus longus muscle causes peroneal neuropathy predominantly presenting as foot drop [30].

## **1.2 Clinical Repair of Nerve Injuries and Current Research**

### **1.2.1 Significance**

Axons of the peripheral nervous system retain the capacity for regrowth. However, repair and reconstruction of nerves in many peripheral nerve injuries is challenging and often leave patients with life-long deficits. In the United States, an estimated 20 million people live with the long-term effects of peripheral nerve injury resulting in a high economic burden of \$150 billion [31]. Even the injuries with the best prognosis must go through the same complex repair and recovery process described in Section 1.1. This process can be restricted by slow nerve

regeneration, tissue adhesion, scar tissue formation, muscle atrophy, neuromuscular junction degradation, and other limiting factors. As a result, current re-innervation practices rarely show complete recovery of function with only a 51.6% rate of satisfactory motor recovery and 42.6% rate of satisfactory sensory recovery [32].

### **1.2.2 Clinical Approaches**

Neuropraxia and axonotmesis injuries have favorable functional recovery and as such little to no interventions are undertaken at the time of injury. In most cases, these patients are observed for the first 3-6 months before surgical repair is considered [30]. While most of these patients begin to show recovery within this time-period, lack of recovery signals either a more serious injury or complications necessitating a surgical intervention. Even for those that begin to recover in 3-6 months, axonotmesis injuries can take months to even years to fully recover. Currently, surgeons prefer not to take initial action with these types of injuries because there are no therapies that provide significant improvement without running the risk of affecting the already healthy recovery rates.

For transection injuries where a tensionless repair is not possible by direct anastomosis, the gold standard is the use of a nerve autograft. The sural nerve is the most common nerve graft, especially when a larger amount of graft material is required. Although sural nerve donor site morbidity is minimal, it does involve a second operation site that results in numbness of the lateral foot. This second operation site can increase operative time especially when the original nerve injury is in a different extremity to the sural nerve. The sural nerve is not the only available nerve graft. Several upper-extremity sources for nerve autograft also exist which pose several potential advantages when repairing upper-extremity nerve injuries, including confining donor morbidity to

the affect limb, limiting additional incisions, and simplifying harvest. In addition to the common Sural nerve graft, several upper-extremity nerve grafts are described in Table 2 (adapted from previously published work[33]).

**Table 2: Partial list of available nerves for autograft repairs**

Modified from: Drislane, F. W., et al. (2014). Blueprints Neurology. Philadelphia, PA, Wolters Kluwer Health.

<b>Donor nerve</b>	<b>Harvestable length</b>	<b>Cross-sectional area</b>	<b>Disadvantage</b>
Medial antebrachial cutaneous nerve	Up to 28 cm	2-3.15 mm <sup>2</sup>	Medial arm scar
Lateral antebrachial cutaneous nerve	5-8 cm	1.3-1.8 mm <sup>2</sup>	Visible forearm scar
Third webspace branch of median nerve	24.5 cm	4.4 mm <sup>2</sup>	Sensory loss in hand (non-critical)
Palmar cutaneous branch of median nerve	5 cm	2.4 mm <sup>2</sup>	Sensory loss in palm
Dorsal cutaneous branch of ulnar nerve	Up to 28 cm	2.4 mm <sup>2</sup>	Sensory loss to dorsal-ulnar hand and digits
Posterior interosseous nerve	2.5 cm	0.5-0.8 mm <sup>2</sup>	Visible dorsal incision Small diameter graft
Sural	30-50 cm	2.5-4 mm <sup>2</sup>	Positioning difficult Requires second extremity
Obturator	11.5 cm	3 mm <sup>2</sup>	Loss of gracilis as possible future free functional flap

While donor nerve alternatives exist to the sural nerve graft, they still possess similar disadvantages including either a need for a second surgery, a loss of sensation, or limited availability. A variety of nerve repair products have been approved as alternatives to the nerve autograft (Table 3). These products range from hollow tube conduits and wraps to decellularized allografts. These products are compared on metrics including tissue specificity, persistence in the body, mechanical support for regenerating axons, possible carrier for small molecules or cells, and their appropriate use in compression, transection, and short (<3cm) and large (>3cm) gap defect injuries. Green denotes high affinity or accepted use for the category. Yellow denotes a moderate or neutral affinity. Red represents a negative quality.

Hollow tube conduits are nonneural, tubular structures designed to bridge the gap of a sectioned nerve while protecting the nerve from scar infiltration and guiding the regenerative fibers towards the distal nerve stump. Available conduits and nerve connectors includes the Axoguard connector (Axogen), Neuragen (Integra), Neuroflex (Styker), Neurotube (Synovis), and Hydrosheath (Salubridge). These products are made from a variety of materials including small intestinal submucosal ECM (SIS), collagen I, poly-glycolic acid (PGA), and polyvinyl alcohol (PVA). Clinical use of the hollow tube conduits is limited predominately to only short gaps and does not produce outcomes that match the nerve autograft repair [34-38]. Wraps made from ECM including Axogen (Axoguard protector), Integra (Neurawrap), and Styker (Neuromend) exist on the market. Wraps are flat or rolled sheets made from SIS or collagen I that can be approximated around an injury. Most commonly these products are employed around anastomoses of transected nerves to protect the site from scar infiltration and to add mechanical support to the suture site. Axogen's Avance nerve graft is alone in its category and is regulated under HCT/P (Human Cellular and Tissue-based Product). The Avance is a decellularized human nerve that is available

in a range of lengths and diameters. Avance is currently the only nerve extracellular matrix (ECM) scaffold available to the market to bridge nerve discontinuities. The Avance graft has been successful in repairing nerve gaps and is a viable alternative to the nerve autograft but is limited to nerve gap injuries [38-40].

**Table 3: Clinically available nerve repair products and alternatives to the nerve autograft**

	Hollow Tubes/Conduits				Wraps			Decell Allograft
	Axogen Axoguard Connector	Integra Neuragen	Stryker Neuroflex	Synovis Neurotube	Axogen Axoguard Protector	Integra Neurawrap	Stryker Neuromend	Axogen Avance Graft
Material	Small intestinal submucosa (SIS)	Collagen type I	Collagen type I	Woven poly-glycolic acid (PGA)	SIS matrix	Collagen Type I	Collagen Type I	Nerve matrix
Form	Solid sheet	Gel tube	Gel tube	Solid mesh	Solid sheet	Gel sheet	Gel sheet	Solid sponge
Cost	\$700	\$1470-1670	\$1,838	--	\$1400-1725	\$1470-2000	\$1828-2000	\$1300-3000
Tissue specificity	Yellow	Yellow	Yellow	Red	Yellow	Yellow	Yellow	Green
Persistence	4-8wks	6-12mos	4-8mos	6-12mos	4-8wks	6-12mos	4-8mos	4-8wks
Mechanical support for regenerating axons	Yellow	Yellow	Yellow	Yellow	Yellow	Yellow	Yellow	Green
Carrier for small molecules or cells	Red	Red	Red	Red	Red	Red	Red	Yellow
Compression injury	Red	Red	Red	Red	Red	Red	Red	Red
Transection	Red	Red	Red	Red	Green	Green	Green	Red
Transection w/ short gap	Green	Green	Green	Green	Green	Green	Green	Green
Transection w/ long gap	Red	Red	Red	Red	Yellow	Yellow	Yellow	Green

While many alternatives exist, some with outcomes that come close or match the nerve autograft, many surgeons still prefer the traditional gold-standard over any alternative solutions. Surgeons that routinely repair peripheral nerve injuries have a high barrier of entry for new products and require alternatives that not only match but exceed current practices. Therefore, current research has explored new ways of improving current repair practices.

### **1.2.3 Current Research**

Numerous approaches for delivery of matrix components, immunomodulatory or growth factors, and cells to the site of nerve repair have been used. The majority of studies have investigated single or combinations of a small number of additives to common hollow tube nerve guidance conduits with the goal of altering the local environment and improving recovery through the addition of growth factors such as Brain Derived Neurotrophic Factor (BDNF), Glial Derived Neurotrophic Factor (GDNF), Nerve Growth Factor (NGF), Neurotrophin-3 (NT-3) or accessory cells into a supportive matrix [41-50]. A review of current research on lumen filler for nerve conduits can be found in Table 4. While many of these studies have reported positive outcomes, limitations include tailoring growth factor release profiles, optimizing the mechanical environment of the substrate used at the site of repair, and maintaining cell viability after transfer [51]. One alternative to engineering a complex microenvironment is to mimic the native microenvironment of healthy peripheral nerve using a decellularized tissue-based hydrogel. This strategy may be able to compete with both the Avance graft and the gold-standard nerve autograft.

**Table 4: Review of current research on lumen fillers for nerve conduits**

Reused with permission (4546560968632). [52]

<b>Growth Factor/ Cell</b>	<b>Matrix</b>	<b>Conduit material</b>	<b>Animal model</b>	<b>Conclusions</b>	<b>Ref</b>
BDNF	Collagen	Collagen	Rabbit facial nerve; 15 mm, n = 10	BDNF did not appear to promote better regeneration than collagen matrix only.	[53]
GDNF	Fibrin	Silicone	Rat sciatic nerve; 13 mm, n = 12	GDNF delivery system generated significantly less nerve fibers at middle line of conduit than isograft but fibers were more mature.	[54]
	EVA/BSA	EVA	Rat sciatic nerve; 15 mm, n = 10	GDNF promoted approximately 20% and 35% regeneration of motor and sensory neurons respectively.	[43]
	Fibrin	Silicone	Rat femoral nerve; 5 mm, n = 7	Controlled delivery of GDNF led to enhanced nerve regeneration that was not significantly different then isograft control.	[46]
NGF	Fibrin	Silicone	Rat sciatic nerve; 13 mm, n = 6	NGF was not significantly different from the isograft control including showing similar nerve maturity and density.	[44]
	EVA/BSA	EVA	Rat sciatic nerve; 15 mm, n = 10	Only 5% of the total number of motor and sensory neurons regenerated with treatment of NGF after 6 weeks.	[43]
NT-3	Collagen	PHEMA-MMA	Rat sciatic nerve; 10mm, n = 6	The introduction of a high dose of fibroblast growth factor (FBF-1) was comparable to isograft and was significantly better than NT-3, BDNF, and matrix alone.	[45]

Table 4 (continued)

Schwann Cells	Collagen	PLGA	Rat sciatic nerve; 12 mm, n = 9	The bone marrow stromal cell derived Schwann cells produced better histologic and functional outcomes than matrix alone but did not match autograft control.	[47, 55]
	Alginate/fibronectin	PHB	Rat sciatic nerve; 10 mm, n = 6	Transplanted Schwann cells and fibronectin had an additive effect on regeneration over negative controls.	[47]
	Gelatin	PLGA	Rat sciatic nerve; 10 mm, n = 6	The addition of Ginkgo biloba extract with Schwann cells increased motor unit action potential at 6 weeks after injury over autograft control.	[56]
	Matrigel	Collagen	Mouse sciatic nerve 6 mm, n = 9	Allogeneic Schwann cells did not provide a benefit over matrix only control but the addition of FK506, an immunosuppressant, improved results over negative control.	[49]
Matrix Alone	Keratin	Silastic	Mouse tibial nerve; 4 mm, n = 5	Keratin increase histologic and electrophysiologic measures of recovery over autograft, however these results did not translate to muscle function recovery after 6 weeks.	[48]
	Keratin	Silicone	Mouse tibial nerve 5 mm, n = 6	Keratin hydrogel improved electrophysiologic and histologic measurement of recovery over empty conduits and autograft controls.	[41]

### 1.3 Extracellular Matrix

Tissues are not solely comprised of cells, instead a substantial volume is made up of extracellular matrix (ECM). The ECM is an intricate network of macromolecules including proteoglycans and fibrous proteins [57, 58]. Proteoglycans fill the majority of the extracellular and interstitial space in tissues creating a hydrated gel [58]. Collagen is the most abundant fibrous protein but other fibrillar proteins of the ECM include elastins, fibronectins, and laminins [59]. The composition of the ECM of tissues is quite complex with hundreds of possible ECM molecules described today [58, 60, 61]. It has been long understood that the extracellular matrix (ECM) not only provides structural support but also regulates cell growth [62, 63], survival, maturation, differentiation [64, 65], and development [66] of resident cells [67]. ECM is not a static scaffold but subject to dynamic reciprocity with its host cells [68] responsive to and responsible for the changing structure, mechanical, metabolic, and functional needs of these cells. Components of ECM such as thrombospondin-1, thrombospondin-2, SPARC, tenascin-C and osteospondin all do not function as structural proteins but modulate cell-matrix interactions and cell function [69, 70].

Peripheral nerve tissue also has its own unique extracellular matrix. The ECM of peripheral nerves are made up of macromolecules including collagen (I, II, IV, and V), laminin, fibronectin, and chondroitin sulfate proteoglycans[71]. The predominant component in peripheral nerve ECM is collagen I, making up about 90% of the composition [71, 72]. Collagen has been seen throughout the three layers of the peripheral nerve; epineurium, perineurium, and endoneurium[73]. Laminin is another common component of peripheral nerve ECM. Laminin is mainly produced by Schwann cells and is found in the basement membranes in a tight network with glycoproteins, collagen IV, and proteoglycans [73]. Laminin can also be found in the perineurium. Along with collagen, laminin has been shown to play an essential role in enhancing axonal growth [71, 73]. Fibronectin

is found around the perineurium and within the epineurium. Both laminin and fibronectin are important constituents of peripheral nerve development. Fibronectin has been shown to play a role in migration and differentiation in neural crest cells while laminin maturation through Schwann cell myelination of axons [73].

#### **1.4 ECM Scaffolds in Soft Tissue Repair**

ECM scaffolds are derived from the removal of cellular components within whole tissue and retain the micro- and macro-scale structural components and functional ECM proteins. These components include collagen molecules (e.g. types I, III, IV, among others), laminin, fibronectin, and glycosaminoglycans (GAGs) as well as a variety of growth factors (e.g. vascular endothelial growth factor (VEGF), basic fibroblast growth factor (bFGF), transforming growth factor  $\beta$  (TGF $\beta$ )) [67, 74-78]. The ECM of urinary bladder, small intestine, dermis, pericardium, and nervous tissue are all examples of FDA approved or clinically available scaffolds for soft tissue repair (Table 5), adapted and updated from [79] [80]. These ECM scaffolds have been used in a number of different configurations to meet the exact clinical needs. These configurations include two-dimensional sheets, powders, multi-laminate sheets, tubular structures, powder pillow devices, and whole organs [81]. Recently, a method for fabricating ECM scaffold degradation products into injectable, temperature responsive, hydrogels has been described [36, 37], enabling delivery in multiple settings without prior fabrication of solid matrices into specific shapes and sizes.

**Table 5: Partial list of commercially available extracellular matrix-based scaffolds**

Modified from Swinehart, I. T., & Badylak, S. F. (2016). Extracellular matrix bioscaffolds in tissue remodeling and morphogenesis. *Developmental dynamics* : an official publication of the American Association of Anatomists, 245(3), 351-60. [82]

<b>Product</b>	<b>Vendor</b>	<b>Scaffold Source</b>
MatriStem®	ACell Inc.	Porcine urinary bladder matrix (UBM)
AxoGuard® Nerve Connector	AxoGen	Porcine small intestinal submucosa (SIS)
AxoGuard® Nerve	AxoGen	Porcine small intestinal submucosa (SIS)
Oasis® Wound matrix	Smith&nephew	Porcine small intestinal submucosa (SIS)
Biodesign®	Cook Medical	Porcine small intestinal submucosa (SIS)
AlloDerm	Biohorizons	Human dermis
ArthroFLEX ®	Arthrex	Human dermis
AlloMax™	BD (C. R. Bard)	Porcine dermis
Permacol™	Covidien	Porcine dermis
XenMatrix Surgical graft	BD (C. R. Bard)	Porcine dermis
Zimmer Collagen Patch®	Zimmer	Porcine dermis
PriMatrix™	Integra LifeScience	Fetal bovine dermis
SurgiMend™	Integra LifeScience	Fetal bovine dermis
TissueMend®	Integra LifeScience	Fetal bovine dermis
Dura-Guard®	Baxter	Bovine pericardium
Peri-Guard®	Baxter	Bovine pericardium
Vascu-Guard®	Baxter	Bovine pericardium
Veritas®	Baxter	Bovine pericardium
Avance® Nerve graft	AxoGen	Human peripheral nerve (HCT/P)

These ECM scaffolds have been successfully used in a range of applications to support constructive remodeling, or the deposition of site-appropriate tissue. The precise mechanisms that drive the process of ECM mediated constructive remodeling are only partially understood. However, it has been shown that scaffold degradation, recruitment of endogenous stem cells, and modulation of the innate immune system are important determinants of outcome. ECM scaffolds are rapidly infiltrated by host cells, especially macrophages which degrade the matrix via matrix metalloproteinases (MMPs) and other proteases. This degradation of the scaffold releases bioactive molecules such as growth factors and cytokines. Furthermore, bioactive cryptic peptides can be created by cleavage of molecules such as collagen, fibronectin and laminin [83, 84]. These bioactive molecules in combination with scaffold degradation initiate a robust remodeling activity that includes immunomodulatory, chemotactic, proliferative, and differentiation activity for a variety of cell types. Macrophages are an important cell population altered by the interaction with ECM scaffolds. Macrophages exist on a phenotypic and functional spectrum (i.e., M1, M2a, M2b, M2c). ECM scaffolds have been shown to promote a shift towards a regulatory, anti-inflammatory macrophage phenotype (M2) and this shift is strongly correlated to downstream constructive remodeling response.

Within the peripheral nervous system, macrophages play an important role in injury recovery. After injury, macrophages arrive to the site within 24 h and their population peaks by 14-21 day [85]. They account for the bulk of phagocytosis within these days and play critical roles in scavenging debris, growth factor production such as NGF and IL-6 [86, 87], and remodeling of the ECM of the distal nerve [24, 88]. It has been shown that modulating macrophages within the peripheral nerve injury towards an M2 like phenotype results in enhanced Schwann cell infiltration and substantially quicker axonal growth in rodent animal models [89]. Furthermore the ratio of

pro-remodeling (M2) macrophages to pro-inflammatory (M1) macrophages has been shown to have a linear relationship with the number of axons that are found at the distal end of nerve scaffolds [89].

While individual ECM components have been isolated from native tissues and investigated, whole ECM is a highly complex milieu that is not fully understood. This prevents the creation of artificially engineered scaffolds with the same ECM composition and distribution. Collagen type 1 is the most abundant ECM protein in many adult tissues and is easily extracted. Collagen can be formed into sheets, hydrogels, and sponges and has been used in applications that include peripheral nerve conduits and lumen fillers (Table 3, Table 4). However, in many applications the response of simple collagen scaffolds does not match that of a comparable whole ECM scaffold.

While many components of the ECM are conserved across several tissue types, each tissue is believed to possess a unique composition and mechanical and ultrastructural characteristics [90, 91]. Recently, scaffolds have been derived from ECM sourced from a variety of tissues including skin, fat, pericardium, heart, skeletal muscle, and liver for both *in vivo* and *in vitro* experiments to examine the effects of using application specific ECM sources [67, 92-95]. These scaffolds have been observed to assist with constructive remodeling or the formation of site-appropriate tissue when used as a biomaterial *in vivo* [96] and in some cases these ECM scaffolds have tissue-specific effects on cellular behavior [83, 84, 93, 97-101]. In these cases, a homologous ECM source has maintained tissue-specific cell phenotypes [84, 99-101], promoted cell proliferation [93, 100], induced tissue-specific differentiation [98], and enhanced the chemotaxis of stem cells [97, 102, 103]. While a preference or necessity for tissue-specific ECM has not been shown for all

therapeutic applications [102, 104, 105], research suggests that the peripheral nerve system is a candidate for a peripheral nerve specific ECM scaffold over non-nerve specific sources [97, 106, 107].

## **1.5 Specific Aims of Dissertation**

Through decellularization, whole nerve-specific ECM scaffolds can be created that would contain the same structural and functional molecules found within the autologous nerve graft. These components have been shown to enhance the natural regenerative response. Key elements found within the peripheral nerve ECM (PNM) such as laminin, fibronectin, and collagen have been shown to enhance the Schwann cell response with the greatest results where proteins were combined [108]. Further research has shown that the presence of laminin in co-cultures of Schwann cells and NG108-15 cells activated transcription factors in Schwann cells which in turn promoted growth of longer neurites by the neuronal cells [108]. In addition, ECM scaffolds have been shown to promote a shift in infiltrating macrophage phenotype towards M2, an anti-inflammatory and tissue repair phenotype. It has been demonstrated that M2 polarized macrophages play a neuroprotective role and as such, shifting the neurodegeneration-induced immune responses towards an M2 response could be an important therapeutic strategy [22]. As the hydrogel degrades, these components, among others, are released into the surrounding area and we believe that they will cause a cascade of effects including Schwann cell migration and a shift towards anti-inflammatory M2 macrophages [109, 110] and will have positive effects on axonal outgrowth and functional outcomes.

This dissertation investigates the use of a novel extracellular matrix hydrogel derived from peripheral nerve tissue as a lumen filler for nerve guidance conduits and more broadly in enhancing peripheral nerve regeneration after injury. The methods and techniques developed in this dissertation provide a better understanding of PNM, characterization of a novel lumen filler, and possible new therapies for peripheral nerve injuries. Furthermore, the results of this dissertation provide insight into the phenotypic role of macrophages during the nerve healing response and correlations between benchtop metrics and functional outcomes of nerve repair.

The objective of this dissertation was to investigate the effects and mechanisms of action of a peripheral nerve specific ECM in the regeneration of peripheral nerve injury. The specific aims of this proposal are designed to answer the following questions:

Does a peripheral nerve specific ECM hydrogel provide a preferred microenvironment over non-nerve specific ECM hydrogels for peripheral nerve repair?

Does PNM generate enhanced recovery through mechanisms beyond simple structural support in a critical length sciatic nerve defect injury model?

Does PNM generate improved functional recovery after a critical length sciatic nerve defect injury as compared to the gold standard, the autologous nerve graft?

**1.5.1 SPECIFIC AIM 1: Characterize a PNM Hydrogel and Determine if PNM Hydrogels Provide a Preferred Microenvironment for Peripheral Nerve Repair as Compared to Non-Nerve-specific ECM (SIS and UBM) Hydrogels.**

Because the extracellular matrix is generated by the resident cells of each tissue and organ, scaffolds derived from different tissues will logically vary in structure and composition. This

complex structure and composition cannot be artificially engineered, thus decellularization represents an ideal approach to the generation of tissue specific substrates. Previous studies have suggested scaffolds derived from a site specific tissue may be better suited for constructive tissue remodeling than non-site specific tissue sources [107]. We hypothesized that PNM would be a better scaffold for peripheral nerve repair than non-nerve ECM. This included that ECM derived from peripheral nerves would contain important nerve associated structural and functional constituents. PNM would have a greater effect on neurite outgrowth and Schwann cell migration than a non-nerve-specific ECM (sub-intestinal submucosa ECM and porcine dermis ECM). Furthermore, PNM was expected to promote a macrophage phenotype similar to M2.

### **1.5.2 SPECIFIC AIM 2: Determine if PNM Generates Enhanced Recovery Via Mechanisms Beyond Simple Structural Support by Assessing PNM's Effect on the Regenerative Response in a Peripheral Nerve Defect Injury Model**

ECM scaffolds have been shown to promote a process of new, site-appropriate, functional tissue formation. These studies have also demonstrated that ECM scaffold materials play a bioactive role and promote a shift in the macrophage response from M1 (proinflammatory) to M2 (anti-inflammatory). M2 macrophages have been shown to have a positive effect on the Schwann cell response to injury [22]. PNM was expected to have a bioactive response on Schwann cells, axons and macrophages. The corollary hypothesis was that use of PNM when repairing a sciatic nerve defect injury of rat sciatic nerves will increase the rate of axonal growth, Schwann cell migration and presence of M2 polarized, anti-inflammatory macrophages.

### **1.5.3 SPECIFIC AIM 3: Determine the Translational Potential of PNM by Investigating Functional Recovery Outcomes After a Critical Length Sciatic Nerve Defect Injury.**

Even when successful regeneration of axons across the injury site occurs, reinnervation of the target tissue does not always follow. Misdirected axons which do not distally reconnect will ultimately undergo progressive withdrawal [111]. These axons will also likely not undergo maturation (myelin sheath formation). Since axon misdirection is believed to play a significant role in poor functional recovery, this proposal seeks to investigate the link between nerve fiber maturity following PNM application and function outcomes [112]. To test this PNM will be compared to the autograft procedure (gold standard), conduit without lumen filler, and no repair controls (negative control). Our hypothesis was that the PNM enhanced regenerative response during acute timepoints would lead to enhance electrophysiological measurements and functional dynamic and static parameters of downstream function.

## **2.0 Development and Characterization of a PNM Scaffold and Hydrogel for Peripheral Nerve Repair**

### **2.1 Introduction**

ECM scaffolds are an attractive material that have not been fully investigated for possible benefits in the peripheral nervous system. ECM based scaffolds that have been appropriately decellularized have been shown to promote constructive remodeling following injury [79, 106, 107, 109, 110, 113, 114]. However, over or under decellularizing tissue results in poor outcomes. The insufficient removal of DNA and other immunogenic materials leads to an increased inflammatory response and possible rejection of the implanted scaffold [1, 2]. The use of overly harsh decellularization methods can successfully remove unwanted native constituents of the tissue but can also damage structural and signaling proteins [115-117]. While many methods for decellularization of tissues have been described and are accepted to work, no method is broadly accepted as optimal for all tissues and organs due to variability in tissue composition and structure [1, 2]. Even for decellularization of peripheral nerve tissue, a wide range of protocols exist [116-140]. A summary of these methods can be found in Table 7. The goals of decellularization are the removal of cells, elimination of genetic material, preservation of ECM components, and the retention of mechanical properties. Decellularization methods described have used mechanical, chemical, and enzymatic techniques to remove cellular debris while limiting the disruption to the ECM. These methods have been previously described [141] and have been summarized and expanded upon in the table below (Table 6).

These methods all have their own advantages and disadvantages as described (Table 6) and as such several techniques are often combined to complement each other with the goal of maintaining the desired tissue characteristics. This can involve all categories, chemical, enzymatic, and mechanical and each constituent's parameters need to be optimized to suit a particular tissue.

**Table 6: Summary of decellularization agents and techniques**

Category		Examples	Advantages and Disadvantages	Tissue Types	References
					PNS
Detergent	Class				
	Ionic	Sodium dodecyl sulfate (SDS)	(-) Cytotoxic: requires extensive wash process [142] (-) Alters microstructure (i.e., collagen fibers)[143]	sciatic nerve, tibial nerve, femoral nerve, median nerve, caudia equine	[34, 133, 136, 139, 144, 145]
		Sodium deoxycholate (SDC)	(-) Causes agglutination of DNA when used without DNase [146]	sciatic nerve, tibial nerve, femoral nerve, caudia equine	[52, 115, 117, 120, 121, 132, 147, 148]
		Triton X-200	(-) Discontinued	sciatic nerve, tibial nerve, femoral nerve, human peripheral nerve	[38-40, 116, 120, 122, 123, 138, 144, 149, 150]
	Nonionic	Triton X-100	(-) Less damaging to structure of tissue than ionic surfactants [83, 92]	sciatic nerve, tibial nerve, femoral nerve, median nerve, caudia equine	[52, 115, 117, 121, 130, 132, 136, 147, 151, 152]
	Zwitterionic	Sulfobetaine-10 (SB-10)	(+) Solubilization of oleosins (+) works over a broad pH range (+) effectively removes cells with mild disruption of ultrastructure in thin tissues [149]	sciatic nerve, tibial nerve, femoral nerve, human peripheral nerve	[38-40, 116, 120, 122, 123, 138, 144, 149, 150]
		Sulfobetaine-16 (SB-16)	(+) solubilizes membrane proteins (+) works over a broad pH range (+) effectively removes cells with mild disruption of ultrastructure in thin tissues [149]	sciatic nerve, tibial nerve, femoral nerve, human peripheral nerve	[38-40, 116, 120, 122, 123, 138, 144, 149, 150]
		CHAPS	(+) Maintains structural ECM proteins (-) Remnant cytoplasmic proteins (+) Maintains ultrastructure [153]	sciatic nerve, tibial nerve, femoral nerve	[130]

Table 6 (continued)

<b>Chemical</b>	Peracetic acid	(-) Insufficient cell removal (-) Highly corrosive (+) Oftentimes used for sanitization (-) Increases stiffness of ECM [142, 154]	UBM, sciatic nerve	[34, 52, 79, 120, 121, 132, 135, 145, 151, 155]
	EDTA	(-) Commonly used with trypsin but ineffective when used alone (-) Decreases salt- and acid-soluble ECM proteins [156]	sciatic nerve	[52, 157, 158]
<b>Enzyme</b>	Trypsin	(-) Prolonged exposure can disrupt ECM ultrastructure (-) Removes ECM constituents such as collagen, laminin, fibronectin, elastin, and GAG [141]	Sciatic nerve	[52, 157, 158]
	DNase	(-) Difficult to remove from the tissue and could invoke an immune response [141], [153]	sciatic nerve	[132, 147, 151, 152, 157-159]
	RNase		sciatic nerve	[132, 147, 152, 157, 158]
	Chondroitinase ABC	(-) Prolonged exposure could disrupt ECM ultrastructure [118, 137]	sciatic nerve, human peripheral nerve	[38-40, 118, 122, 137, 138]

The majority of application of decellularized ECM towards the PNS have sought to improve nerve grafting by generating decellularized allografts [119, 120, 130-132, 145, 147, 152, 157, 159] or xenografts (Wang et al. 2013). Others have processed decellularized nerve [52, 160] or urinary bladder sources[151] to produce hydrogels or wraps to augment existing repair procedures. While the methods vary, they often utilize a combination of ionic and non-ionic detergents and sometimes enzymatic processes to decellularize the peripheral nerve tissues.

In order to study PNI, researchers have developed two primary models: Transection or Gap Injury and Crush Injury. The transection or gap injury model aims to address the impacts of severe PNI, where a segment of the nerve is completely removed, to mimic the physiological limit upon which natural nerve regrowth is not possible. The crush injury model represents a mild injury prognosis, where the nerve is expected to make a full recovery post injury. Each model provides a deeper insight into the critical factors necessary to assist nerve regeneration for PNI patients.

Serious trauma to the peripheral nervous system resulting in a full transection requires coaptation surgery and is often further complicated by retraction of the nerve stumps. [161] If nerve ends cannot be coapted directly without tension, the current gold standard repair involves the use of an autologous nerve graft to bridge the gap. Often using the sural nerve as donor tissue, the autologous nerve graft procedure results in donor site morbidity. As an alternative, decellularization techniques have been utilized to create acellular nerve grafts from allogeneic and xenogeneic sources that emulate the same structure and ECM composition of the autologous nerve graft.

**Table 7: Partial list of decellularization methods for peripheral nervous system**

Study model	Source Tissue	Added Comp. / Post Processing	Method Type	Decellularization Method				Notable Results	Ref			
				#	Step	T	rpm					
In vitro analysis of decellularization	Rat sciatic nerve	N/A	Detergent	Sondell et al. 1998 Method				The study found that the Sondell method of decellularization disrupted the nerve ECM more than the Hudson method. Hudson method also produced a greater degree of demyelination and improved adhesive ratios when scaffolds were co-cultured with adipose-derived stem cell. The study suggests that greater ECM disruption in the Sondell method could be from switching between the tissue shrinkage of sodium deoxycholate and swelling of distilled water.	[115-117, 121, 123, 150]			
					distilled water	7h						
				2x	3% Triton X-100	12h						
					4% Sodium deoxycholate	24h	yes					
					distilled water							
				Hudson et al. 2004 Method								
					distilled water	7h						
					125 mM sulfobetaine-10	15h	yes					
					50 mM phosphate and 100mM sodium	15m						
					0.14% Triton X-200, 0.6 mM sulfobetaine-16, 10 mM phosphate and 50 mM sodium	24h	yes					
				3x	50 mM phosphate and 100mM sodium	5m						
					125 mM sulfobetaine-10	7h	yes					
					50 mM phosphate and 100mM sodium	15m						
					0.14% Triton X-200, 0.6 mM sulfobetaine-16, 10 mM phosphate and 50 mM sodium	15h						
3x	50 mM phosphate and 100mM sodium	15m										
	Distilled water				7h	yes						
1.5 cm rat sciatic nerve defect	Rat sciatic nerve	N/A	Detergent	1 M Sodium chloride				15h	yes	This method decellularized the nerve to a similar degree to the Hudson T. method but displayed better ECM preservation. In a rat sciatic nerve gap model, the detergent less method outperformed the Hudson T. method in nerve histomorphometry and muscle mass but did not outperform the nerve autograft controls.	[130]	
				2.5 nM Triton X-100				24h	yes			
				1X PBS				15m	yes			
				Distilled water				7h	yes			
				1 M Sodium chloride				15h	yes			
				100 nM CHAPS				24h	yes			
				5x	1X PBS				5m			yes

Table 7 (continued)

In vitro characterization and effect on PC12 cells	Rat sciatic nerve	axially aligned channels	Detergent and Enzymatic	distilled water	7h		Testing showed that the method effectively decellularized the tissue and significantly increased pore size and created axially aligned channels. In vivo work has not been published but in vitro work showed enhanced PC12 cell migration both in number and depth into the graft.	[132]	
				2x	3% Triton X-100	12h			yes
					2% deoxycholic acid in 50nM Trizma base	24h			yes
				DNase and RNase (5 U/ml) in 10nM magnesium chloride	12h				
				0.1% peracetic acid	1h				
3.5cm Rat sciatic nerve gap defect	Rat sciatic nerve	N/A	N/A	DMEM 10% FBS 2% pen/strep/amph	2wk	yes	In a rat sciatic nerve gap model, histologic results indicated that nerve autograft outperformed both the detergent free and detergent decellularized grafts. Only nerve autograft and detergent free grafts showed functional recovery inn muscle force testing	[131]	
				PBS	1wk	yes			
In vitro characterization and subcutaneous implantation	Rat sciatic nerve	Apoptosis assisted	Enzymatic	DMEM with camptothecin (5 or 10uM) 37°C	1-3d	14	The apoptosis decellularization method was able to decellularize the tissue while maintaining basal lamina microarchitecture while being less cytotoxic then detergent decellularization methods. The apoptosis-assisted method also produced less inflammatory infiltrate and stromal remodeling compared to autograft control. More work will need to be done to look at downstream outcomes for nerve regeneration.	[159]	
				4X PBS	24h				
				2X PBS	30m				
				3x 1X PBS	30m				
				75 U/mL DNase	36h				
				2x 1X PBS	30m				
In vitro characterization	Rat sciatic nerve	N/A	Detergent and Enzymatic	10 mM TRIS-HCl; pH 8.0		yes	Decellularization method reduced DNA content by greater than 95% but preserved collagen, laminin, and fibronectin.	[145]	
				2x 0.1% SDS with 10 kIU/mL Aprotinin and 0.1% EDTA		yes			
				3x 1X PBS	30m	yes			
				1 U/mL Benzonase	3h	yes			
				1.5 M NaCl		yes			
				0.1% peracetic acid in PBS	3h	yes			
				3x 1X PBS at 4C	30m	yes			
				1X PBS at 4C	48h	yes			

Table 7 (continued)

1cm and 1.5cm rat sciatic nerve defect models	Rat sciatic nerve and rabbit median nerve	N/A	Detergent	1X PBS			Decellularization method was performed on both an allogeneic and xenogeneic tissue source and were compared in vivo to isograft control. Function, electrophysiological, and histomorphological analyses were performed after 24 weeks. Limited macrophage infiltration was observed but a large number of axons and Schwann cells were shown migrating into the bridge. Testing showed no difference between allo- and xenogeneic sources of decellularized nerve graft. However, both were inferior to isograft control. This was different than previous results from the group in Wakimura et al. 2015, where isograft and decellularization allograft was found to have similar outcomes in the same model and tests.	152]	[136,	
				1% SDS	24h	yes				
				Distilled water	30m					
				1% Triton X-100	1h	yes				
				Distilled water	30m					
				100 U/mL penicillin-G, 100 ug/mL streptomycin, 0.25 ug/mL amphotericin B	7d					
In vitro characterization	Rat sciatic nerve	N/A	Detergent and Enzymatic	50 nM Tris buffer	12h		Methods developed were compared to Sondell et al. and Hudson et al. methods. Method proposed by Roosens et al. showed a better removal of DNA content and preservation of ECM components.	121, 157, 158]	[116,	
				2x	1% Triton X-100 in 50 nM Tris buffer at 4°C	24h				
					HBSS	24h				24
				2x	40,000 U/L DNase, 20 mg/L RNase, 100 mg/L Trypsin at 37C	45m				yes
					1% Triton X-100 in 50 nM Tris buffer at 4°C	12h				
				3x	HBSS at 4°C					

Table 7 (continued)

1.5 cm rat sciatic nerve defect	Porcine sciatic nerve	Processed into an ECM hydrogel	Detergent	distilled water	7h		The goal of the study was to generate an alternative to human decellularized nerve allograft by decellularizing a porcine sciatic nerve. This was tested as a solid scaffold as well as an ECM hydrogel filler for a polymer conduit. The decellularization method closely resembles the Sondell method but the authors found that repeated detergent washes stripped to much ECM for effective gelation formation. This study found that repeated detergent washes was not necessary to produce a scaffold with significant residual DNA removal. In vivo the peripheral nerve ECM was able to augment a conduit with similar electrophysiology results to xenograft. However, both were inferior to autograft control for electrophysiology and sciatic functional index testing.	[127]
				3% Triton X-100	12h			
				4% Sodium deoxycholate	24h	yes		
				3x distilled water	15m	yes		
				Ethanol:Dichloromethane (1:2)	24h			
				distilled water				
1.5 cm rat sciatic nerve defect model	Rat sciatic nerve	N/A	Detergent	Distilled water	6h		New decellularization method developed by altering Hudson et al. method while still using similar detergent combinations (sulfobetaine-10, sulfobetaine-16, Triton X-200, and sodium deoxycholate). Method sought to reduce residual myelin present in the original Hudson et al. method. The modified method did produce a higher degree of demyelination than the Hudson method. Comparing these two methods to the nerve autograft, the modified method had a reduce immune response in vivo and had remyelination that was more similar to autograft than the Hudson method. However, morphologic assessment of axon regrowth showed no difference between the two methods.	[120]
				125mM sulfobetaine-10	12h	yes		
				3x 1X PBS	10m			
				0.14% Triton X-200, 0.6 mM sulfobetaine-16	24h	yes		
				1X PBS	10m			
				Distilled water	10m			
				125mM sulfobetaine-10	12h	yes		
				4% Sodium deoxycholate	24h	yes		
				3x 1X PBS	2h			
				0.1% Peracetic acid	3h			
				3x				
				1X PBS	1h			

Table 7 (continued)

Rabbit tibial nerve	Rabbit tibial and femoral nerves	N/A	Detergent	Method 1: Hudson Method (control)		The main goal of the study was to develop a protocol that limited the hands-on time necessary to decellularize peripheral nerve in order to avoid postprocessing sterilization steps. Results suggested that both method 2 and 3 were less harsh than the Hudson method with small amount of DNA fragments and Schwann cells still present after decellularization. Furthermore, method 2 produced a more prominent uneven decellularization towards the center of the graft. The Triton X-100 and SDS method did remove most of the myelin sheets, axons and DNA residue to a satisfactory degree and maintained the nerve ECM well.	[144]	
				125 mM SB-10, 10 mM phosphate, 50 mM sodium	15h			yes
				2x 0.14% Triton X-200, 0.6 mM SB-16, 10 mM phosphate, 50 mM sodium	24h			yes
				Method 2: Triton X-100 based Method				
				125 mM SB-10, 0.2% Triton X-100, 1% penicillin-streptomycin	48h			yes
				Sonication at 40 Hz	2m			
				Method 3: Triton X-100 and SDS method				
				125 mM SB-10, 0.2% Triton X-100, 1% penicillin-streptomycin	48h			
freeze-thaw cycle								
3x 1X PBS	30m							
0.25% SDS and sonicated for 5m every 30m at 40 Hz	3h							
rat trigeminal, intraorbital sciatic nerve transection model	Porcine fetal urinary bladder matrix	Pressed and lyophilized into a sheet. ETO sterilized	Mechanical and Detergent	8x	Nanopure water	30m	The method was done under a vacuum in a specially designed pressure chamber that cycled between ambient pressure and 0 psi at a rate of 1min/cycle. This wrap enhanced epi- and endoneurial organization and increased angiogenesis and growth associated protein-43 expression at peripheral nerve repair sites at 28 d post-surgery. However, the number of axons, myelination, and whisker-evoked functional responses were unaltered.	[151]
					3% Triton X-100	30m		
					3 M NaCl	30m		
					DNase	1h		
					0.1% Peracetic acid/ 4% ethanol	1h		
					1X PBS			
				3x	Nanopure water			

Table 7 (continued)

Rat sciatic nerve gap model	Rat sciatic nerve	N/A	Mechanical, Detergent, and Enzymatic	Method 1: Sondell method (control)				Histology showed lower immunogenicity for all three decellularized groups compared to native control, however the freeze-thaw combined with enzymatic degradation showed the lowest inflammatory response. This was marked by fewer inflammatory cells and less necrosis at the downstream muscle. In addition, the native and first two methods displayed expression of MHC-II antigen in the neural scaffolds while the freeze-thaw enzyme method did not. Furthermore, all three decellularization techniques had similar mechanical properties to the native nerve.	[147]
					distilled water	12h	yes		
				2x	3% Triton X-100	12h			
					4% Sodium deoxycholate	24h			
				Method 2: Low detergent method					
					ultrapure water	1h	yes		
					0.5% Triton X-100	48h	yes		
					ultrapure water	48h			
					DNase and RNase at 37°C	12h			
				Method 3: Freeze-thaw method					
					hypotonic solution at 4°C	12h			
					hypotonic solution at -80°C	6h			
					hypotonic solution at 37°C	30m			
	0.05% pancreatin	6h							
	DNase and RNase at 37°C	12h							
1.5 cm rat sciatic nerve defect model	Rat caudia equine	Decellularized cauda equina allograft embedded within chitosan conduit	Detergent	3x	1X PBS			Caudia equine does not possess an epineurium which the study hypothesized would allow for less harsh decellularization methods. The paper found that the caudia equine tissue required half the time (12h) in SDS to achieve similar decellularization results. This was combined with a chondroitin conduit and compared in vivo to conduit alone, acellular sciatic nerve, and autograft. Acellular sciatic nerve inferior to the acellular caudia equine embedded conduit in histologic, electrophysiologic, and functional metrics. The caudia equine conduit device performed similarly to the autologous nerve graft.	[139]
					0.5% SDS at 16°C	12h	40		
	10x			penicillin (100 U/mL) and streptomycin (0.1 mg/mL) in PBS					
				1X PBS	12h				
	Rat sciatic nerve			10x	1X PBS				

Table 7 (continued)

In vitro analysis	Porcine caudia equine	Homogenized caudia equine ECM combined with PLGA to form an electrospun scaffold	Detergent	distilled water			Method successfully removed genetic material and differential centrifugation was able to incorporate insoluble proteins of the caudia equine ECM into an aligned, electrospun PLGA material. This incorporation of ECM proteins enhanced neurite outgrowth of dorsal root ganglion cells compared to PLGA material alone.	[148]
				3% Triton X-100	2h	yes		
				4% Sodium deoxycholate	2h	yes		
				1X PBS rinse				
				Homogenized				
				Centrifugation steps to isolate ECM precipitate				
In vitro analysis	Rat sciatic nerves	Nerve ECM coated onto PCL based conduits	Detergent	distilled water	15m		Polydopamine (PDA) was coated onto polycaprolactone (PCL) conduits to successfully increase attachment of peripheral nerve ECM as a surface modification. This was shown to have potentially beneficial changes in Schwann cell behavior when cultured on the material in vitro.	[34]
				0.5% Triton X-100 in 1M NaCl distilled water	2h	yes		
				1% SDS in 1M NaCl distilled water, solution changed daily	2d	yes		
				0.1% peracetic acid and 4% EtOH in 1M NaCl	4h			
				distilled water	4h			
				lyophilized				
1.0 cm rat sciatic nerve defect model	Rat sciatic nerve	Acellular nerve graft augmented with additional NGF or GDNF	Mechanical and Enzymatic	3x	Liquid nitrogen	2m	This study compared the chondroitinase ABC treated acellular nerve grafts to those imbibed with NGF or GDNF. In vivo results showed that NGF significantly enhanced motor axon outgrowth into the graft during the first week and the number of myelinated axons present at 8 weeks. However, sensory nerve outgrowth was significantly stunted compared to control and GDNF groups. In vitro experiments with dorsal root ganglion outgrowth in the presence of chondroitinase ABC and NGF showed no effect on sensory neurite outgrowth. Authors suggest that NGF in the presence of chondroitinase ABC might promote apoptosis of the measured IB4-positive sensory neurons.	137]
					Thawed in water bath at 37°C	2m		
					2 U/mL chondroitinase ABC in PBS at 37°C	16h		
				2x	Rinsed in lactated Ringer solution			
					Incubated with NGF (10ug/mL) or GDNF (20 ug/mL) solution	1h		
					Rinsed in lactated Ringer solution			

Table 7 (continued)

Clinical study of trigeminal nerve repair	Human peripheral nerve	gamma irradiated	Detergent and Enzymatic	distilled water	7h		Rinker et al., 2017 reviewed 28 patients with digital nerve injuries that were treated with the Avance nerve graft from Axogen. Of these, 86% recovered meaningful function which matched historic data of autograft repair (60-80%). Isaacs & Safa, 2017 looked at a small number of patients that required large diameter repairs. If repaired with autograft, these 4-5 mm wide nerves might require a cabled repair to avoid limitations of large diameter grafts. This study examined clinical data to see if similar concerns exist when using the largest diameter Avance nerve allografts. The study suggests that the acellular graft does not have this same limitation as autograft, presenting similar motor and sensory recovery as the gold-standard. Finally, Yampolsky, Ziccardi, & Chuang, 2017 reviewed the data of the Avance graft being used in the reconstruction of <2 cm trigeminal nerve injuries. In this case, 15 of 16 patients regained sensory function.	[38, 39, 122, 138]
Clinical study of large diameter cable repairs				125 mM sulfobetaine-10	15h	yes		
Clinical study of digital nerve gaps >2.5cm				50 mM phosphate and 100mM sodium	15m			
				0.14% Triton X-200, 0.6 mM sulfobetaine-16, 10 mM phosphate and 50 mM sodium	24h	yes		
				3x 50 mM phosphate and 100mM sodium	5m			
				125 mM sulfobetaine-10	7h	yes		
				50 mM phosphate and 100mM sodium	15m			
				0.14% Triton X-200, 0.6 mM sulfobetaine-16, 10 mM phosphate and 50 mM sodium	15h			
				3x 50 mM phosphate and 100mM sodium	15m			
	Chondroitinase ABC 37°C							

Sondell M. et al. was one of the first investigators to decellularize peripheral nerve for use as an allograft. [121]Rat sciatic nerves were treated using Triton X-100 and SDC. (*Table 3*) This process was repeated once and then the graft was washed in distilled water and stored in PBS. Early understanding of peripheral nerve decellularization was enhanced by Hudson et al., who compared the effects of many different detergents on cellular clearance and ECM preservation. An anionic detergent, Triton X-200 was found to be the most effective decellularization agent and combined with two amphoteric detergents to further increase effectiveness [116, 149]. This method was more effective at decellularizing the peripheral nerve tissue while better preserving the ECM when compared to the Sondell et al. method. [115-117, 149]This foundation led to a wide range of work optimizing the methods, structure, and composition of decellularized nerve grafts.

Despite advantages of the detergents Hudson et al. method identified, variations of the Sondell et al. method using Triton X-100 and sodium deoxycholate are still investigated [52, 132, 148]. Sridharan et al. used a modified Sondell et al. method to decellularize rat sciatic nerves but imparted an axially aligned channel structure through controlled freezing [132]. The study hypothesized that native pore size of basal lamina tubes was not ideal for nerve regeneration and sought to increase the pore size to enhance axon penetration. They showed that their methods were able to effectively decellularize the tissue and significantly increased pore size and the channels remained axially aligned. Briefly, the sciatic nerves were placed into insulating molds and stood upright, perpendicular to the freeze-dryer plate. Freezing rate was controlled to a constant rate of 1 °C/min to a final temperature of -30 °C. This was held for 1 hr before warming to -10 °C to lyophilize for 24 hr. In vivo work has not been published, however in vitro work showed enhanced PC12 cell migration both in number and depth into the graft.

Remnant detergents can be cytotoxic to infiltrating cells, so investigators have tried reducing or removing the detergent load [118, 130, 131, 137, 147, 159]. Kim et al. devised a method that used minimal detergent concentrations to decellularize rat sciatic nerves [130]. This method decellularized the nerve to a similar degree to the Hudson method but displayed better ECM preservation. In a rat sciatic nerve gap model, the method without the detergents outperformed the Hudson method in nerve histomorphometry and muscle mass, but ultimately the nerve autograft controls showed greater recovery. Several decellularization methods have been developed that use no detergents to create acellular grafts [118, 130, 131, 137, 147, 159]. Both Wang et al. 2013 and Boyer et al. 2015 explored the use of mechanical and enzymatic decellularization method to replace detergent based methods. Wang et al. 2013 performed a signal freeze-thaw cycle and used DNase and RNase to finish the decellularization of rat sciatic nerves. This method produced less inflammation in vivo compared to the Sondell et al. method and a light detergent method which showed expression of MHC-II within the scaffolds [147]. To enhance removal of chondroitin sulfate proteoglycans, a known inhibitor of regrowth, Boyer et al. 2015 used a method that combined multiple freeze-thaw cycles with chondroitinase ABC. The reduction of chondroitin sulfate proteoglycan with chondroitinase ABC was shown to increase axon growth into critically long grafts [118]. Boyer et al. 2015 augmented the scaffold with NGF and found enhanced motor neuron survival and growth [137]. Cornelison R. C. et al. used camptothecin, hypertonic PBS solution, and 75 U/ml DNase to decellularize sciatic nerves without the use of detergents and using the Hudson method as a comparison [159]. Their apoptosis-assisted decellularization method was able to successfully decellularize the tissue while maintaining basal lamina microarchitecture while being less cytotoxic than detergent decellularization methods. The apoptosis-assisted method also produced less inflammatory

infiltrate and stromal remodeling compared to the autograft control. Vasudevan S. et al. developed a decellularization method that utilized a yet undescribed technique [131]. Rat sciatic nerves were cultured in DMEM with 10% fetal bovine serum and 2% penicillin/streptomycin/amphotericin for 2 weeks under constant agitation. After the 2-week culture period, the nerves were transferred to a new tube containing only PBS and kept for 1 week under constant agitation. The abrupt termination of nutrient supply was expected to aid in decellularization. In a rat sciatic nerve gap model, histologic results indicated that nerve autografts outperformed both the detergent-free and detergent decellularized grafts. Only nerve autograft and detergent free grafts showed functional recovery in muscle force testing.

Another approach to replacing the nerve autograft is nerve guidance conduits. While outcomes of current nerve guidance conduits are often inferior to the nerve autograft, researchers have investigated numerous approaches to improve these devices. The inclusion of ECM is one such strategy. This dissertation proposes the inclusion of a hydrogel from a decellularized sciatic nerve as a lumen filler for a nerve guidance conduit.

## **2.2 Methods**

### **2.2.1 Preparation of Peripheral Nerve ECM**

As most ECM scaffolds used in clinical settings are of a xenogeneic nature, and due to the amount of material required for processing, sciatic nerve tissue was originally harvested from an equine source for use in canine experiments. PNM was first developed using equine sciatic nerve harvested from healthy, adult horses euthanized for reasons unrelated to nerve injury or

neurological disease. These tissues were frozen for at least 16h at -80° C. The outer portion of the epineurium of the nerve was stripped by sharp dissection and mechanical delamination, leaving the nerve bundles intact. The tissue was then sectioned longitudinally and cut into lengths of less than 5 cm and quartered lengthwise prior to treatment.

Tissues were then processed using a modification of a protocol for spinal cord decellularization as previously described [107]. Briefly, the decellularization process consisted of a series of agitated washes: water (type 1, ultrapure, Milli-Q<sup>®</sup> purified water, 14 hours at 4° C), 0.02% trypsin (HyClone)/0.05% EDTA (Invitrogen, Waltham, MA USA) (60 minutes at 37° C), 3.0% Triton X-100 (Sigma, 60 min), water rinse (type 1, repeated until agitation no longer produced bubbles), 1M sucrose (Thermo Fisher, Waltham, MA USA, 15 min), 4.0% sodium deoxycholate (Sigma, St. Louis, MO, USA 60 min), 0.1% peracetic acid/4% ethanol (Sigma, 120 min), 1X PBS (15 min), water (14 hours), 1X PBS (15 min). Following treatment, samples were frozen (-80° C) and then lyophilized.

Further studies utilized both canine and porcine sciatic nerves also harvested following euthanasia of adult animals for reasons unrelated to nerve injury or neurological disease. These tissues were also frozen for at least 16 h at -80° C. The epineurium was left intact, but the nerves were halved longitudinally and segmented into smaller 0.5 cm sections. The same protocol as above was performed with the addition of another water rinse (type 1, repeated until agitation no longer produced bubbles) after the 4.0% sodium deoxycholate wash.

Enzymatic degradation products were generated from the above PNM and UBM scaffold materials as previously described [21]. Briefly, lyophilized scaffold materials were powdered and solubilized at a concentration of 20 mg/mL in a solution containing 2.0 mg/mL pepsin (Sigma) in 0.01 N HCl (ACROS organic) at a constant stir rate for 48h and then frozen for future use.

Finally, the porcine sciatic nerve was sourced from clinical grade, traceable, market-weight pigs (Tissue Source; LLC, Lafayette, IN). The tissue was then frozen for at least 16 h at -80° C. The tissue was quartered longitudinally and cut into sections of less than 5 cm. Decellularization was performed as previously described [162]. Enzymatic degradation products were produced from solid ECM scaffold material as previously described [162]. Enzymatic degradation products were aliquoted and lyophilized. Immediately before use, lyophilized degradation products were rehydrated using sterile water. Gelation was then initiated by adjusting the pH of the digest to 7.4 and 0.5X PBS concentration through the addition of 0.2 M NaOH and 10X PBS.

Comparisons were made with both canine and porcine ECM. Urinary bladder matrix (UBM) from a canine source and both UBM and small intestine submucosal matrix (SIS) from porcine sources were used as a control for characterization of decellularization and biochemical composition. Urinary bladder matrix was chosen as a control as it is a well characterized source for tissue decellularization, protocols resulting in effective decellularization have been established. Canine urinary bladder matrix was prepared as previously described [163]. Briefly, the tissue was bisected into a sheet and mechanically delaminated to remove the outer muscular layers, leaving the urothelial basement membrane and underlying connective tissue intact. The delaminated tissue was then subjected to washes in 0.1% peracetic acid/4% ethanol (Sigma, 120 min), 1X PBS (15 min), water (14 hours), 1X PBS (15 min). All tissues were then treated in a manner like that described for PNM. Porcine urinary bladder extracellular matrix (UBM) was also prepared using the previously described method [164].

### **2.2.2 Formation of Hydrogel from Enzymatic Degradation Products**

ECM hydrogels were formed from the degradation products as previously described [165]. Briefly, gelation was induced by adjusting the pH of the pepsin digest to 7.4 through the addition of one-tenth the digest volume of 0.1 M NaOH, one-ninth the digest volume of 10X PBS, and then diluting to the desired final ECM concentration in 1X PBS. Dilutions were performed on ice and the gel solution was placed in a non-humidified incubator at 37° C and allowed to gel for 1 h for benchtop confirmation of gelation. Concentrations between 8 and 15 mg/mL were examined visually for their ability to form a hydrogel. Hydrogels were prepared and evaluated under SEM using a standard preparation procedure and imaged at 4,000 magnification.

### **2.2.3 Confirmation of Decellularization**

Qualitative and quantitative assessments of cellular content was performed on all three tissue sources including histologic staining, immunofluorescent labeling, and dsDNA quantification. Fixation of lyophilized ECM scaffolds was performed in 10% neutral buffered formalin (Electron Microscopy Sciences, Hatfield, PA, USA). Samples were embedded in paraffin, sectioned, and stained with hematoxylin and eosin (H&E) or with 4',6-diamidino-2-phenylindole DAPI to verify removal of nuclei. Additional samples were stained using Luxol fast blue to determine removal of myelin as an additional metric of decellularization.

Qualitative assessment of DNA content was conducted by digesting the ECM scaffold in 0.1 mg/mL proteinase K solution (Invitrogen). Protein content was removed from the sample by repeated phenol/chloroform/isoamyl alcohol (Thermo Scientific) extraction and centrifugation (10,000 G) until no protein precipitate was observed at the interface. The aqueous layer was mixed

with 3 M sodium acetate (Fisher Scientific) and 100% ethanol. The solution was frozen using dried ice and centrifuged to produce a DNA pellet. The pellet was rinsed with 70% ethanol, centrifuged (10,000 G), and dried. Double-stranded DNA was then quantified using Quant-iT™ PicoGreen dsDNA assay kit (Life Technologies) following kit instructions. Statistical significance was assessed using one-way ANOVA with Tukey post-hoc test. Additionally, agarose gel electrophoresis was performed to assess base pair length of any remaining DNA.

#### **2.2.4 Assessment of Extracellular Matrix Ultrastructure and Components**

Maintenance of tissue-specific extracellular matrix components was assessed using histologic staining, immunolabeling, and scanning electron microscopy (SEM). Scaffold materials were fixed in 10% neutral buffered formalin, embedded in paraffin and sectioned at 5 µm. Immunolabeling was performed with antibodies specific to ECM components (collagen I, III, and IV). Briefly, after deparaffination, all slides were subjected to antigen retrieval by immersion in 95°C–100° C in citric acid solution (Acros Organics, Waltham, MA USA, 10 mM, pH 6.0; 20 min) followed by rinsing in a 1X Tris buffered saline/Tween-20 solution (0.1% Tween 20, Fisher Scientific, v/v, pH 7.4; 3 washes, 5 minutes each). Samples were then washed in PBS and treated with a pepsin digestion (0.05% pepsin, Sigma, w/v in 10 mM HCl, 15 minutes at 37° C. solution for further antigen retrieval. Samples were blocked against nonspecific binding using a solution consisting of 2% horse serum, 1% bovine serum albumin, 0.1% Tween-20, and 0.1% Triton X-100 in PBS for 30 minutes at room temperature. Primary antibodies for collagen I, III, and IV (Sigma, 1:200) were applied to sections overnight at 4° C. Samples were washed in PBS and appropriate fluorescently labeled secondary antibodies (AlexaFluor 488, 1:250) were applied for 60 minutes at room temperature.

For SEM, lyophilized samples were fixed in cold 2.5% (v/v) glutaraldehyde and processed using an established method [164]. The dried samples were mounted onto aluminum stubs and sputter coated with a 3.5 nm layer of gold–palladium alloy prior to imaging

Quantitative assessment of collagen (hydroxyproline) and GAG content was performed through spectrophotometric assays. 100 mg of dry tissue was digested overnight at 60° C in 0.125 mg/ml papain (Sigma) in phosphate buffer with 0.01 M EDTA and 0.01 M cysteine (Sigma). Afterwards, GAG content was assessed by mixing aliquots of the resultant digest with the dye 1,9-dimethylmethylene blue (Fisher Scientific) and reading the absorption of a 525 nm wavelength. Hydroxyproline content was analyzed as per a published protocol [166].

The concentrations of nerve growth factor (NGF) and ciliary neurotrophic factor (CNTF) in NP40-glycerol extracts (20 mM Tris containing 1.0% NP40, 10% glycerol, and protease inhibitors) of native nerve, PNM, and UBM were determined using human  $\beta$ -NGF and human CNTF ELISA kits (Sigma). These ELISA assays are cross-reactive with porcine and equine growth factors and indicative of concentration but not activity. Assessment of growth factor composition was performed only on PNM harvested from equine sources; however, all other assessments were performed on both canine and equine PNM samples.

### **2.2.5 Mechanical and Morphologic Aspects of the Resultant Hydrogels**

For scanning electron microscopy (SEM), lyophilized samples were fixed in cold 2.5% (v/v) glutaraldehyde and processed using a standard SEM preparation procedure. The dried samples were mounted onto aluminum stubs and sputter coated with a 3.5 nm layer of gold–palladium alloy prior to imaging.

To test the mechanical properties of the resultant PNM hydrogel an AR2000 dynamic rheometer was used to measure gelation time and shear storage ( $G'$ ) and loss moduli ( $G''$ ). The concentration of PNM reconstituted into a hydrogel was varied (8, 10, 15 and 20 mg/mL). Measurements were acquired using a time sweep with a frequency of 0.1 Rad and using a 40mm plate with a 0.5 mm gap over 2000 sec. A frequency sweep between 5 and 0.1 will also performed.

## **2.3 Results**

### **2.3.1 Confirmation of Decellularization**

#### **2.3.1.1 Equine Sciatic Nerve Decellularization**

Following decellularization, Decellularized canine sciatic nerve shows significant removal of nuclei through H&E staining (Figure 3A) compared to native sciatic tissue (Figure 3B). No nuclei were visible in hematoxylin and eosin (H&E) stained sections under light microscopy (Figure 3A-B). DAPI stain in decellularized (Figure 3C) and native (Figure 3D) shows similar results with a small number of disrupted nuclei remaining. In some samples, a small number of nuclei (2-3

nuclei/40X field) were observed when labeled with DAPI (Figure 3E-F). When present, retained nuclei were observed within the central most nerve fascicles relative to the whole nerve tissue or within the dense perineurium of the treated tissues.

DNA remaining in the scaffold is highly fragmented ( $< 400\text{bp}$ ) (Figure 3E). Quant-iT™ PicoGreen assay for dsDNA content shows dsDNA content of the decellularized tissue of PNM was significantly decreased as compared to native tissue ( $p < 0.05$ ,  $n = 5$ ) (4F). dsDNA content was decreased by approximately 85% in the decellularized tissue ( $158.1 \pm 34.5 \text{ ng/mg}$ ) compared to native tissue ( $1,043.6 \pm 291.2 \text{ ng/mg}$ ) (Figure 3F). Error bars denote standard deviation. These values are consistent with those reported for multiple FDA approved, commercially available ECM scaffold materials [29].

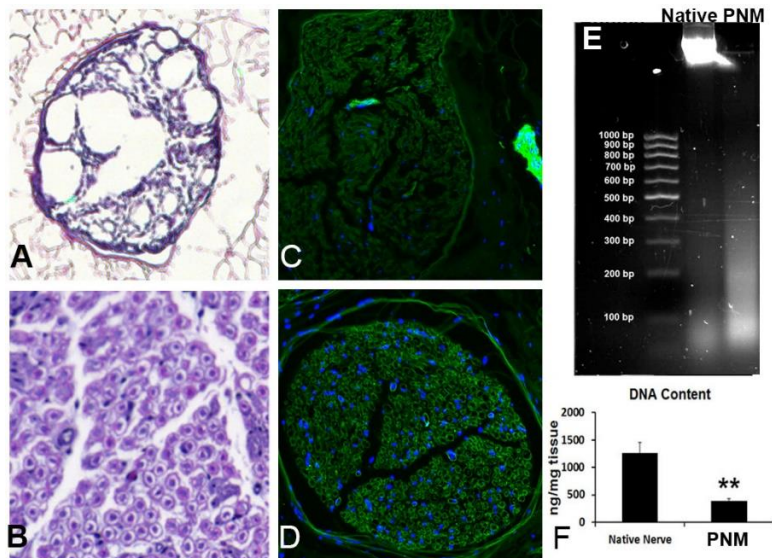


**Figure 3: Confirmation of decellularization for an equine sciatic nerve**

### 2.3.1.2 Canine sciatic nerve decellularization

Decellularized canine sciatic nerve shows significant removal of nuclei through H&E staining (Figure 4A) compared to native sciatic tissue (Figure 4B). Following decellularization of canine sciatic nerve, few nuclei were visible in hematoxylin and eosin (H&E) stained sections under light microscopy (Figure 4A–B). DAPI stain in decellularized (Figure 4C) and native (Figure 4D) shows similar results with a small number of disrupted nuclei remaining. In some samples, a small number of nuclei (5–10 nuclei/20X field) were observed when labeled with DAPI (Figure 4C–D). When present, retained nuclei were observed within the central most nerve fascicles relative to the whole nerve tissue or within the dense perineurium of the treated tissues. Luxol Fast Blue staining was used to assess myelin content in decellularized (Figure 4E) and native (Figure 4F) sciatic nerve. Myelin, a potentially immunogenic axonal component [167], was reduced within the endoneurial tissue compared to dark circles of myelin in native tissue after decellularization process (Figure 4E–F).

PicoGreen assay for DNA content shows dsDNA content of the decellularized tissue of both PNM and urinary bladder matrix was significantly decreased as compared to native tissues ( $p < 0.05$ ,  $n = 5$ ) (Figure 4G). The dsDNA that remains within PNM was highly fragmented ( $< 400\text{bp}$ ) compared to dsDNA extracted from native tissue (Figure 4H). The dsDNA content was decreased by approximately 85% in the decellularized tissue ( $158.1 \pm 34.5 \text{ ng/mg}$ ) compared to native tissue ( $1,043.6 \pm 291.2 \text{ ng/mg}$ ) (Figure 4G). These values are consistent with those reported for multiple FDA approved, commercially available ECM scaffold materials [168].

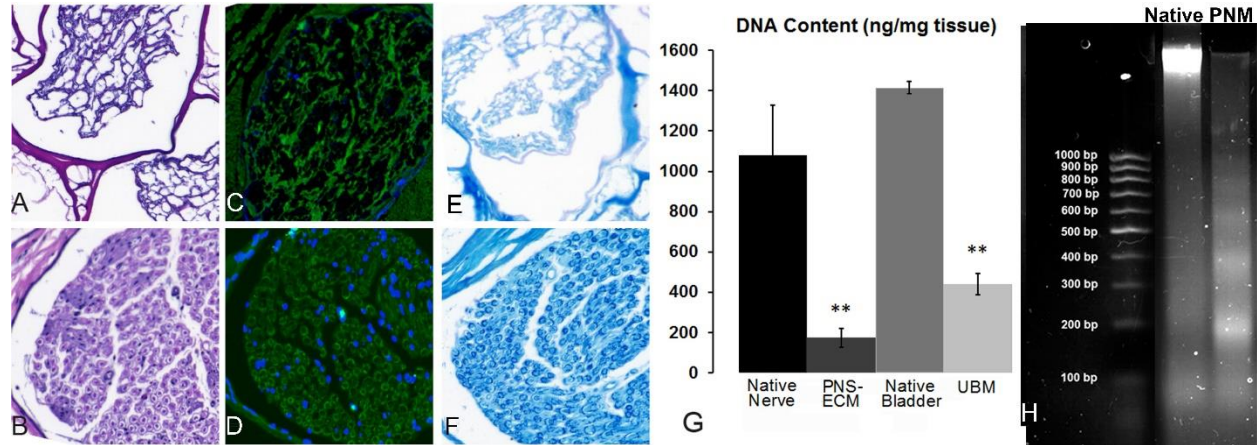


**Figure 4: Confirmation of decellularization of a canine sciatic nerve**

Decellularized canine sciatic nerve shows significant removal of nuclei through H&E staining (A) compared to native sciatic tissue (B). DAPI stain in decellularized (C) and native (D) shows similar results with a small number of disrupted nuclei remaining. Luxol Fast Blue staining myelin dark blue is reduced after decellularization (E) within the endoneurial tissue compared to dark circles of myelin in native tissue (F). (G) PicoGreen assay for DNA content shows dsDNA content of the decellularized tissue of both PNM and urinary bladder matrix was significantly decreased as compared to native tissues (\*\*,  $p < 0.05$ ,  $n = 5$ ). (H) The dsDNA that remains within PNM was highly fragmented ( $< 100$ bp) compared to dsDNA extracted from native tissue. Reused with permission (4546560968632). [52]

### 2.3.1.3 Porcine sciatic nerve decellularization

Decellularization was confirmed qualitatively through DAPI staining and SEM imaging (Figure 5A-D). DAPI stain for nuclei in native (Figure 5A) and decellularized sections (Figure 5B) of sciatic nerve. DAPI staining showed a full reduction in whole nuclei within the solid nerve scaffold (Figure 5A, B). SEM images shows dense tissue both between and within individual

fascicles before decellularization (Figure 5C). After decellularization, the tissue is porous with tubules where the axons previously resided. The original structures, including endoneurium and perineurium are well preserved within the scaffold (Figure 5D). Quantitative results showed effective removal of cellular content and high degree of fragmentation after decellularization (Figure 5E, F). Gel electrophoresis shows highly fragmented remnant DNA after decellularization with the majority below 400bp (Figure 5E) Quant-iT™ PicoGreen assay for dsDNA showed a statistically significant ( $p < 0.01$ ) reduction of 84% in residual dsDNA after decellularization (Figure 5F). Error bars show standard deviation of a  $n = 5$ .

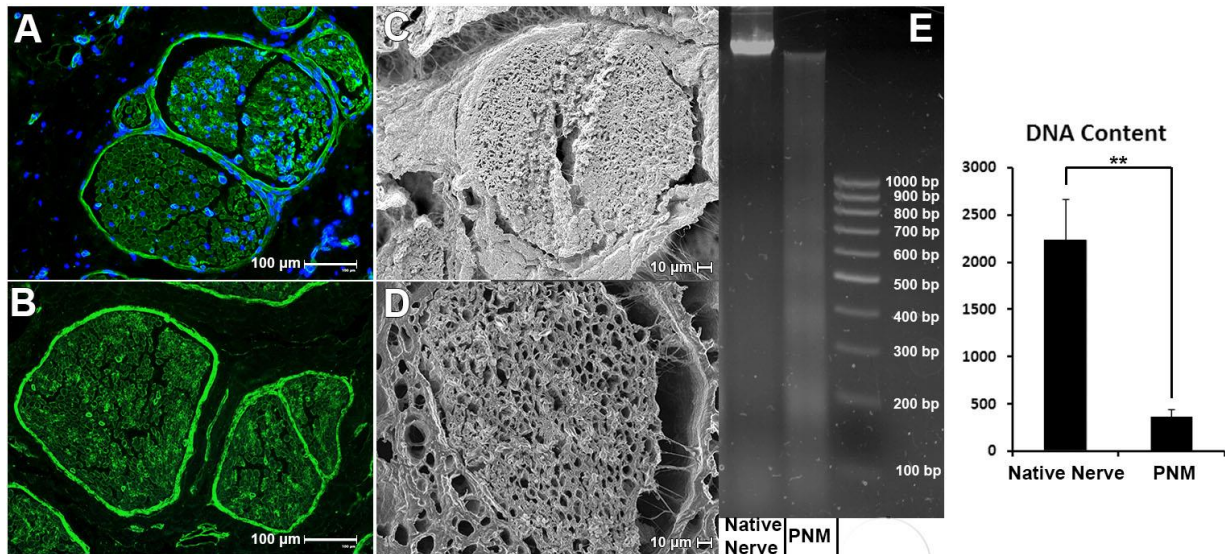


**Figure 5: Conformation of decellularization of a porcine sciatic nerve**

Qualitative assessment of decellularization was confirmed through DAPI staining of native (A) and decellularized (B) as well as SEM imaging of native (C) and decellularized (D). Gel electrophoresis was performed to assess dsDNA fragmentation (E). The dsDNA that remains

within PNM was highly fragmented (<100bp) compared to dsDNA extracted from native tissue.

(F) PicoGreen assay for DNA content shows dsDNA content of the decellularized tissue of PNM was significantly decreased as compared to native tissues (\*\*,  $p < 0.05$ ,  $n = 5$ ).

## 2.3.2 Maintenance of Extracellular Matrix Ultrastructure and Components

### 2.3.2.1 Equine Sciatic Nerve Decellularization

Biochemical testing was performed to assess the quantity of basic ECM components including hydroxyproline and GAG as well as nerve-specific growth factors including ciliary neurotrophic factor (CNTF) and nerve growth factor (NGF). Hydroxyproline content increased from  $34.9 \pm 9.1 \mu\text{g}/\text{mg}$  in native nerve tissue to  $65.0 \pm 9.4 \mu\text{g}/\text{mg}$  after decellularization ( $p = 0.027$ ). PNM was observed to contain less hydroxyproline than UBM ( $65.0 \pm 9.4 \mu\text{g}/\text{mg}$ ) ( $p = 0.001$ ) (Figure 6A). GAG content decreased with decellularization (native  $51.3 \pm 8.0 \mu\text{g}/\text{mg}$  to  $31.0 \pm 16.7 \mu\text{g}/\text{mg}$ ). Homogeneity of variances was violated; therefore, a Games-Howell post-hoc test was used to reveal a difference between native nerve and UBM ( $p = 0.001$ ) but no significant difference between PNM and native nerve ( $p = 0.15$ ) or UBM ( $p = 0.33$ ) (Figure 6B). Levels of NGF in PNM ( $177.0 \pm 33.2 \text{ pg}/\text{g}$ ) were retained at 26% of the native nerve ( $680.9 \pm 160.8 \text{ pg}/\text{g}$ ) after decellularization ( $p < 0.001$ ). Despite a non-nerve tissue origin, UBM was observed to have a similar amount of NGF ( $161.0 \pm 38.5 \text{ pg}/\text{g}$ ) as PNM ( $p = 0.953$ ) (Figure 6C). After decellularization, 50% of CNTF was preserved from native nervous tissue ( $457.5 \pm 60.9 \text{ pg}/\text{g}$ ) to PNM ( $228.2 \pm 38.4 \text{ pg}/\text{g}$ ) ( $p < 0.001$ ). A comparable amount of CNTF was found in UBM ( $301.6 \pm 58.3 \text{ pg}/\text{g}$ ) ( $p = 0.953$ ) (Figure 6D). Differing letters denote statistical significance ( $p < 0.05$ ) and error bars show standard deviation.

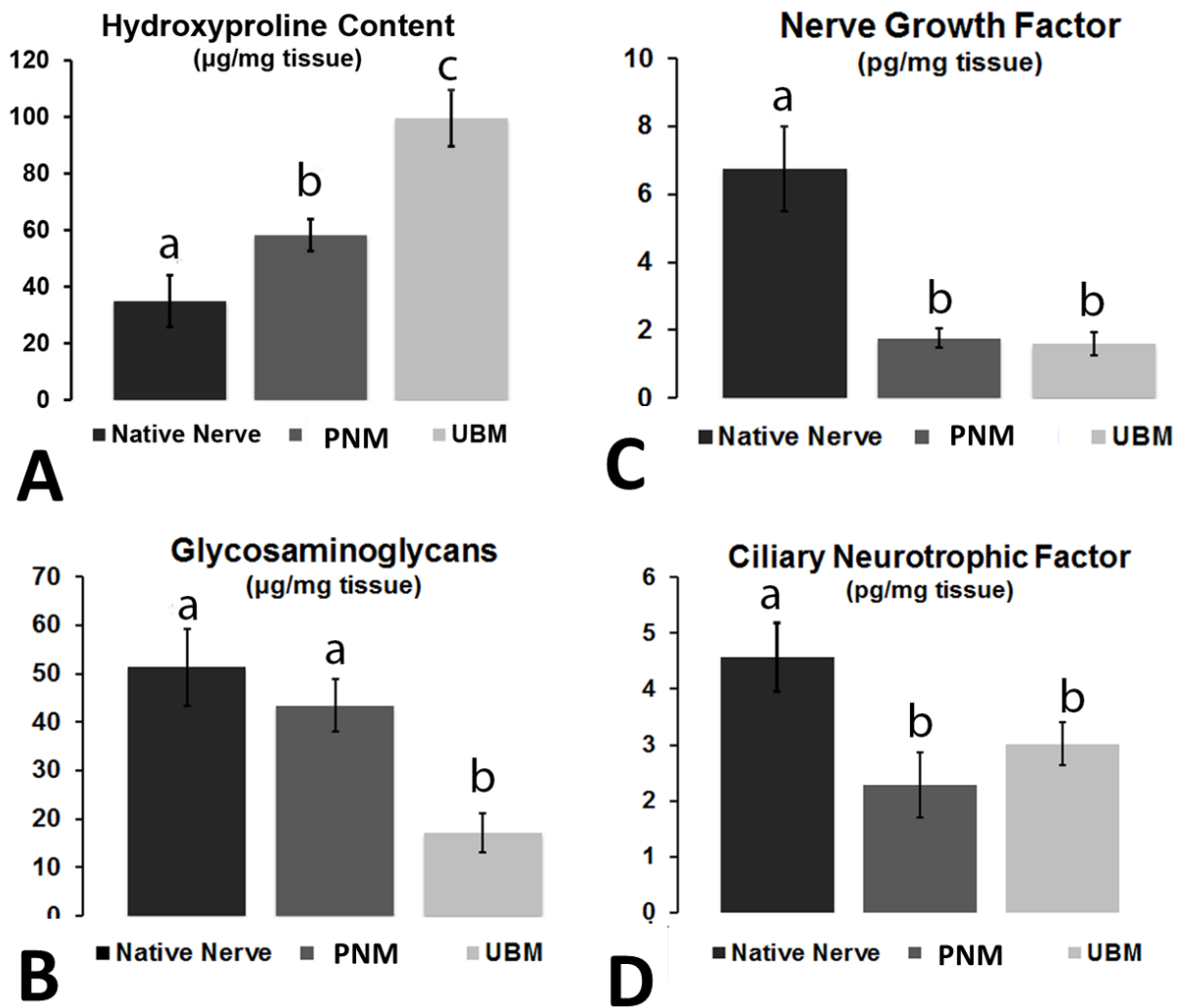


**Figure 6: Composition analysis of equine sciatic nerve**

Quantification of hydroxyproline, glycosaminoglycan, nerve growth factor, and ciliary neurotrophic factor content in equine sciatic nerves. (A) Relative hydroxyproline content, a proxy for collagen content, was found to increase after decellularization. This could be caused by an overall reduction of cells within the tissue. PNM was observed to have less hydroxyproline than UBM. (B) Glycosaminoglycan content did not change after decellularization and content was

greater than seen in UBM. (C-D) Nerve specific growth factors were significantly reduced by decellularization and were similar between PNM and UBM. Differing letters denote statistical significance ( $p < 0.05$ ) and error bars show standard deviation.

### **2.3.3 Canine Sciatic Nerve Decellularization**

Individual components of the ECM were examined through immunofluorescent staining of collagen I, collagen III, and collagen IV before and after decellularization (Figure 7A-F). Collagen I was seen both within the endoneurial and epineurial space before decellularization (Figure 7A) but was reduced by decellularization (Figure 7B). Little positive staining of collagen III was seen in both native (Figure 7C) and decellularized (Figure 7D) sciatic nerve tissue sections. Maintenance of the basal lamina was investigated through staining of collagen IV, a major constituent of the basal lamina. While immunofluorescent labeling showed that the content and organization of collagen I and III was affected by decellularization (Figure 7A-D), collagen IV within individual nerve bundles was strongly preserved (Figure 7E-F). Strong positive staining within the decellularized samples both within the endoneurial basal lamina and within the perineurium (Figure 7E-F) with a similar pattern of staining between the decellularized and native samples, suggests a strongly preserved basal lamina structure. The intensity of the staining within the endoneurium, however, was less than the perineurium and the architecture was slightly disrupted as compared to native tissue.

Low (Figure 7G, H) and high (Figure 7I, J) magnification scanning electron microscopy (SEM) images of native and decellularized sciatic nerve. Cross-sectioned native (Figure 7G) and decellularized (Figure 7H) tissue at 150X magnification shows a dense epineurial space that it is largely cleared by decellularization but perineurium and endoneurium structure largely

maintained. Enhanced magnification (1000X) of the same samples, native (Figure 7I) and decellularized (Figure 7J) endoneurial tissue. Images show the presence (Figure 7I) and removal of (Figure 7J) axons within the endoneurium. Biochemical assays for hydroxyproline (Figure 7K) and glycosaminoglycans (GAG) (Figure 7L) did not reveal any significant changes to either component after peripheral nerve decellularization ( $p = 0.57$   $n = 5$ ,  $p = 0.26$   $n = 5$ ). These components were compared to urinary bladder matrix (UBM) which had significantly more hydroxyproline ( $p = 0.001$ ) (Figure 7K) but significantly less GAG ( $p = 0.001$ , Figure 7L) than PNM and native nerve. Different letters denote a significant difference ( $p < 0.05$ ).

The solubilized PNM can be reconstituted into a stable hydrogel at concentrations as low as 8 mg/ml. This was visually confirmed by depositing the neutralized PNM solution within a stainless-steel ring and incubating at 37° C for 30 min (Figure 7M). Under SEM, the hydrogel was characterized by a highly porous network of fibular proteins (Figure 7N). Image shows macroscopic (Figure 7M) and SEM image (Figure 7N) of an 8 mg/ml equine PNM hydrogel

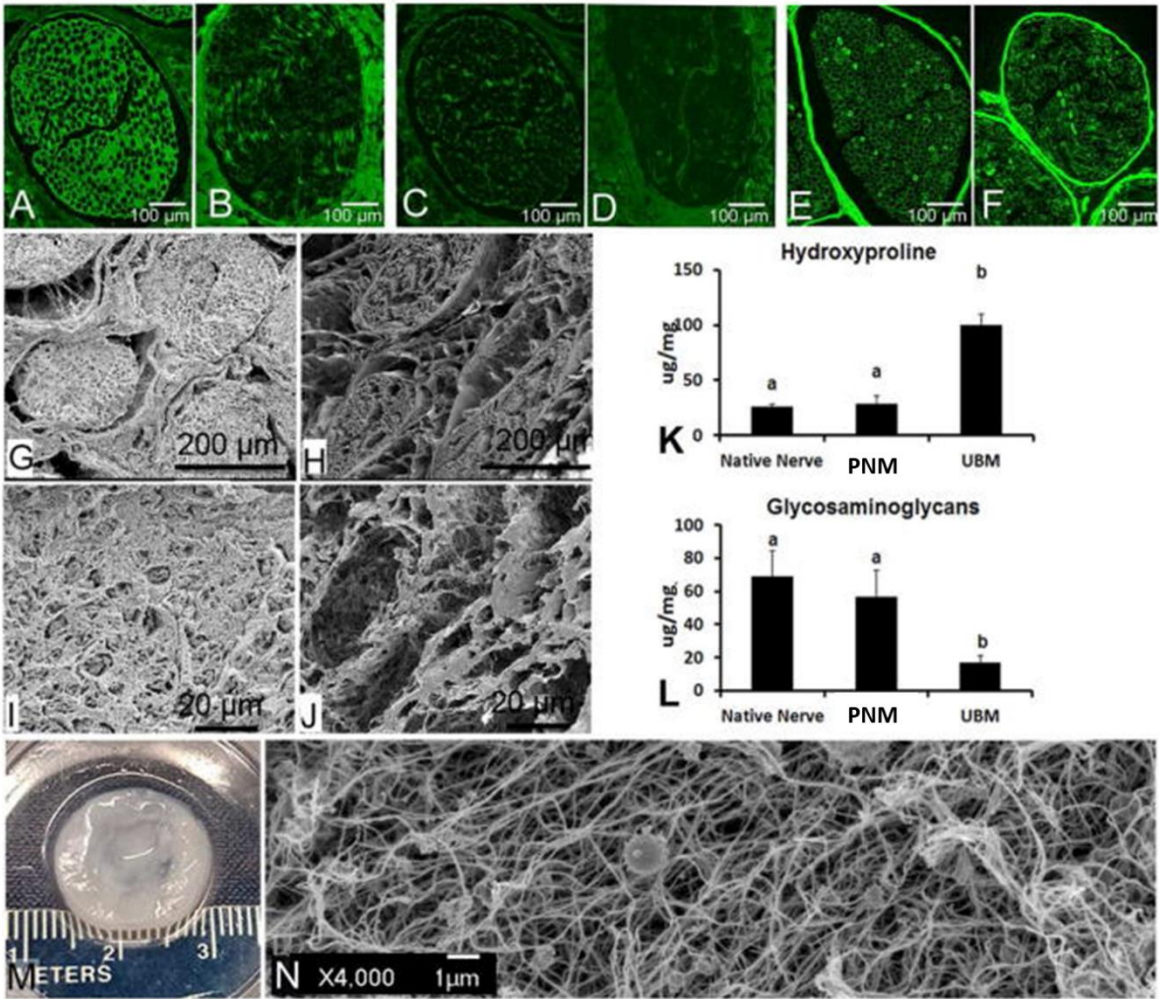


**Figure 7: Characterization of remaining content within canine sciatic nerve after decellularization**

(A–F) Immunofluorescent staining of collagen I, collagen III, and collagen IV before and after decellularization. Collagen I was seen both within the endoneurial and epineurial space before decellularization (A) but was reduced by decellularization (B). Little positive staining of collagen III was seen in both native (C) and decellularized (D) sciatic nerve tissue sections. Collagen IV, a major component of the basal lamina had strong staining around the individual nerve fibers, in the endoneurial space, and in the perineurium in native nerve (E). The same pattern of collagen IV

staining was seen in the decellularized nerve tissue (F) suggesting a preservation of the basal lamina. (G, H) Low and (I, J) high magnification scanning electron microscopy (SEM) images of native and decellularized sciatic nerve. Cross-sectioned native (G) and decellularized (H) tissue at 150X magnification shows a dense epineurial space that it is largely cleared by decellularization but perineurium and endoneurium structure largely maintained. Enhanced magnification (1000X) of the same samples, native (I) and decellularized (J) endoneurial tissue. Images show the presence (I) and removal of (J) axons within the endoneurium. Biochemical assays for hydroxyproline (K) and glycosaminoglycans (GAG) (L) did not reveal any significant changes to either component after peripheral nerve decellularization ( $p=0.57$   $n=5$ ,  $p=0.26$   $n=5$ ). These components were compared to urinary bladder matrix (UBM) which had significantly more hydroxyproline but significantly less GAG than PNM and native nerve. Different letters denote a significant difference ( $p<0.05$ ). Image shows macroscopic (E) and SEM image (F) of an 8 mg/ml equine PNS-ECM hydrogel. Reused with permission (4546560968632). [52]

### **2.3.3.1 Porcine sciatic nerve decellularization**

The qualitative presence of tissue-specific extracellular matrix components was confirmed using immunofluorescent staining methods. Samples were stained with antibodies specific to collagen I, III, IV and laminin. Native and decellularized porcine nerve sections on the top and bottom rows respectively stained for collagen I (Figure 8A, B), collagen III (Figure 8C, D), collagen IV (Figure 8E, F), and laminin (Figure 8G, H). Collagen I was seen predominately within the epineurial space around the nerve bundles before decellularization ( 8A) but was completely reduced by decellularization (Figure 78B). Little positive staining of collagen III was seen in both

native ( 8C) and decellularized ( 8D) sciatic nerve tissue sections. Maintenance of the basal lamina was investigated through staining of collagen IV and laminin, a major constituent of the basal lamina. While immunofluorescent labeling showed that the content and organization of collagen I and III was affected by decellularization ( 8A–D), collagen IV and laminin within individual nerve bundles was strongly preserved ( 8E–H). Strong positive staining within the decellularized samples both within the endoneurial basal lamina and within the perineurium ( 8E–F) with a similar pattern of staining between the decellularized and native samples, suggests a strongly preserved basal lamina structure

Quantitative assessment of ECM components hydroxyproline (Figure 8I) and glycosaminoglycans was determined through direct spectrophotometric assays (Figure 8J). No significant differences were observed in either hydroxyproline or glycosaminoglycan content between native and decellularized porcine sciatic nerve tissues.

Assessment of nerve specific growth factors including brain derived neurotrophic factor (BDNF) ( 9A), neurotrophic factor 3 (NT-3) ( 9B), ciliary neurotrophic factor (CNTF) ( 9C), and nerve growth factor (NGF) ( 9D) in PNM as compared to native tissues and decellularized tissues from other anatomic locations (UBM- urinary bladder, SIS- small intestine submucosa) was assessed using ELISA kits. Some similarities between PNM and both SIS and UBM were observed. PNM had similar levels as SIS of BDNF and similar levels to UBM for NGF. In addition to these similarities, both SIS and UBM showed significantly higher concentrations of NT-3 ( $p < 0.05$ ,  $n = 5$ ). However, in all four nerve-specific growth factors surveyed PNM most closely matched the normal profile of the native nerve source. This suggests that PNM might more closely match the overall growth factor profile of normal nerve tissue.

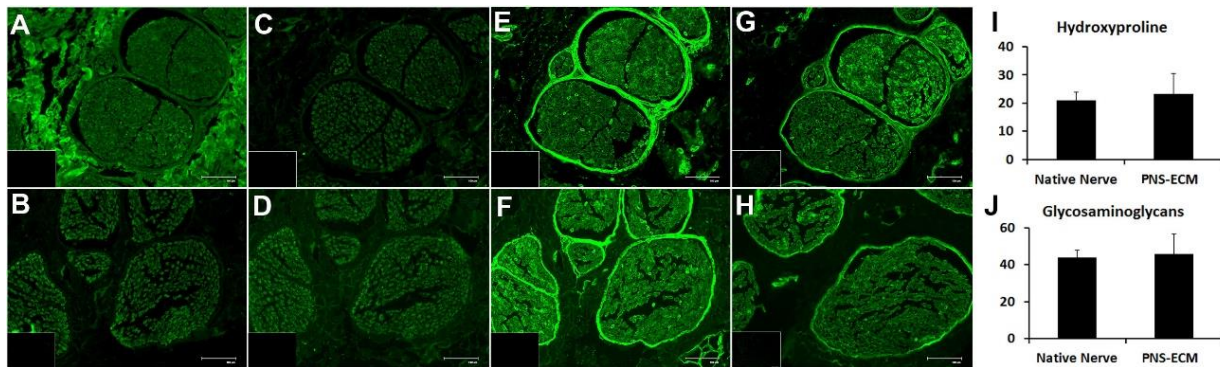


**Figure 8: Structural ECM components of porcine sciatic nerve**

(A–F) Immunofluorescent staining of collagen I, collagen III, collagen IV, and laminin before and after decellularization. Collagen I was seen both within the endoneurial and epineurial space before decellularization (A) but was reduced by decellularization (B). Little positive staining of collagen III was seen in both native (C) and decellularized (D) sciatic nerve tissue sections. Collagen IV, a major component of the basal lamina had strong staining around the individual nerve fibers, in the endoneurial space, and in the perineurium in native nerve (E). The same pattern of collagen IV and laminin staining was seen in the decellularized nerve tissue (F) suggesting a preservation of the basal lamina. Biochemical assays for hydroxyproline (I) and glycosaminoglycans (GAG) (J) did not reveal any significant changes to either component after peripheral nerve decellularization ( $p=0.6$   $n=5$ ,  $p=0.4$   $n=5$ ).

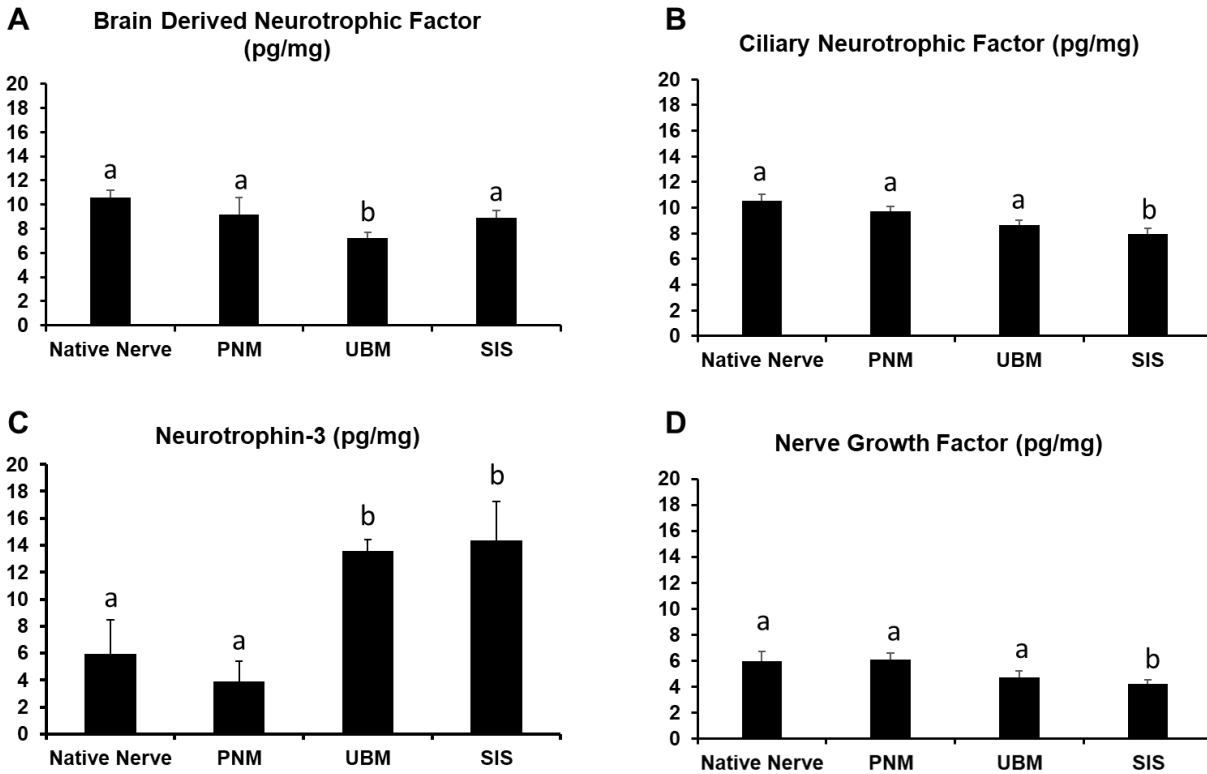


**Figure 9: Bioactive components in porcine PNM**

Assessment of nerve specific growth factors including brain derived neurotrophic factor (BDNF)(A), neurotrophic factor 3 (NT-3) (B), ciliary neurotrophic factor (CNTF)(C), and nerve growth factor (NGF)(D) in PNM as compared to native tissues and decellularized tissues from other anatomic locations (UBM- urinary bladder, SIS- small intestine). PNM was found to have similar levels of nerve specific growth factors including brain derived neurotrophic factor (BDNF)(A), neurotrophic factor 3 (NT-3)(B), ciliary neurotrophic factor (CNTF)(C), and nerve growth factor (NGF)(D) as compared to native tissues, but significantly increased levels as compared to decellularized tissues from other anatomic locations (UBM- urinary bladder, SIS- small intestine).

### **2.3.4 Maintenance of Extracellular Matrix Ultrastructure and Components**

Maintenance of the basal lamina was investigated through staining of collagen IV, a major constituent of the basal lamina. While immunofluorescent labeling showed that the content and organization of collagen I and III was affected by decellularization (Figure 8A-D), collagen IV within individual nerve bundles was strongly preserved (Figure 8E-H). Strong positive staining within the decellularized samples both within the endoneurial basal lamina and within the perineurium (Figure 8E-H), suggests a strongly preserved basal lamina structure. The intensity of the staining within the endoneurium, however, was less than the perineurium and the architecture was slightly disrupted as compared to native tissue.

PNM was found to have similar levels of nerve specific growth factors including brain derived neurotrophic factor (BDNF) (Figure 9A), neurotrophic factor 3 (NT-3) (Figure 9B), ciliary neurotrophic factor (CNTF) (Figure 9C), and nerve growth factor (NGF) (Figure 9D) as compared to native tissues. In most cases, PNM had significantly increased levels as compared to decellularized tissues from other anatomic locations (UBM- urinary bladder, SIS- small intestine) except for NT-3 where both native nerve and PNM had significantly less than UBM and SIS.

### **2.3.5 Assessment of Mechanical and Morphometric Characteristics of Resultant PNM**

#### **Hydrogel**

The hydrogel was formed by returning the digested ECM to a pH of 7.4 and raising the temperature to 37 ° C. A time sweep was run showing gelation within 10 minutes and a maximum storage modulus of 70 Pa ( 10A, B). Analysis of morphometric properties of the gel showed minimal difference in fibrinous connections and porosity with changing concentration ( 10C, D). Examples

of the PNM hydrogel at 8, 10, and 15 mg/mL can be seen in 10E. A max of 70 Pa was a very weak hydrogel that may not hold up to surgical conditions. However, based on literature nervous tissue prefers weaker materials. Study suggest that scaffolds stiffer than 500 Pa limit neurite growth [169]. Therefore, our goal was to tailor the PNM hydrogel to a stiffness between 100-200 Pa. This would still be a soft matrix that neurons prefer but stable enough for clinical use.

Based on previously published work on ECM hydrogels, we were able to alter mechanical properties of the hydrogel by changing salt concentrations [170]. We found that lowering the ionic concentration to 0.5X PBS significantly increased the storage modulus of the PNM hydrogel (\*,  $p < 0.05$ , 11A, B). When the ionic concentration was again tested with multiple concentrations, we found that PNM hydrogels at 15 and 20 mg/mL fell within our desired range ( 12A, B). In addition, results suggest that the current PNM hydrogel has an upper stiffness of ~150 Pa as increasing concentration did not increase stiffness above 15 mg/mL.

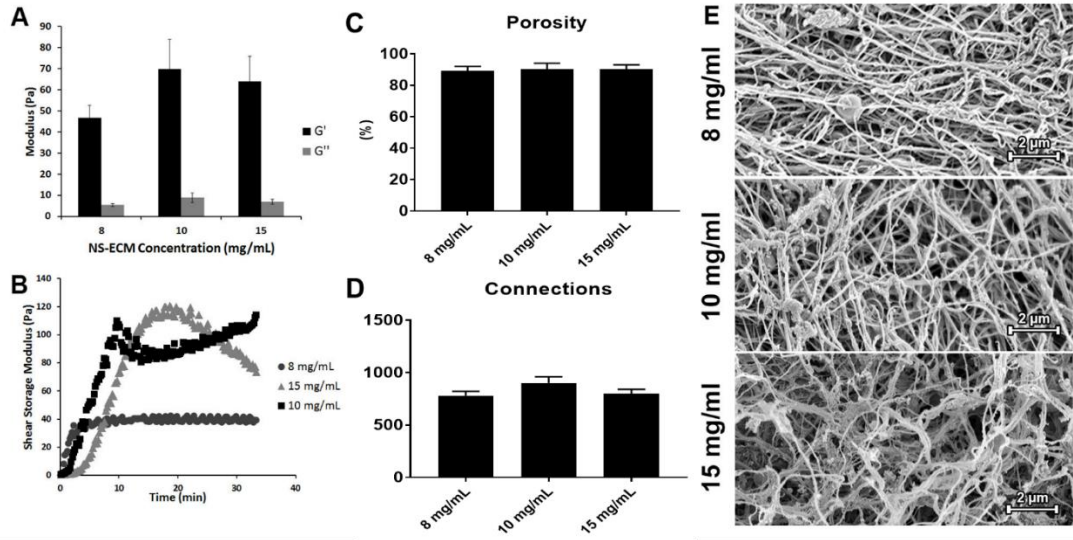


**Figure 10: Mechanical and morphometric properties of canine PNM hydrogel**

(A) Rheometry of PNM hydrogel at 8, 10, and 15 mg/mL. No significant differences were observed but batch to batch variability of early samples increased experiment variability (n=5). (B) Sample trace of a single rheometry run of the 8, 10, and 15 mg/mL PNM hydrogel. The 10 mg/mL hydrogel reaches peak storage modulus by 10 minutes. (C-D) SEM images of the PNM hydrogels were assessed for porosity and fibrillar connections but no differences were observed. (E) Sample SEM images of the PNM hydrogel at 8, 10, and 15 mg/mL.

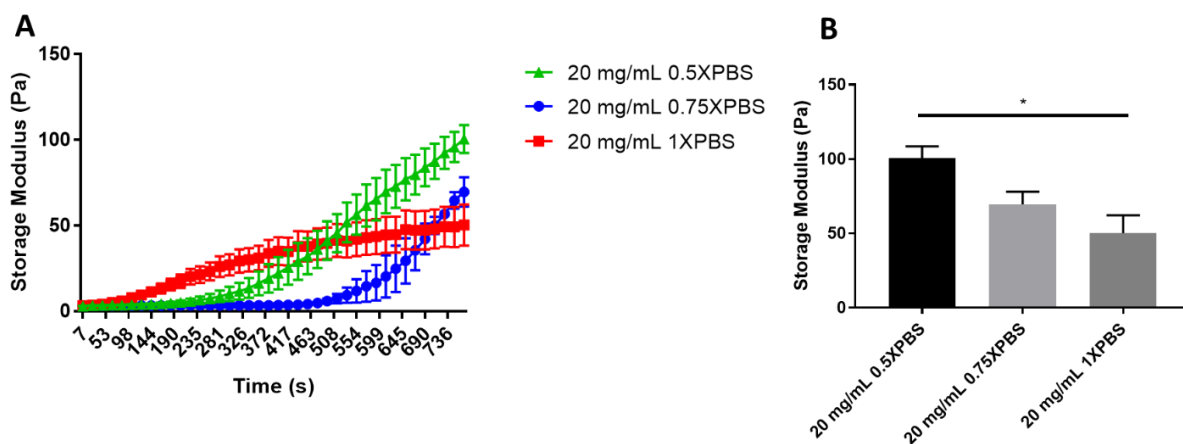


**Figure 11: Varying salt concentration changes mechanical properties of porcine PNM hydrogel**

(A) Sample trace of a single rheometry test of a 20 mg/mL porcine PNM hydrogel with varied ionic strength. (B) Reducing ionic strength by using 0.5X PBS produced the most stable hydrogel.

(\* ,  $p < 0.05$ ,  $n = 5$ )

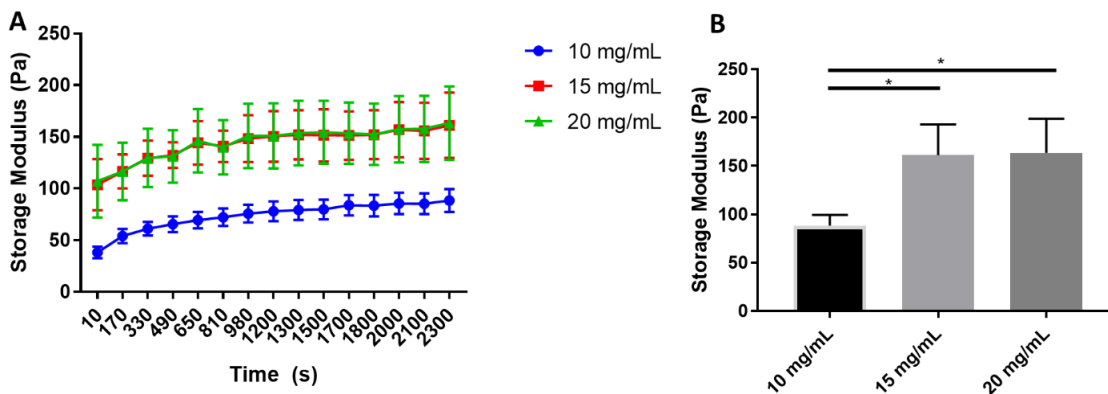


**Figure 12: Porcine PNM hydrogel shows a maximal storage modulus**

(A) Sample trace of a single rheometry test using 0.5X PBS at 10, 15, and 20 mg/mL using porcine PNM. (B) Storage modulus increases between 10 to 15 mg/mL but did not increase from 15 to 20 mg/mL. (\*,  $p < 0.05$ ,  $n = 5$ )

### 2.3.6 Defining Best Practices for Injectable Hydrogel

PNM was previously observed to form a stable hydrogel *in vitro* between concentration of 8-15 mg/mL. PNM was then assessed for the ability to form a hydrogel *in vivo*. The PNM hydrogel was tested in a rat model of sciatic nerve defect and repair. A silicone conduit was filled with the PNM hydrogel at 10mg/ml as a lumen filler and removed after 1 hour. Different sized conduits were tested as well as different methods of injecting and gelating the PNM to define best practices for delivering the hydrogel. A larger conduit with an inner diameter of 2.5 mm, approximately 0.5 mm larger than the sciatic nerve was tested first. The hydrogel was first injected into the conduit

and allowed to gel in a non-humidified incubator at 37° C before implantation ( 13A). Most of gel was lost during manipulation of conduit into place. The conduit was not refilled, and the hydrogel was not present at all after 1 hour ( 13B). The same conduit was tested but implanted before injecting the PNM digest ( 13C). The hydrogel was slowly leaking out and was down to 50% during muscle suturing. Only a small gel plug remained after 1 hour ( 13D). The same process was repeated with a conduit with an inner diameter comparable to the rat sciatic nerve (1.98 mm inner diameter.) Gelling the PNM hydrogel prior to implantation still caused liquid to leak out during manipulation of conduit and only 50% remained at muscle closure ( 13E). However, the 50% appeared to remain after 1 hour ( 13F). ( 13G, H) The same PNM hydrogel was injected in the conduit after placement. ( 13G) Only a very small amount of the hydrogel was observed to exit the conduit. ( 13H) The conduit appeared to remain full of the 10 mg/mL PNM hydrogel after 1 hour.

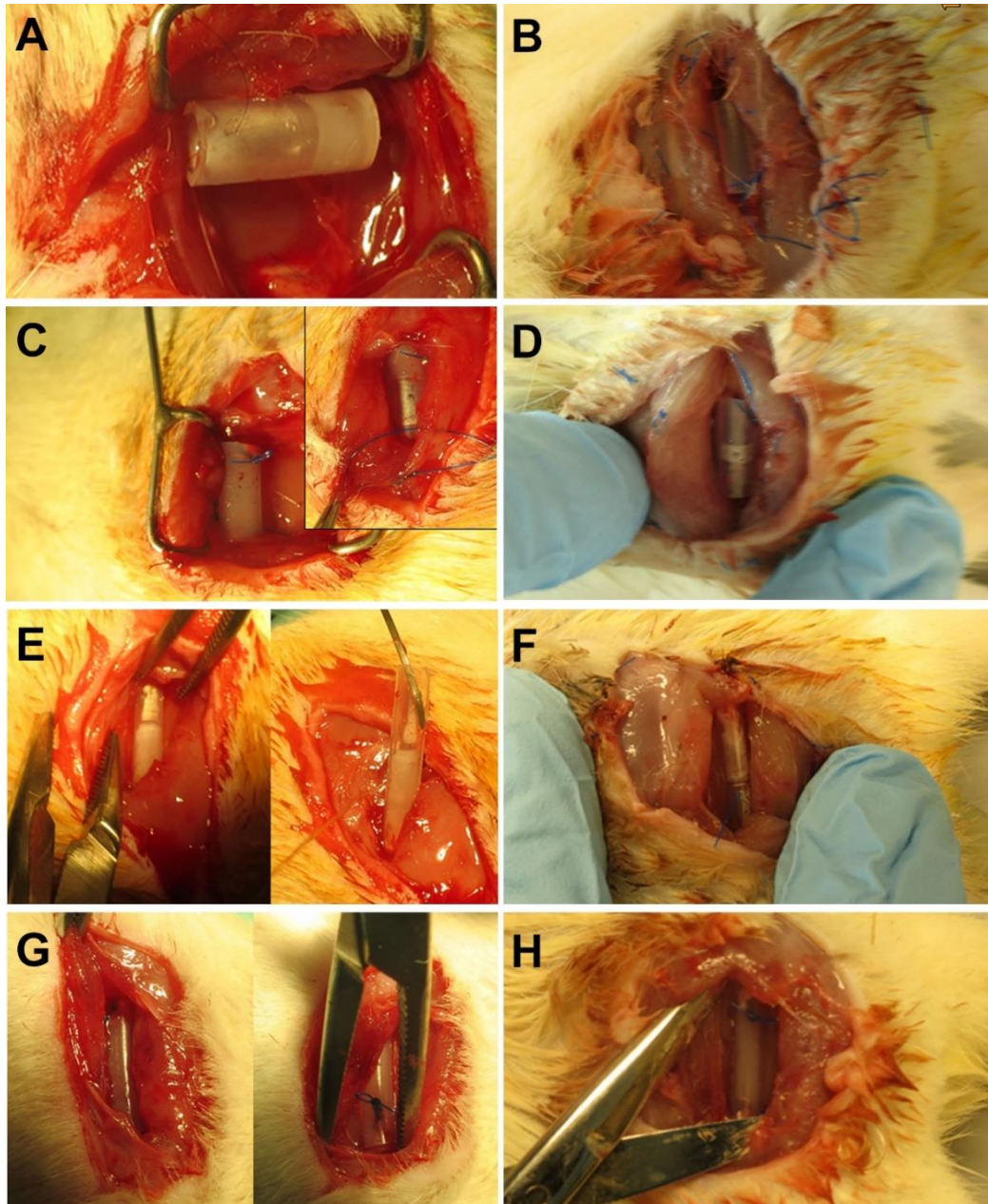


**Figure 13: Testing different protocols for *in vivo* injection of PNM hydrogel into a silicone conduit**

(A) PNM hydrogel injected into 2.5mm diameter conduit prior to implantation. (B) After 1 hour, conduit was empty. (C) PNM hydrogel injected into 2.5mm diameter conduit after implantation but only a small amount remained after 1 hour (D). (E) PNM hydrogel injected into

2.0mm diameter conduit prior to implantation. (F) Some PNM hydrogel was lost during the manipulation of implantation. (G) PNM hydrogel injected into 2.0mm diameter conduit after implantation. (H) All of the PNM hydrogel remained in the conduit after 1 hour.

## **2.4 Discussion**

ECM based scaffold materials such as those used in the present study have been derived from a wide variety of tissues and organs through decellularization. These materials have subsequently been used in a similarly wide variety of preclinical and clinical studies to promote constructive tissue remodeling at the implantation site [171, 172]. The majority of the scaffold materials which are used clinically are derived from xenograft sources; however, a smaller number of decellularized tissue based products are sourced from cadaveric human tissues. In the present study, we chose to utilize a xenogeneic scaffold material composed of canine sciatic nerve. All three tissue sources used (equine, canine, and porcine) were utilized due to local availability, and the necessity of a large animal tissue source to provide sufficient tissue to complete the study. It is noted that most of the commercially available products utilize source tissues from porcine and bovine sources. Regardless of the tissue source, the development of effective decellularization protocols is essential to remove the majority of immunogenic cellular constituents while maintaining the tissue-specific structural and functional components intact [97, 109, 173]. For this reason, it is generally desirable to use the mildest, least disruptive protocol possible that yields an

acellular material with the least interference to the structural and functional components of the ECM.

PNM was developed from three different sciatic nerve sources, equine, canine, and porcine. The decellularization process was adapted slightly for each source to account for the different size ranges but the predominate process was kept consistent. The three different nerve-specific ECMs generated by decellularization in this dissertation was demonstrated to be effectively decellularized with an 85-90% decrease in DNA content when compared to native tissue, yielding a material with similar or less DNA content than many commercially available ECM-based materials [168]. Removal of genetic material from the PNM scaffolds was consistent across animal sources. Furthermore, the remaining ECM components of the nerve tissue was also well preserved with each of the three PNM scaffolds. The results of this chapter suggest that PNM can be generated from multiple animal sources while still producing a highly similar nerve specific ECM scaffold.

The PNM used in this study retained many of the structural and functional components of native nerve following processing to remove cellular content. SEM demonstrated an ultrastructure like that of native nerve, with retention of epineural and endoneural architecture including the basal lamina. This was confirmed by immunofluorescent labeling that demonstrated preservation of large amounts of collagen IV, a component of the basal lamina. Previous studies have demonstrated that UBM also maintains tissue-specific structural features including an intact basement membrane rich in collagen IV as well as the underlying submucosal connective tissues [19]. In the present study, a shift in the balance of hydroxyproline to GAG content was observed when comparing PNM and UBM. Likely, UBM contains an increased hydroxyproline content due to the maintenance of the underlying submucosal tissues during decellularization, while the PNM scaffold materials are enriched in non-fibrillar collagens and laminin, comparatively. ELISA

further demonstrated maintenance of nerve specific growth factors such as NGF and CNTF at similar levels within both the PNM and UBM scaffold materials. These results are consistent with previous studies comparing UBM to central nervous tissue derived materials [17].

While differences were observed between PNM and UBM and SIS, many similarities still exist between these ECM sources. While exact ratios may differ between ECM sources, PNM still share basic ECM constituents with UBM and SIS such as collagen IV and laminin. Furthermore, PNM, UBM, and SIS all showed the presence of nerve-specific growth factors. Concentration and ratios of exact growth factors were found to differ between sources but the hypothesis that only PNM would possess nerve-specific growth factors was found to be false. We still believe that PNM was the closest approximation to the peripheral nerve ECM and therefore could provide an advantaged benefit when used as a scaffold for peripheral nerve repair and regeneration. Our findings, though suggest that UBM and SIS could still provide factors beneficial to nerve regeneration.

The prominent component of most ECM is collagen. Collagen alone has been processed into an injectable solution, which can self-assemble under certain conditions into a hydrogel [174, 175]. It has been shown that the same process can be performed with ECM of multiple sources, including peripheral nerve sources [52, 97, 106, 127, 176, 177]. The formation of the collagen into fibril within ECM hydrogels is dependent upon electrostatic and hydrophobic interactions [174, 175]. This provides alternatives to cross-linking agents for manipulating the mechanical properties of the hydrogel. Previous literature has shown that altering the ionic salt concentration can increase the storage modulus of ECM hydrogels [170, 178] and this was also shown within this dissertation for PNM hydrogels. Reducing the ionic salt concentration has the effect of enhancing interactions between electrostatically charged amino acid side chains [174, 178]. Using 0.5X PBS has been

shown to have little effect on hydrogel swelling but it is not known how infiltrating cells would tolerate salt concentration lower than physiologic conditions [170]. It is also yet unknown how soon the salt concentration would normalize due to native swelling of the injury.

ECM hydrogels were found to be a practical solution for supporting nerve repair. Both the PNM and UBM degradation products begin to gel within 60 seconds after neutralizing to 7.4 pH at body temperature (37° C). The injectable substance was easy to handle and deliver to the site of injury. In a clinical setting, ECM hydrogels could be readily injected into an inert or bioactive conduit so that the liquid filled the available space before forming a hydrogel. Alternatively, the hydrogel could be delivered directly at the site of nerve coaptation.

In summary, it was shown that an ECM scaffold could be produced from peripheral nerve tissue and that this scaffold can be processed into a collagen-based hydrogel. Furthermore, we characterize and show the bioefficacy of the PNM hydrogel. The pilot animal study suggests that extracellular matrices should play a role in augmenting nerve repair in clinical patients.

### **3.0 PNM hydrogel Enhances Recovery Through Increase in Axon Extension, Schwann Cell Recruitment, and Phenotypic Changes in Macrophages**

#### **3.1 Introduction**

Many studies have investigated the use of lumen fillers for nerve guidance conduits to affect the local environment and favor better recovery outcomes through the addition of growth factors or accessory cells into a supportive matrix [41-50, 53, 55, 56]. While many of these studies reported positive results, very few report results nearing those achieved with an autograft procedure. Additionally, there are numerous practical problems associated with many approaches to nerve conduits and lumen fillers: the addition of growth factors is expensive and the factors are not always stable, cells require tissue harvesting and time to culture, and a bulk of donor Schwann cells undergo apoptosis and die during the first weeks after introduction [179]. The use of matrix fillers that are engineered to last the duration of the recovery are often too dense and impede cell growth through the nerve conduits. These studies explore lumen fillers that incorporate single cell or growth factor suspensions that were selected based on their roles on nerve regeneration.

Extended axonal regrowth cannot occur without closely apposed Schwann cells (SC) [180] and the specificity of this process is enhanced both by extracellular matrix (ECM) components, such as collagen IV or laminin, which provide basement membrane support for SC migration. Studies have shown that axon regeneration is severely limited when SC proliferation or migration are artificially inhibited. Inversely, the addition of SCs to a nerve defect injury has been shown to support improved regrowth. Schwann cells provide a large number of cues to support regeneration including classic neurotrophins (NGF, BDNF, NT-3, and NT-4/5), neuropoietic cytokines (CNTF

and IL-6), other neurotrophic factors (IGT-1 and Glial Derived Neurotrophic Factor (GDNF)), cell adhesion molecules (NCAM, L1, and N-cadherin), and ECM proteins (laminin, tenascin C, fibronectin, and heparan sulfate proteoglycan) [4]. These molecules influence the peripheral nerve regeneration through endogenous Schwann cell support or supporting axon outgrowth or survival. Axon, in turn signal Schwann cell to proliferate upon injury and then myelinate if they can reconnect with an appropriate end organ [180, 181]. Axons as well as macrophages responding to the injury provide mitogenic molecules to SCs including neuregulins, PDGF- $\beta$ , TGT- $\beta$ , and FGFs.

Macrophages are a key component of the host response to nerve injury [181], providing important signaling and support molecules to axons and SCs, clearing cellular debris from the injury through phagocytosis, and stimulating neovascularization [180-185]. Macrophages have been described as having diverse and plastic phenotypes along a continuum between M1 (classically activated; proinflammatory) and M2 (alternatively activated; remodeling, homeostatic) extremes. M1 macrophages are characterized by the secretion of reactive oxygen species and proinflammatory cytokines and chemokines. Persistence of M1 macrophages can lead to tissue damage and destruction. In contrast, M2 macrophages secrete anti-inflammatory immune modulators and participate in the constructive healing and remodeling phase of the tissue remodeling response by promoting tissue deposition and in growth.

Macrophages are critical for regeneration within the peripheral nervous system. Macrophage arrive to the site within 24 h after injury and their population peaks by 14-21 day [85]. They play critical roles in scavenging debris, growth factor production such as NGF and IL-6 [86, 87], and remodeling of the ECM of the distal nerve [24, 88]. In multiple injury models, the process of inducing a shift from M1 to M2 like macrophage phenotype has positive benefits on downstream healing, including the generation of site appropriate tissue [87, 109, 110]. It has been

shown that modulating macrophages within the peripheral nerve injury towards an M2 like phenotype results in enhanced Schwann cell infiltration and substantially quicker axonal growth in rodent animal models [89]. In addition, the ratio of pro-remodeling (M2) to pro-inflammatory (M1) population macrophages in the injured nerve tissue has been shown to have a linear relationship with the number of axons at the distal end of nerve scaffolds [89].

Scaffolds composed of ECM derived through the decellularization of intact tissues and organs have been shown to promote a process of constructive remodeling following injury [172], including the formation of new, functionally innervated, site-appropriate host tissue [186, 187]. While the exact mechanisms which underlie the ability of these materials to promote such remodeling are unknown, a number of studies have now shown that the release of bioactive tissue specific molecules and a shift in the local inflammatory response at the site of implantation are key occurrences during the remodeling process [172]. A number of ECM scaffolds have been demonstrated to be supportive substrates for axonal growth and the degradation products of such materials have been demonstrated to be bioactive and chemotactic for SC [96, 186].

The native microenvironment of nerve regeneration is a complex mixture of signaling and support cues produced by SCs, macrophages, and axons. A limitation of many existing studies is the limited scope of growth factor or cellular incorporation. This is partly scientifically motivated to fully understand one element at a time. However, artificially engineering a microenvironment that approaches the native nerve milieu becomes increase difficult. One alternative to engineering a complex microenvironment is to use the natural microenvironment of healthy peripheral nerve harvested through decellularization. Scaffolds composed of ECM derived through the decellularization of intact tissues and organs have been shown to promote constructive remodeling following injury [172] including the formation of new, functionally innervated, site-appropriate

host tissue [186]. Studies implanting porcine derived ECM scaffolds into a rat model of abdominal wall defect and canine model of esophageal reconstruction found the presence of new nervous tissue within the graft area. Mature nerve, immature nerve, and Schwann cells were found within the remodeled ECM scaffolds after 28 days in the rat and 91 days in the canine model demonstrated that ECM can act as a substrate for the formation of functionally innervated tissue. This dissertation also shows that PNM is a friendly substrate for axonal growth and the degradation products of the materials have been demonstrated to be bioactive and chemotactic for SC [186]. Furthermore, PNM stimulates macrophages to produce PDGF- $\beta$  possibly enhancing the SC proliferation response to injury. While PDGF- $\beta$  is thought primarily to be a mitogen for mesenchymally derived cells, PDGF- $\beta$  along with other factors (bFbF, neuregulin-1, neurotrophin-3, and IGF-1) have been already reported to play a role in the development from Schwann cell precursor cells into early Schwann cells [188]. Schwann cells must undergo proliferation after injury and it has been shown that PDGF- $\beta$  is a potent mitogen for Schwann cells and has a neuroprotective action to nerves after injury [189, 190].

In this chapter, the PNM was examined *in vitro* and *in vivo* for its effect on axons, SCs, and macrophages. Both macrophages and Schwann cells involvement is critical for peripheral nerve regeneration [4, 24, 85, 88, 89, 181]. Macrophages account for the majority of debris phagocytosis, produces growth factors, and remodels the ECM of the distal nerve [24, 85, 88, 89]. Furthermore macrophages with an M2 like phenotype enhance Schwann cell infiltration and improve axonal growth [22]. Schwann cells proliferate upon injury and provide many signaling and survival cues to support regeneration [4]. These molecules support axon outgrowth and survival. Finally, Schwann cell myelinate axons that are able to reconnect with an appropriate end organ [180, 181]. It for these reasons that the chapter focuses on PNM effect on increasing

Schwann cell migration into the site of injury and macrophage phenotype and involvement. To test this *in vivo*, canine PNM was used in a rat sciatic nerve critical length defect model and assays focused upon two key early events in the remodeling process: modulation of the host macrophage response and recruitment of Schwann cells.

## **3.2 Methods**

### **3.2.1 Evaluation of Effects of Enzymatic Degradation Products Upon Neurite Outgrowth**

Neurite outgrowth was tested with ECM produced from both equine and porcine sciatic nerve sources. Spinal cord neurons were isolated from embryonic day 14 Sprague–Dawley rat pups. Spinal cords were collected in cold Hanks' buffered salt solution without  $\text{Ca}^{2+}$  and  $\text{Mg}^{2+}$  (Gibco, Carlsbad, CA, USA), minced into pieces and enzymatically dissociated in 2 ml 0.25% trypsin solution containing 0.05% collagenase L1 (MP Biomedicals, Solon, OH, USA) at 37° C for 20 minutes. Cell digestion was inhibited by adding 2 ml SBTI-DNAse solution (0.52 mg/ml soybean trypsin inhibitor; 3.0 mg/ml BSA; 0.04 mg/ml bovine pancreas DNAse, D-4263; Sigma). The cell suspension was gently triturated and centrifuged at 800×g for 5 minutes. The resulting pellet was then resuspended in plating medium and gently triturated. The plating medium consisted of 20% horse serum (Gibco), 5 ml HBSS without  $\text{Ca}^{2+}$  and  $\text{Mg}^{2+}$  (Gibco) and 9.8 ml Dulbecco's modified Eagle's medium with L-glutamine (DMEM; Sigma). All non-dispersed tissue was discarded. Spinal cord neurons were seeded on poly-L-lysine-coated coverslips (12.5 µg/ml in H<sub>2</sub>O; Sigma) in plating medium with a plating density of 3×10<sup>5</sup> cells/mL and allowed to adhere for 4 h in culture conditions of 5% CO<sub>2</sub> and 37° C. After 4 h, the medium was exchanged with 1

ml serum-free culture medium containing Neurobasal-A (NBA, Gibco), and 1 mM Glutamax (Gibco). ECM degradation products were neutralized by adjusting the pH to 7.4 prior to dilution in PBS to the desired concentration. Medium was either supplemented with PNM or UBM digestion products (at concentrations of 125, 250, and 500 µg/mL), 1×B27 supplement (Gibco, positive control), or with 50 µg/ml pepsin (negative control). Low concentrations were used to prevent the digestion products from polymerizing within the cell culture media and to focus analysis strictly on ECM component bioactivity. Three images at 20X magnification were taken per well on days 1, 2 and 4 post seeding. Three images at 20X magnification were taken per well. The number of cells with neurite extensions and the length of neurite extensions were counted using NeuronJ (ImageJ, NIH). Difference in length of neurite extensions between groups (Media supplemented with 50 µg/ml pepsin solution, B27 supplement, or the protein digest of PNM or UBM at concentrations of 125, 250 and 500 µg/ml) was determined using ANOVA with Tukey's post hoc test.

### **3.2.2 Evaluation of Enzymatic Degradation Products of Porcine PNM Upon Schwann**

#### **Cell Migration**

A Schwann cell line (RT4-D6P2T) obtained from ATCC was used. The Schwann cell line was cultured in medium containing DMEM, 10% FBS, 100 U/mL penicillin, and 100 µg/ml streptomycin and passaged 2-4 times and allowed to reach 70-80% confluence before starving in serum-free DMEM for 16 hours. After starvation, cells were trypsinized with 0.25% trypsin and 0.53 mM EDTA for 2 minutes. Cells were then centrifuged at 1200 RPM for 5 minutes. The resultant pellet was re-suspended in serum-free DMEM and incubated (37° C) for 1 hour. Polycarbonate PFB filters (8 µm pores) was coated on both sides with 0.05 mg/mL collagen type

1. Digested ECM peptide fragments were plated in the bottom chamber before assembling and sealing the top chamber. Approximately 30,000 cells were placed in to each well followed by incubation for 3 hours. Afterwards, cells facing the upper chamber were scraped off and the cells facing the lower chamber were fixed in methanol and stained with anti-S-100 antibody (1:100, Sigma) and corresponding secondary antibody (1:100, Alexafluor).

### **3.2.3 Assessment of Macrophage Phenotype in Vitro Using a NanoString's nCounter**

#### **Technology**

Briefly, murine bone marrow derived macrophages were cultured for 7 days before running experiment. Macrophages were exposed to low concentrations of PNM (100, 300, 500, 700  $\mu\text{g}/\text{mL}$ ) or IL-4 to promote an M2 like phenotype or IF $\gamma$  to promote an M1 like phenotype. The cells were then lysed, and RNA was isolated with RNeasy microkit (Qiagen). Nanodrop spectrophotometer (ND-1000, Saveen Werner) was used to measure RNA concentration, and 100 ng was applied from each sample for RNA expression analysis, running one strip of 12 samples at a time on a nCounter analysis system (Nanostring Technologies). The procedure was performed according to the manufacturer's instructions. The kit used was a fixed codeset for mRNA analysis, nCounter GX Human Immunology Kit v2 (Nanostring Technologies).

### **3.2.4 Assessment of Macrophage Response and Schwann Cell Migration in an Animal Model of Sciatic Nerve Defect Injury**

To determine the effects of cell PNM on macrophage and Schwann cell migration animals underwent creation of a sciatic nerve gap defect followed by repair with a silicone conduit alone (n = 7) or a silicone conduit with PNM (n = 7). Rats (Sprague Dawley, females, 200–250 g) were pre-medicated with subcutaneous buprenorphine (2 mg/kg), anesthetized with isoflurane and maintained under anesthesia with isoflurane/oxygen. The sciatic nerve was exposed and transected and a 15 mm critical-length defect [191] was created within a 17 mm silicone nerve conduit (Tuzic, Siliclear tubing, 4.6 mm OD, 3.4 mm ID). Proximal and distal nerve stumps were aligned and sutured 1 mm into the conduit with 9-0 suture. Conduits were filled with PNM hydrogel at a concentration of 8 mg/ml, prepared as described above. The hydrogel was brought to room temperature 5 minutes prior to injection into the conduit. The hydrogel was observed to gel within the silicone conduit with 5 minutes. Excess gel was removed, and the site irrigated with saline solution. Muscular and cutaneous layers were closed routinely. Post-surgical pain control was provided by subcutaneous meloxicam (2 mg/kg) injection immediately postoperatively and 12 hours after surgery. Rats were euthanized with pentobarbital (I.P.) 21 days after implantation and the conduit and proximal and distal stumps removed intact. Samples were fixed in Zamboni's solution for immunofluorescent labeling as described below.

### 3.2.5 Immunolabeling and Quantitative Analysis

Samples were embedded in paraffin and sectioned longitudinally at 4  $\mu\text{m}$  for immunofluorescent labeling to assess the host macrophage, and Schwann cell response. Complete consecutive sections were used for M1, M2 and Schwann cell labeling. Three slides from each rat were generated for each label. After deparaffinization and rehydration, antigen retrieval was performed by steaming in 10 mM citrate (pH 6.0) for 20 min followed by incubation for 20 min at room temperature. Sections were then processed with a MicroProbe System (Fisher Scientific) and phosphate buffered saline containing 0.05% Neonate 20 (PBST) was used for washing between each of the steps described below. Slides were blocked in a solution of 2x casein and 10% antibody host species matched serum for 30 minutes at room temperature. The sections were then incubated with a mixture of antibodies specific for markers of M1 macrophages (CD68, CCR7), M2 macrophages (CD68, CD206), and Schwann cells (GFAP) for 90 minutes at room temperature. Incubation in appropriate AlexaFluor 488 and Texas Red conjugated secondary antibodies was performed sequentially for 30 minutes each at room temperature. Sections were coverslipped in an aqueous mounting media containing DAPI (Vectashield, Vector Laboratories). For negative control, the primary antibodies were replaced with a mixture of isotype IgG at equivalent concentrations. Antibody species, isotype, dilution, and supplier information are provided in Table 8.

**Table 8: List of antibodies used**

Reused with permission (4546560968632). [52]

Antibody	Host species	Isotype	Dilution	Source
CD206 (C-20)	goat	IgG, polyclonal	1:50	Santa Cruz
CCR7 (Y59)	rabbit	IgG, monoclonal	1:500	Abcam
CD68 (ED1)	mouse	IgG1, monoclonal	1:50	BioRad
GFAP	rabbit	IgG, whole antiserum	1:500	Abcam

High resolution images of the entire proximal stump and regenerative bridge were obtained from fluorescently labeled slides (Zeiss 510). The original site of transection was identified in each image and a straight line drawn perpendicular to the long axis of the nerve at that level to allow identification of individual cells relative to this line (Volocity Image Analysis Software, Perkin Elmer). The location of all individual macrophages (M1, CD68+ CCR7+; or M2, CD68+ CD206+) and Schwann cells (GFAP+) and their location relative and perpendicular to the transected proximal nerve stump were then determined (Volocity) with concealment of group allocation. Cell position (M1, M2 macrophage or Schwann cell) relative to the original site of transection was binned into 500 $\mu$ m increments, log transformed and treated as a categorical variable to allow for non-linear effects. M2:M1 ratio was calculated for each section as the total number of

CD68/CD206+ macrophages divided by the total number of CD68/CCR7+ macrophages. The distribution of each cell population was analyzed using a mixed effect models, with animal identity as a random effect. Linear contrasts were used to make specific comparisons when appropriate.

### **3.3 Results**

#### **3.3.1 Bioactivity of Degradation Products**

##### **3.3.1.1 Evaluation of Effects of Enzymatic Degradation Products Upon Neurite Outgrowth**

Degradation products of canine PNM were introduced at different concentrations to primary neurons over four days. Bioactivity of degradation products was analyzed through a neurite outgrowth assay assessed at 1, 2, and 4 days post-plating using ImageJ. Individual days were assessed for statistical significance using a one-way ANOVA followed by a Sidak post-hoc test to correct for multiple comparisons. A trend towards increased neurite outgrowth with increased ECM concentration was observed for both PNM and UBM groups (Figure 11A). The increase in neurite outgrowth for the highest concentration (500  $\mu\text{g/ml}$ ) of PNM produced similar results to the positive control ( $p = 0.98$ ) and was significantly greater than the negative control ( $p = 0.03$ ). Images from neurite outgrowth with pepsin (negative) control, b27 supplement (positive) control, PNM and UBM at 500  $\mu\text{g/ml}$ . Neurite outgrowth analysis images depict increased growth over the four days as well as increase growth over the negative control (Figure 11B).

The degradation products were neutralized, diluted to a concentration of 8 mg/ml and the hydrogel was allowed to form in a non-humidified incubator at 37° C (Figure 11C). Digested decellularized nerve products formed into a stable gel at 8 mg/mL shown both macroscopically and under scanning electron microscopy at 4,000X magnification (Figure 11D).

The same neurite outgrowth performed using primary spinal cord neurons collected from E14 embryonic rat pups to test PNM generated from porcine sciatic nerves. Media was supplemented with PNM at low concentrations (125, 250, or 500 µg/ml), pepsin (50 µg/ml, negative control), or nerve growth factor (NGF 50 pg/ml, positive control) (Figure 15A). Statistical analysis of covariance with Sidak post-hoc test performed with statistically similar groups ( $p < 0.05$ ) for each separate day shown with matching letters. Primary neurites stained with  $\beta$ -Tubulin shows neurites produced after 7 days (Figure 15B)

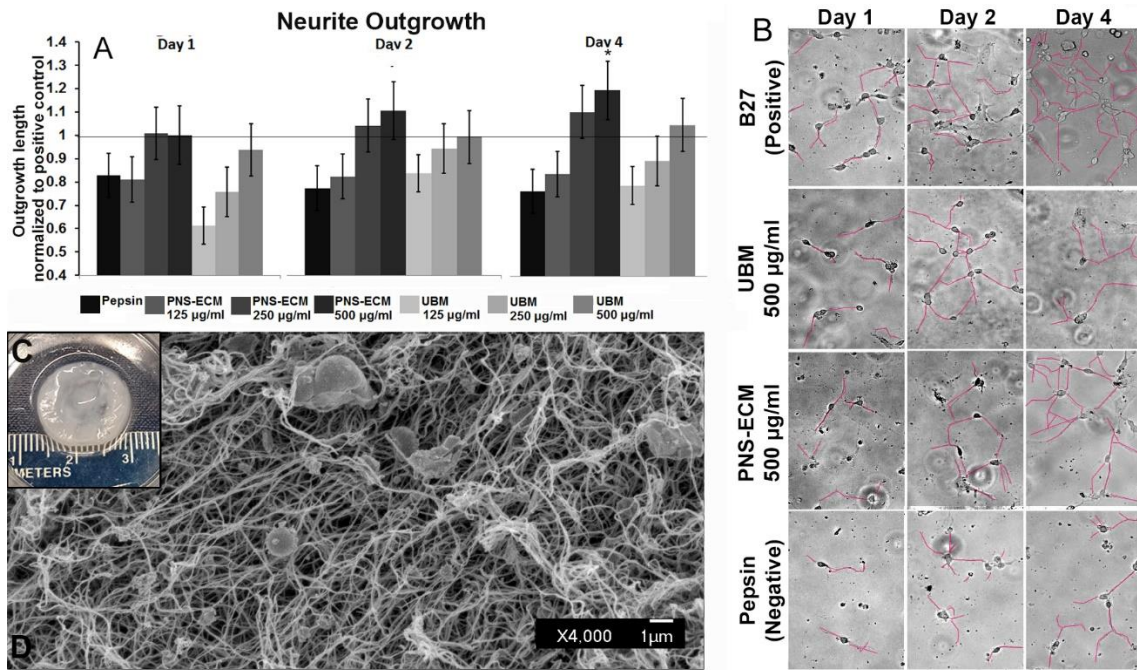


**Figure 14: PNM digestion products promote neurite outgrowth and can be formed into a stable hydrogel**

(A) Degradation products of PNM were introduced at different concentrations to primary neurons over four days. PNM 500 µg/ml was significantly greater than positive control by 4 days (\*,  $p < 0.05$ ,  $n = 5$ ). (B) Images from neurite outgrowth with pepsin (negative) control, b27 supplement (positive) control, PNM and UBM at 500 µg/ml. (C-D) Digested decellularized nerve products formed into a stable gel at 8 mg/mL.

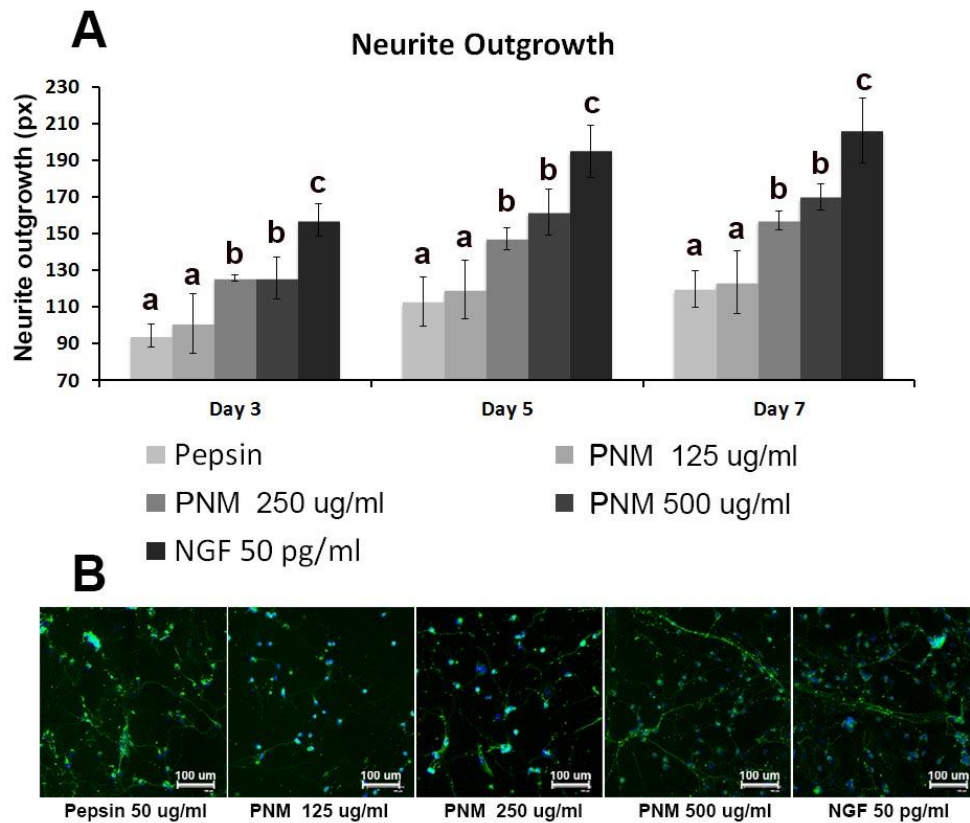


**Figure 15: Porcine PNM effect on primary spinal cord neurite outgrowth**

Neurite outgrowth performed using primary spinal cord neurons collected from E14 embryonic rat pups. Media was supplemented with NS-ECM at low concentrations (125, 250, or 500  $\mu\text{g/ml}$ ), pepsin (50  $\mu\text{g/ml}$ , negative control), or nerve growth factor (NGF 50  $\text{pg/ml}$ , positive control) (A). Statistical analysis of covariance with Sidak post-hoc test performed with statistically similar groups ( $p < 0.05$ ,  $n = 5$ ) for each separate day shown with matching letters. Primary neurites stained with  $\beta$ -Tubulin shows neurites produced after 7 days (B).

### **3.3.1.2 Evaluation of effects of enzymatic degradation products upon Schwann cell migration**

Schwann cell migration was performed using a boyden chamber. Serum-free media supplemented with various concentration of PNM produced similar migration to positive controls (serum supplemented media, with 50 ng/ml NGF, and with 100 ng/ml NGF). Because the cells are serum starved, serum is an accepted positive control for most Schwann cell migration assays. We also included medium supplemented with both 50 and 100 ng/ml of NGF. UBM and SIS was also tested at the highest concentration tests (1000  $\mu\text{g/mL}$ ). PNM treatment showed enhanced Schwann cell migration that was chemoattractant. Poor migration when PNM was added to the cell side of the boyden chamber suggests that PNM is not simply chemokinetic or promoting not directed migration. Conversely, we found that UBM and SIS promoted greater chemokinetic migration rather than chemoattractant migration (16A). Migration stimulated by PNM treatment was significantly greater than that of SIS or UBM ( $p < 0.05$ ,  $n = 5$ ). PNM treatment was also statistically greater than negative controls (pepsin and PNM on cell side only) ( $p < 0.05$ ,  $n = 5$ ). The application of PNM also had an apparent dose dependent effect of Schwann cell migration (16B).

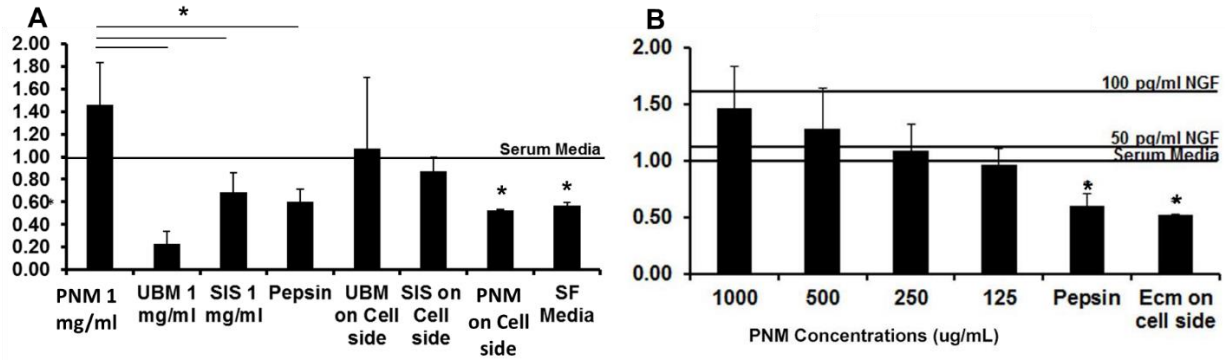


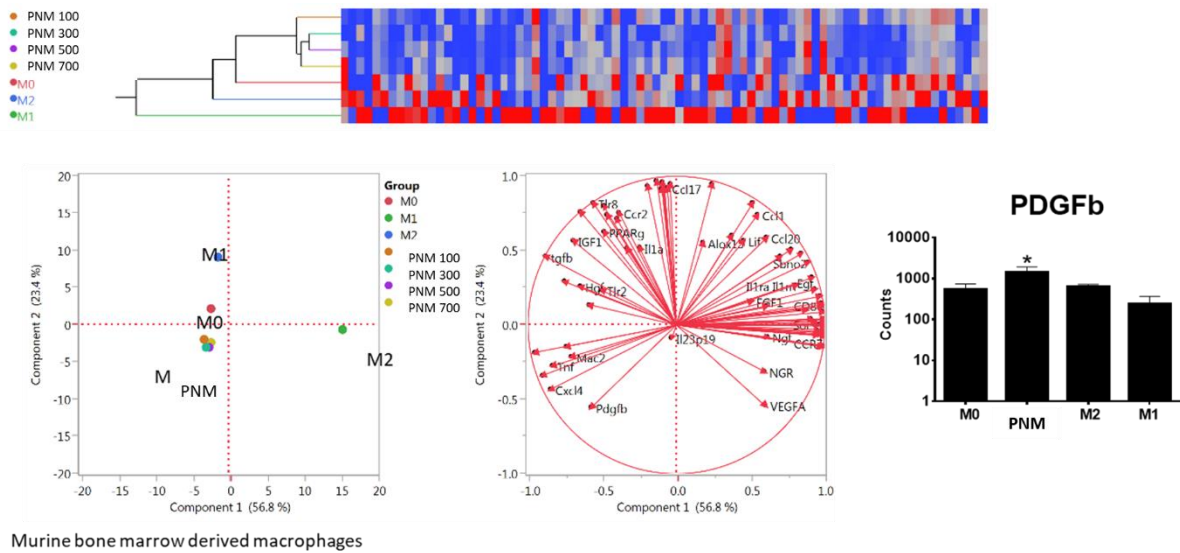
**Figure 16: Porcine PNM effect on Schwann cell migration in vitro**

Schwann cell migration was performed using a boyden chamber. PNM digested products supplemented to serum-free media at 1 mg/mL produced significantly more migration ( $p < 0.05$ ,  $n = 5$ ) than UBM and SIS at the same concentration (A). Serum-free media supplemented with various concentration of PNM produced similar migration to positive controls (serum supplemented media, with 50 ng/ml NGF, and with 100 ng/ml NGF). Treatment was statistically greater than negative controls (pepsin and PNM on cell side only) (\*,  $p < 0.05$ ,  $n = 5$ ) (B).

### 3.3.2 Assessment of Macrophage Phenotype

A nanostring assay was performed on murine bone derived macrophages. Macrophages were exposed to PNM digestive products at dilute concentrations (100, 300, 500, and 700  $\mu\text{g/mL}$ ). Exposure to PNM digestive products promoted a phenotype that was distinct from resting, pro-inflammatory, and anti-inflammatory macrophages and the biggest activity we found was the

expression of an angiogenesis factor, Platelet derived growth factor  $\beta$  (PDGF $\beta$ ) (Figure 17). Angiogenesis is well known to be essential for nerve regeneration. PNM also promoted M2 (regenerative) genes including *Chi313*, *Retnla* and *IL4ra*.



PDGFb – Platelet derived growth factor b – angiogenesis stimulant. Angiogenesis is well known to be essential for nerve regeneration. Abbreviations used: PNM 100  $\mu\text{g}/\text{mL}$ ; PNM 300  $\mu\text{g}/\text{mL}$ ; PNM 500  $\mu\text{g}/\text{mL}$ ; PNM 700  $\mu\text{g}/\text{mL}$ ; PDGFb, Platelet derived growth factor  $\beta$ .

### **3.3.3 In Vivo Test of Macrophage and Schwann Cell Response to PNM Hydrogel**

#### **3.3.3.1 Macrophage Phenotype in a Sciatic Nerve Defect**

Representative longitudinal sections of regenerative bridges were immunohistolabeled for M1 macrophages (18A, CD68+CCR7+) for control (empty conduit) and PNM filled conduits. Sections were also immunolabeling for M2 ( 18B, CD68+CD206+) macrophages in empty and PNM filled conduits. Macrophages within the remodeling site tended to be distributed on the margins of the regenerative bridge (Figure 18) and the number of both M1 and M2 macrophages (M1: CD68+ CCR7+; M2: CD68+ CD206+) was found to be increased in the presence of PNM within rodent sciatic defects (Figure 19A–B) as compared to conduit alone. Insert demonstrates intracellular CD 68 labelling and surface CD206 labelling. No additional extension of proximal stump was observed in control sections. The number of M1 macrophages was significantly increased in the PNM group at 2.5–3.0 mm from the original site of transection ( $p = 0.01$ , linear contrast) and M1 macrophages were identified up to 5.5 mm from the original site of transection, in contrast to the control (3.5 mm). The number of M2 macrophages was also significantly increased in the PNM group at each 500  $\mu\text{m}$  interval from 1.0 to 3.0 mm from the original site of transection (all  $p = 0.001$ , linear contrast) and M1 macrophages were identified up to 5.5 mm from

the original site of transection, in contrast to the control (3.0 mm). The presence of PNM also increased the M2:M1 ratio within the conduit (n = 3 slides/label/animal and 7 animals/group) (p = 0.002, 19C).

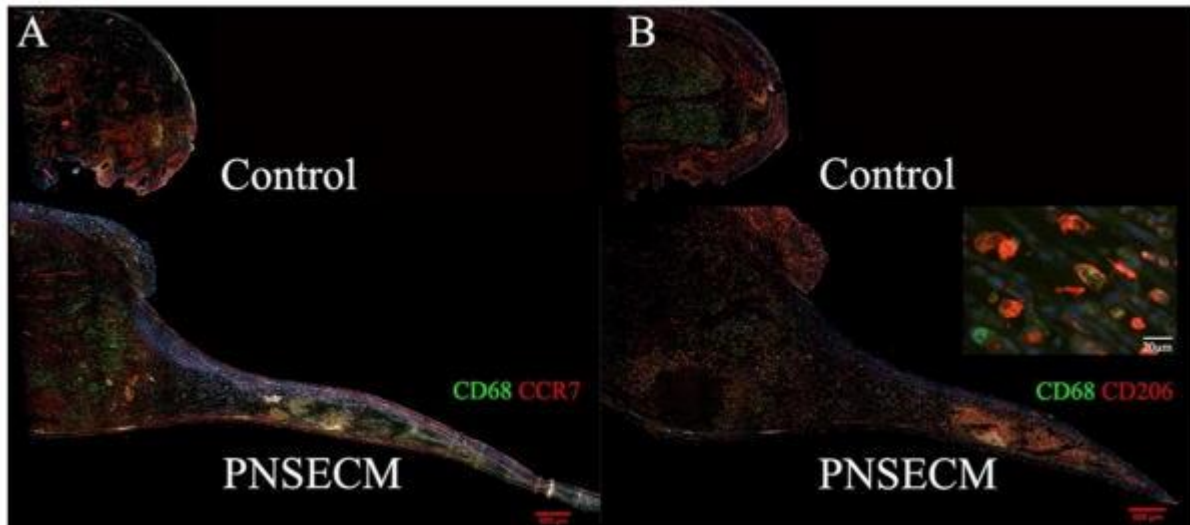


**Figure 18: Representative longitudinal sections of regenerative nerve bridge stained for M1 and M2 macrophage markers**

Representative longitudinal sections of regenerative bridges immunohistolabeled for M1 macrophages (panel A, CD68+CCR7+) for control (empty conduit) and PNM filled conduits. Representative immunolabeling for M2 (panel B, CD68+CD206+) macrophages in empty and PNM filled conduits. Insert demonstrates intracellular CD 68 labelling and surface CD206 labelling. No additional extension of proximal stump was observed in control sections. Reused with permission (4546560968632). [52]

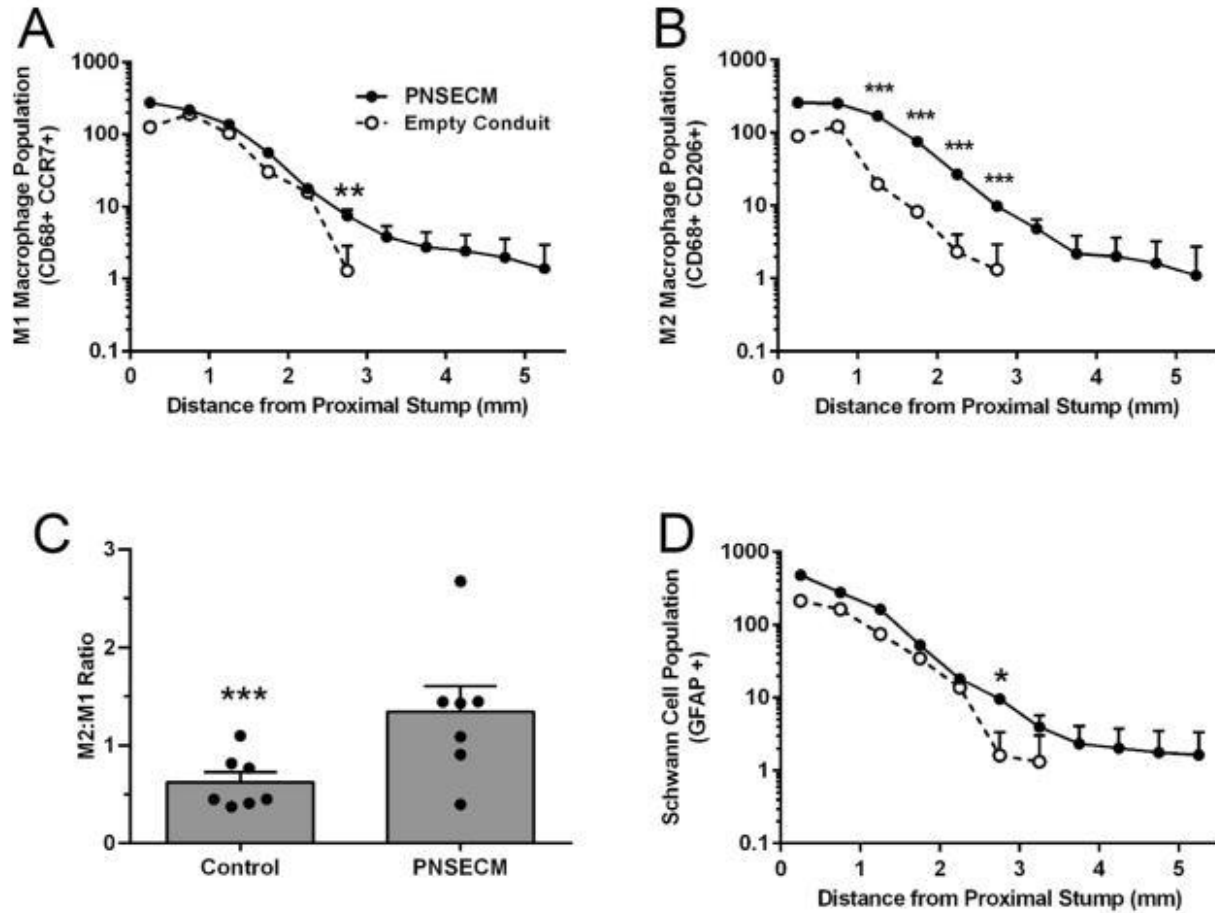


**Figure 19: Macrophage recruitment and Schwann cell migration into nerve bridge**

PNM promotes migration of both M1 (CD68+CCR7+) and M2 (CD68+CD206+) macrophage phenotypes, relative to the original site of transection (A, B); an increased M2:M1 ratio (C) and increased extension of Schwann cells populations relative to the original site of transection (D). Data shown are least square (adjusted) mean and standard error (A, B, D) and mean and standard error (C). n= 3 slides/ label/animal and 7 animals /group. Reused with permission (4546560968632). [52]

### **3.3.3.2 Schwann cell migration in a sciatic nerve defect**

Schwann cells (SC) tended to be distributed on the margins of the regenerative bridge and SC numbers were significantly increased in the PNM group at 2.5–3.0 mm from the original site of transection ( $p = 0.02$ , linear contrast). SC were identified up to 5.5 mm from the original site of transection, in contrast to the control (3.5 mm, 19D). Overall, the use of PNM as a lumen filler increased extension of Schwann cells populations relative to the original site of transection (Figure 19D). Data shown are least square (adjusted) mean and standard error (A, B, D) and mean and standard error (C).  $n = 3$  slides/ label/animal and 7 animals /group.

## **3.4 Discussion**

In this study, we characterized the biological effects of PNM hydrogels upon the early progression of peripheral nerve reconstruction across a critical gap defect. We show that PNM hydrogels largely maintain matrix structure and several growth factors, promote increased macrophage invasion and higher percentages of M2 macrophages and enhance Schwann cell migration when transplanted into a rodent model. These effects have all been associated with improved nerve regeneration in previous studies [87, 89, 108, 112, 181, 192, 193]

Neurite outgrowth assays demonstrated that degradation products formed through pepsin digestion of the intact materials were bioactive, promoting neurite outgrowth and extension. Both UBM and PNM displayed dose dependent effects across the observed time points, showing increasing neurite growth with increasing dose. While lower doses of PNM were not significantly

increased over positive control, by the last time point (day 4) the highest dose of PNM (500  $\mu$ g/ml) showed significantly better growth than both UBM and B27 positive control. Even at this highest dose (500  $\mu$ g/ml), PNM is still significantly more diluted than when it was (8 mg/ml). These results suggest that the resultant PNM hydrogel retained biologically active nerve specific components, although native architecture was lost when the hydrogel was formed.

In the present study, when delivered into a rodent critically sized defect, we observed a switch in the ratio of M1:M2 phenotype macrophages, a phenomenon associated with improved nerve growth, [22] and promotion of Schwann cell migration across a gap defect. This was associated with improved function over time in a non-critical (8 mm) common peroneal defect. We selected the common peroneal nerve as our experimental paradigm for functional studies as the consequence of axonal misdirection is reduced compared to sciatic nerve injury in which inappropriate reinnervation of muscular targets leads to dysfunction after injury [51]. We did not evaluate PNM in comparison to other biomaterials or biopolymers. This is the focus of ongoing work.

The present study does not attempt to investigate the mechanisms by which the injectable ECM promote these phenomena; however, a recent study has described M2 macrophage mediated angiogenesis as a mechanism leading to Schwann cell chemotaxis and downstream regeneration [181]. While ECM mediated shifts in macrophage phenotype have been reported in other applications, as has increased angiogenesis, further investigation of these phenomena in the context of nerve repair is warranted. Similarly, mechanistic studies linking these phenomena to improvements in function downstream should be performed. However, though the exact mechanisms are not clear, these results provide evidence that PNM is an effective tool for improving nerve repair.

In this study, we characterized the biological activity of injectable peripheral nerve-specific ECM hydrogels, determined the biological effects of these hydrogels using both *in vitro* and *in vivo* test for neurite extension, Schwann cell migration, macrophage gene expression as well as an animal model of critical gap defect sciatic assays.

Results of the study demonstrated that the ECM hydrogels tested had significant potential for promoting increased recovery following surgical reconstruction. The decellularized PNM was shown to retain multiple nerve-specific matrix components, including growth factors. Enzymatic degradation products of the PNM scaffolds were shown to promote neurite outgrowth in *in vitro* assays. These same degradation products, when assembled into a hydrogel were demonstrated to promote a switch in the ratio of M1:M2 phenotype macrophages, a phenomenon associated with improved nerve growth [172], and to promote Schwann cell migration across the gap defect. In total, these results provide strong evidence that PNM is effective at altering the response of Schwann cells and macrophages during peripheral nerve injuries. Results from this chapter show that PNM effects important mediators of nerve regeneration, the next step is to investigate if these effects lead to improvement in downstream functional recovery.

## **4.0 PNM Can be Utilized in Both Crush and Nerve Defect Injuries to Increase Axon Growth and Functional Recovery**

### **4.1 Introduction**

Previous work has shown that the PNM retains components of the peripheral nerve ECM including collagen, laminin, and nerve specific growth factors. Furthermore, PNM was able to enhance neurite outgrowth and Schwann cell migration *in vitro* after post processing for hydrogel formation. The PNM hydrogel was also shown to promote a switch in the ratio of M1:M2 phenotype macrophages and to promote Schwann cell migration across a sciatic nerve gap defect. Overall, these results suggest that the PNM hydrogel provides a beneficial microenvironment for nerve regeneration during the initial stages of recovery. We hypothesize that the early effects on the response of Schwann cells and macrophages during peripheral nerve injuries will lead to lasting downstream changes. This involves tracking functional improvements over the full course of recovery to test potential for promoting increased recovery following surgical reconstruction in a pre-clinical study.

There are a number of methods for estimating recovery of peripheral nerve repair in experimental models, including histological measurements of axon count, neuron cell body count, motor endplate count, and motor unit number estimation. However, these metrics are not direct measures of function and do not always correlate with actual nerve function. Axon count and myelination does not give information about whether the axon has reached its appropriate target organ and electrophysiology does not necessarily equate to the function of complex locomotion [194-196]. Therefore, a direct measure functional recovery is important for a well-designed study

for a new nerve repair therapy. Relatively few methods of assessing functional recovery after peripheral nerve injury have been used. These methods have historically focused on behavioral tests and include walking track analysis, sensory function, kinematics, and ground reaction force. Serial assessment of functional recovery reduces the number of animals required for experimentation and reduces some of the variability in testing, as each animal can act as its own control. Quantification of peripheral nerve regeneration in animal models of nerve injury and repair by purely histologic, morphologic, or electrophysiologic parameters do not directly measure the goal of peripheral nerve repair, full functional recovery. These metrics do not necessarily correlate with actual nerve function.

This chapter includes pre-clinical studies that incorporates a wide range of experiments, including histologic, electrophysiologic, and functional metrics. This was done to broaden overall the understanding of the effect that PNM had on peripheral nerve injury. The predominant focus of this dissertation has been on severe fifth degree injuries or neurotmesis resulting in a gap defect. These injuries have the worst outcomes but also have the largest focus from the research community and have several FDA approved devices directed at improving outcomes. However, as discussed previously, peripheral nerve injury exists on a spectrum that can be described by the Sunderland scale. This chapter also seeks to investigate the use of PNM across different categories of peripheral nerve injury, including crush, transection without a gap, as well as transection with a gap.

While having significantly better outcomes, 2<sup>nd</sup>-4<sup>th</sup> degree injuries often do not reach full recovery and take weeks to months to recovery. Currently, there is no accepted treatment or aid for this type of peripheral nerve injury. An off the shelf product that has the potential to improve outcomes for serious nerve injuries and speed the return to function for less severe injuries is an

attractive solution. PNM hydrogel is an easily injectable material in an off the shelf formulation which promotes recruitment of alternately activated M2 macrophages, Schwann cell migration, and axon extension. We believe that PNM can positively impact both crush and gap nerve injuries. This study will expand our understanding of delivery techniques and therapeutic applications for the PNM hydrogel.

In addition to the rat models of sciatic nerve injury, a pilot study was undertaken in a large animal model of recurrent laryngeal nerve transection. An illustration of the anatomy of the path of the recurrent laryngeal nerve which branches from the Vagus nerve (cranial nerve X) and innervates the intrinsic muscles of the larynx can be seen in Figure 22. Injury to the recurrent laryngeal nerve (RLn) results in vocal fold immobility, dysphonia, and potentially life-threatening airway obstruction with major consequences for speech, airway coaptation or by nerve graft [197-199]. The RLn branches off the vagus nerve in the chest and works its way back to the larynx (Figure 22). Injury to the RLn is a possible complication of thyroid surgery and other neck procedures. Despite advances in microsurgical technique and extensive studies on nerve repair, presently used surgical reinnervation methods produce only moderate results and full functional recovery after nerve injury is seldom achieved [200-203]. Therefore, methods that accelerate or improve reinnervation following reconstruction of the RLn are of significant clinical interest.

In this chapter the effect of PNM on functional recovery through numerous animal peripheral nerve injury models, including crush, transection, and nerve defect injuries was investigated. Two pilot studies using rat models of sciatic and common peroneal nerve gap defect injuries was used to establish the sciatic functional index (SFI) experiment. These were also used to get initial functional results on a critical and non-critical length defect injury. Two large studies

investigated a non-critical gap defect and crush injury of the rat sciatic nerve. Finally, a canine model of recurrent laryngeal nerve transection was used to test PNM in a transection and coaptation model of peripheral nerve injury.

## 4.2 Methods

Five studies were used to test PNM across several animal and injury models. The experiments used in these pre-clinical studies are summaries in Table 9.

**Table 9: Diagram of Pre-clinical studies and experiments used**

Experiments	Study				
	Pilot study of rat critical-length sciatic nerve defect	Pilot non-critical defect of rat common peroneal nerve	1cm rat sciatic nerve gap defect model	Rat sciatic nerve crush model	Large animal recurrent laryngeal nerve transection
Nerve histology					
Muscle histology					
SFI/PFI					
Walking track analysis					
Von Frey					
Electrophysiology					

#### **4.2.1 Pilot Study of Critical-length Gap Defect of Rat Sciatic Nerve Surgical Procedure**

After a brief isolation period, the rats underwent behavior testing using the sciatic function index. After the animals' hind legs were dipped in ink, they were persuaded to walk across a paper thereby demonstrating specific gait patterns and documenting toe spread at baseline.

The surgery was performed under ketamine (2-10 mg/Kg, intramuscularly) and acepromazine (1-2 mg/kg, intramuscularly) sedation. Buprenex (0.1-0.25 mg/kg) and gentamicin (2-4 mg/kg) were also administered subcutaneously immediately post induction. An incision using the scalpel was carried out longitudinally along the leg exposing the underlying muscle. Dissection around the muscle exposed the underlying sciatic nerve. The nerve is then cut with a scalpel blade to avoid crush injury. A 5 mm non-branching segment will be removed. Next, a 15 mm collagen conduit will be placed in the gap between the nerve ends. The nerve ends sat in the lumen of the conduit and was sutured in place with two 10-0 nylon sutures. In the experimental groups, the conduit was filled with a 10 mg/mL PNM hydrogel. For the control group the nerve segment was flipped and sutured back as an analog to the nerve autograft. Two animals with nerve defects were not repaired and kept as negative controls. The skin was closed with the 4-0 suture in an interrupted fashion.

The animals were followed for 180 days. Every 14 days, the animals underwent the behavioral testing of the sciatic function test to document progress as well as toe spreading. At the end of the 180 days the animals were euthanized using CO<sub>2</sub> until they ceased to breath and heart function had stopped. As a secondary method of euthanasia, cervical dislocation was used.

#### **4.2.2 Pilot Non-critical Gap Defect of Rat Common Peroneal Nerve Surgical Procedure**

To evaluate the effects of PSECM on functional recovery, a non-critical 8 mm gap defect was created in the common peroneal nerve using a 10 mm conduit in the left hind limb of Sprague Dawley rats (females, 200–250 g). Conduits were filled with PNM or left empty (control, n = 6/group). All surgeries were block randomized and anesthetic and surgical procedures were performed as described above.

#### **4.2.3 Surgical Model of a 1cm Gap Defect Injury of Rat Sciatic Nerve**

The sciatic nerve with its three major branches were exposed through the hamstring through a splitting incision. A 5-10 mm section of the sciatic nerve approximately 5 mm proximal from the main branching point was excised. This segment was either removed and the resultant gap repaired using a conduit or flipped and sutured in place. Afterwards the various treatment and control procedures were performed, and the muscle and skin were closed using 3-0 and 4-0 sutures. Five groups specific to the nerve defect model were used: the autograft repair alone, conduit alone, or conduit with PNM lumen filler at concentrations 10, 20, and 40 mg/mL ( 20).

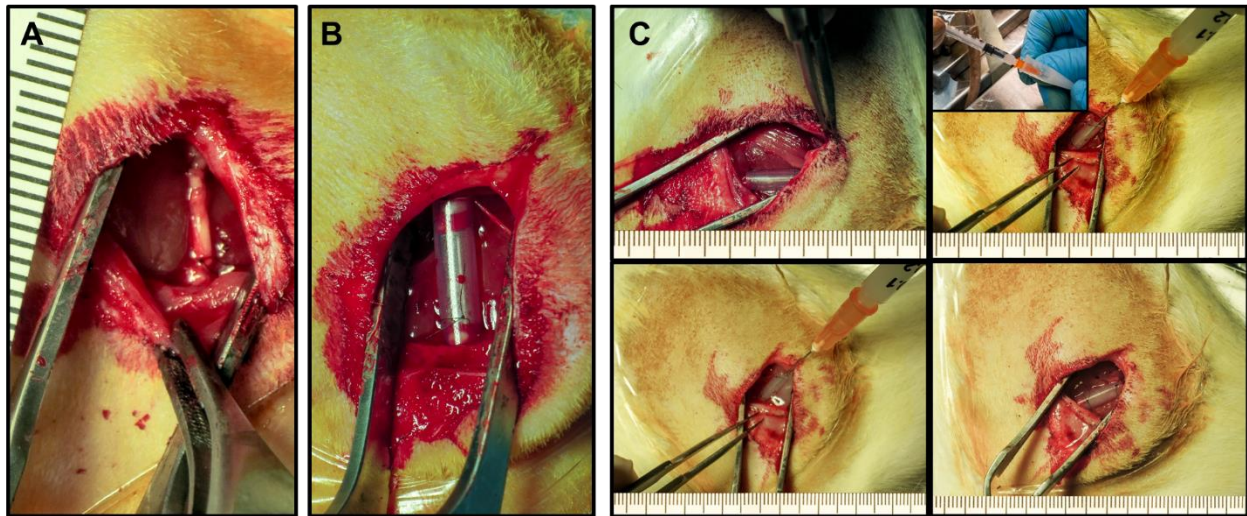


**Figure 20: Representative surgical images of sciatic nerve defect model**

Representative images showing the three major surgical repairs (A) autograft, (B) silicone conduit repair, and (C) silicone conduit repair with PNM lumen filler are varying concentrations.

#### 4.2.4 Surgical Model of Sciatic Nerve Crush Injury

A rat model of sciatic nerve crush resulting in a third degree axonotmesis injury was used. A segment of the sciatic nerve 5 mm proximal to the tibial and common peroneal nerve split was exposed and crushed for 60 seconds using a bulldog clamp calibrated to produce 500 g of force. The nerve was then injected with 25-30  $\mu$ g of PMN hydrogel using a 25G needle. Controls included a crushed sciatic nerve without additional treatment, an uninjured sciatic nerve with injection of PMN hydrogel, a transection and ligation of the nerve at the same location, as well as

sham and uninjured controls (Figure 21). Animals were sacrificed after 90 days at which time their nerves and gastrocnemius were excised. The general procedure of crushing the sciatic nerve as well injected the PNM hydrogel can be seen in Figure 21.

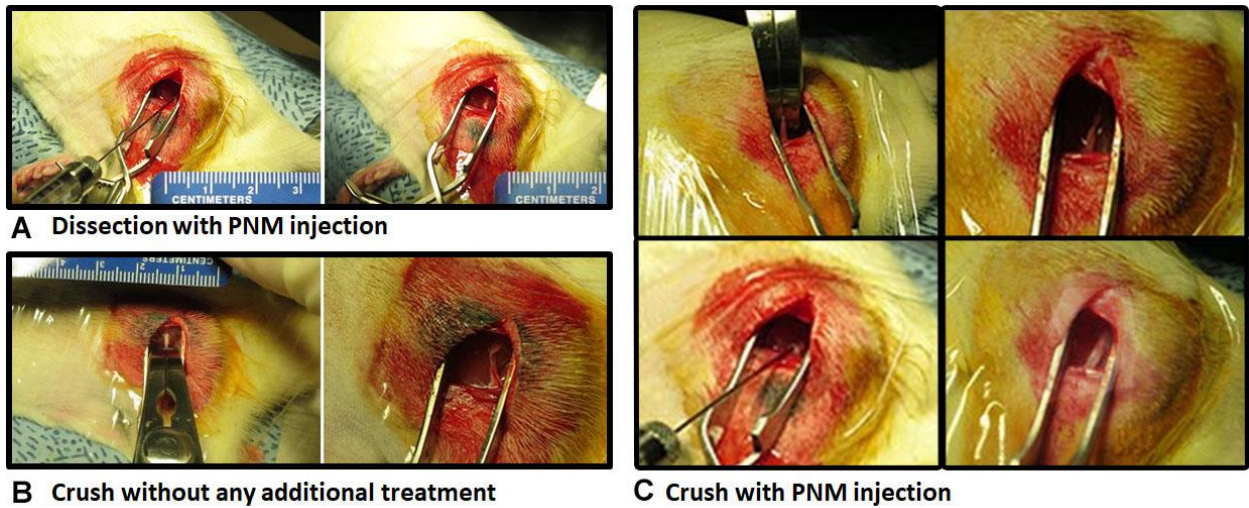


**Figure 21: Representative surgical images of sciatic nerve crush model**

(A) Normal, uninjured nerve was injected with 25-30  $\mu\text{g}$  of PMN hydrogel using a 25G needle (DO-PNMI). (B) Sciatic nerve crushed with a bulldog clamp calibrated to 500g of force (C-NT). (C) Sciatic nerve crushed with same bulldog clamp and then injected with 25-30  $\mu\text{g}$  of PMN hydrogel using a 25G needle (C-PNM). Other controls (sham procedure, SHAM; no injury, NI; transection and ligation, T-NT) not shown.

## **4.2.5 Large Animal Model of Recurrent Laryngeal Nerve Reconstruction**

### **4.2.5.1 Animals and Instrumentation**

This study was performed in accordance with the PHS Policy on Humane Care and Use of Laboratory Animals, the NIH guide for Care and Use of Laboratory Animals, federal and state regulations, and was approved by the Cornell University Institutional Animal Care and Use Committee (IACUC). Animals were brought into the research unit and given a 7-day acclimatization period prior to any procedure. Daily record logs of medical procedures were maintained. Cages with elevated floors were cleaned daily and disinfected biweekly. The animals were fed twice a day to maintain proper body condition and allowed water ad libitum. Group housing provided socialization and ample space for exercise.

Eleven female Beagle dogs (age 5-7 years, body weight  $6.8 \pm 0.7$  kg, range 6.4-8.7kg) with no history of upper airway disease and normal laryngeal function, determined endoscopically, were used. Dogs were chosen at random and fasted for at least six hours before anesthetic procedures. At the end of each procedure, dogs were monitored for one hour before returning to their group housing.

After fasting overnight, each dog was anesthetized with dexmedetomidine (2 mcg/kg IV followed by 2 mcg/kg/hour) and maintained under anesthesia at a constant expired isoflurane concentration (approximately 1MAC, 1.3%). Monitoring consisted of continuous electrocardiogram, pulse oximetry, non-invasive blood pressure, capnography and temperature.

Analgesia was provided with pre-operative Meloxicam (0.2 mg/kg body weight) subcutaneously (SQ), followed by meloxicam given as an oral suspension (0.1 mg/kg body weight), daily for four additional days.

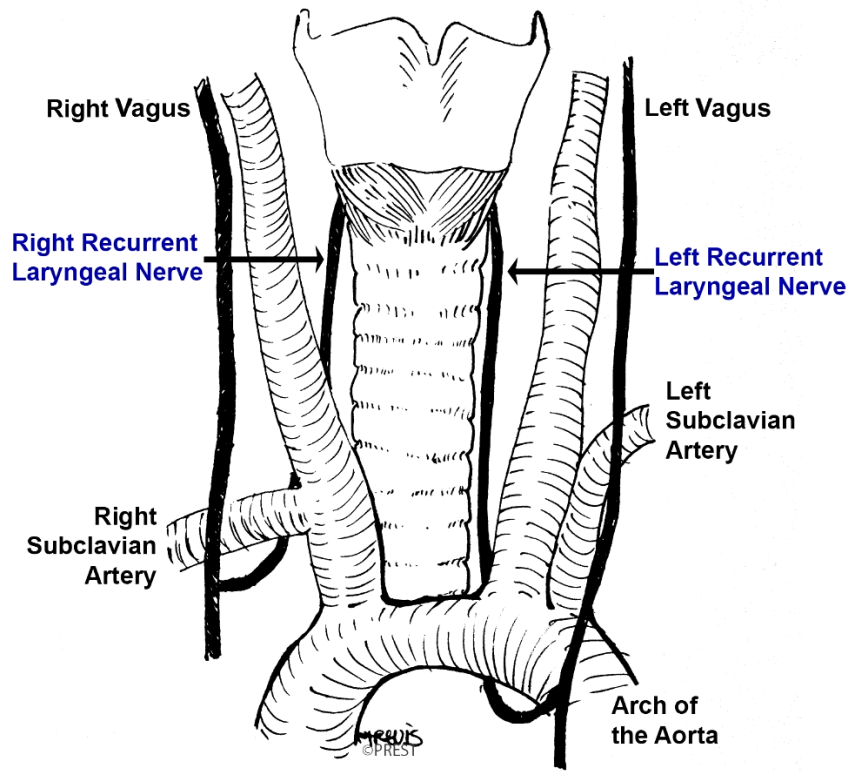


**Figure 22: Anatomy of the recurrent laryngeal nerve**

#### **4.2.5.2 Surgical Method for Canine Model of RLn**

Animals were placed in left lateral recumbency and a lateral approach to the larynx was made in a standard fashion anterior to the right linguofacial vein, the subcutaneous fascia was divided and the main trunk of the right Recurrent Laryngeal nerve (RLn) identified ( 22). The RLn was identified and transected 15 mm inferior to the cricoid. We performed these experiments on the right side of the larynx as there is some evidence for reduced functional recovery of left RLn injury compared to right, although the mechanism for this difference is unclear [204]. Endoscopy using a rigid endoscope (2.7 mm diameter, Olympus) was performed to verify right sided paralysis immediately after surgery.

Animals were randomly (computer generated code) divided into three groups. In the control group RLn transection was immediately followed by end-end RLn-RLn anastomosis performed using 3 epineural stitches of nylon 9-0 suture. Care was taken to avoid driving the needle or suture through the nerve fascicles. The anastomosis was surrounded by a preplaced empty 7 mm silicone conduit (3.5 mm internal diameter, Silastic; Dow Corning, Midland, MI) tagged to the perineurium at either end. In the two treatment groups the conduit was filled with either ECM derived from equine motor nerve (PNM); or with ECM derived from Urinary Bladder Matrix (UBM) and introduced into the conduit lumen via an 18-gauge needle. Hydrogels were brought to room temperature 5 minutes prior to injection into the conduit. The incision was then closed in layers.

Animals were euthanized at 6 months following implantation and laryngeal muscles and nerves harvested bilaterally for histology and immunohistochemistry.

Endoscopy using a rigid endoscope (2.7 mm diameter, Olympus) was performed immediately following surgery, and at 2 and 6 months to assess arytenoid movement under light sedation (dexmedetomidine (1 mcg/kg IV)) [205, 206].

#### **4.2.6 Common Peroneal Functional Index and Sciatic Functional Index**

Walking track analysis was used to determine hind limb function using a modified peroneal functional index (PFI) before injury (week 0) and 2, 4, 8, 12 and 16 weeks after repair [207]. Briefly, a minimum of three walking track assessments were obtained by inking the rat's feet, using an oversized inking pad (Ranger Industries, Tinton, NJ), and then permitting them to run across a single 43 cm long by 10 cm wide piece of plain white paper within a clear Perspex corridor. Three trials for each rat at each time point were retained for analysis, and rejection of a trial occurred if the rat paused or stopped in the middle of the trial or otherwise did not maintain a relatively constant velocity or if the prints made were unusable due to poor inking. Walking tracks were scanned into digital images (CanoScan LiDE 110, Canon USA, Inc, Melville, NY), and measurements for print length (PL, the distance between cranial extent of digit III and caudal extent of the print); total spread (TS, the distance between the centers of paw pad I and paw pad V); intermediate toe spread (IT, the distance between the centers of paw pad II and paw pad IV); distance to the opposite foot (TOF, the vertical distance between the cranial aspects of contralateral prints) and deviation angle (DA, the angle of the foot with respect to the direction of travel; destination = 180°) obtained, with concealment of group allocation, using Photoshop CS6®

software (Adobe Systems, Inc., San Jose, CA). All measurements for all prints were recorded for each trial (usually 2 prints per limb) and mean measurements determined from all ipsilateral prints.

Factors contributing to PFI (PL, IT and DA) were calculated as a percentage of baseline (preinjury) value rather than as a percentage of the contralateral limb. Modified PFI was calculated as  $PFI = (-55.47 \times PL) + (74.87 \times IT) + (163.43 \times DA) - 2.18$ . A mixed effect model was fitted to the data with animal identity as a random effect. Time after injury (weeks) was treated as a categorical variable to allow for a non-linear effect of time and an interaction term (time\*group) included. Tukey's post hoc tests and linear contrasts were used as appropriate. Statistical analysis was performed using one-way ANOVA and Tukey post-hoc with SPSS (IBM Corporation, Armonk, NY, USA) or JMP (SAS Institute, Cary, North Carolina, USA). Significance was set at  $p < 0.05$  throughout.

Standard metrics for Sciatic Functional Index (SFI) was captured at mid-stance phase ( 23). A custom MatLab program was written to collect the measure the data from video stills and to calculate the SFI measurement (Appendix B.1.1). Each measurement was captured 3 times per video.

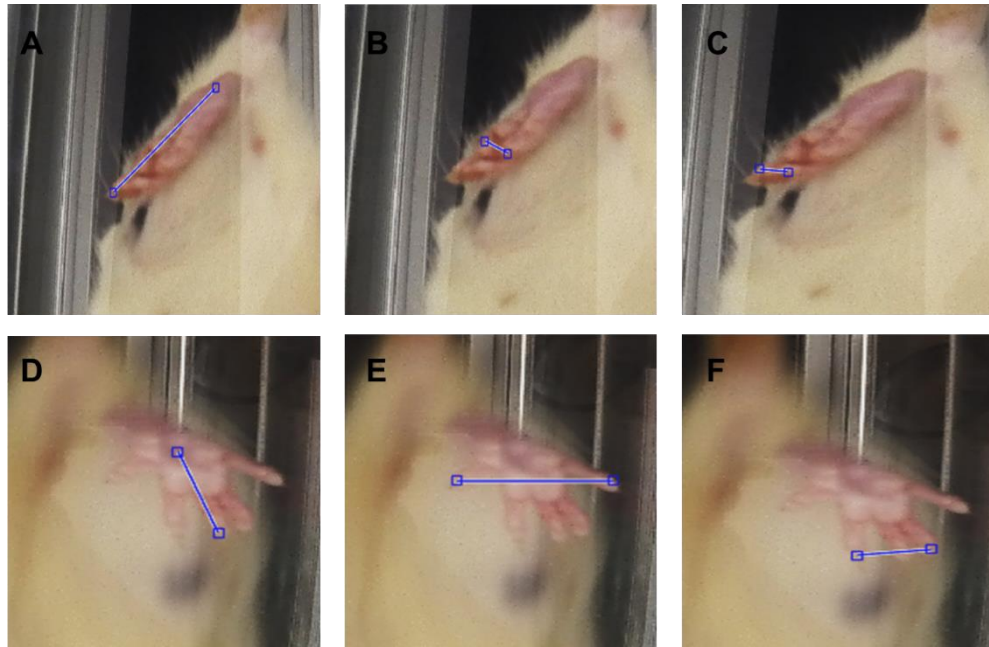


**Figure 23: SFI measurements in a rat model of sciatic nerve defect injury**

(A-C) Measurements for injured side including (A) print length from middle finger to heel, (B) outer toe spread from 1<sup>st</sup> and 5<sup>th</sup> digits, and (C) the inner toe spread from 2<sup>nd</sup> and 4<sup>th</sup> digits. (D-F) Contralateral side measurements including (A) print length, (B) outer toe spread, and (F) inner toe spread.

#### **4.2.7 Kinematics Collection and Analysis**

Functional assessment was performed using MotoRater (TSE systems), a semi-automated system for rodent kinematic gait analysis. Animals were evaluated at weeks 0, 1, 2, 3, 4, and every even week following, out to 24 weeks. Three videos were captured per rat per timepoint. Simi

Motion movement analysis software was used to place tracking dots at various joints of the body and at key phases of gait. Ankle angle was captured at toe-off to assess the function of the gastrocnemius muscle. Tracking dots were placed on the forefoot, ankle, and knee of the rat. These locations were tattooed onto the rat before surgery ( 24).

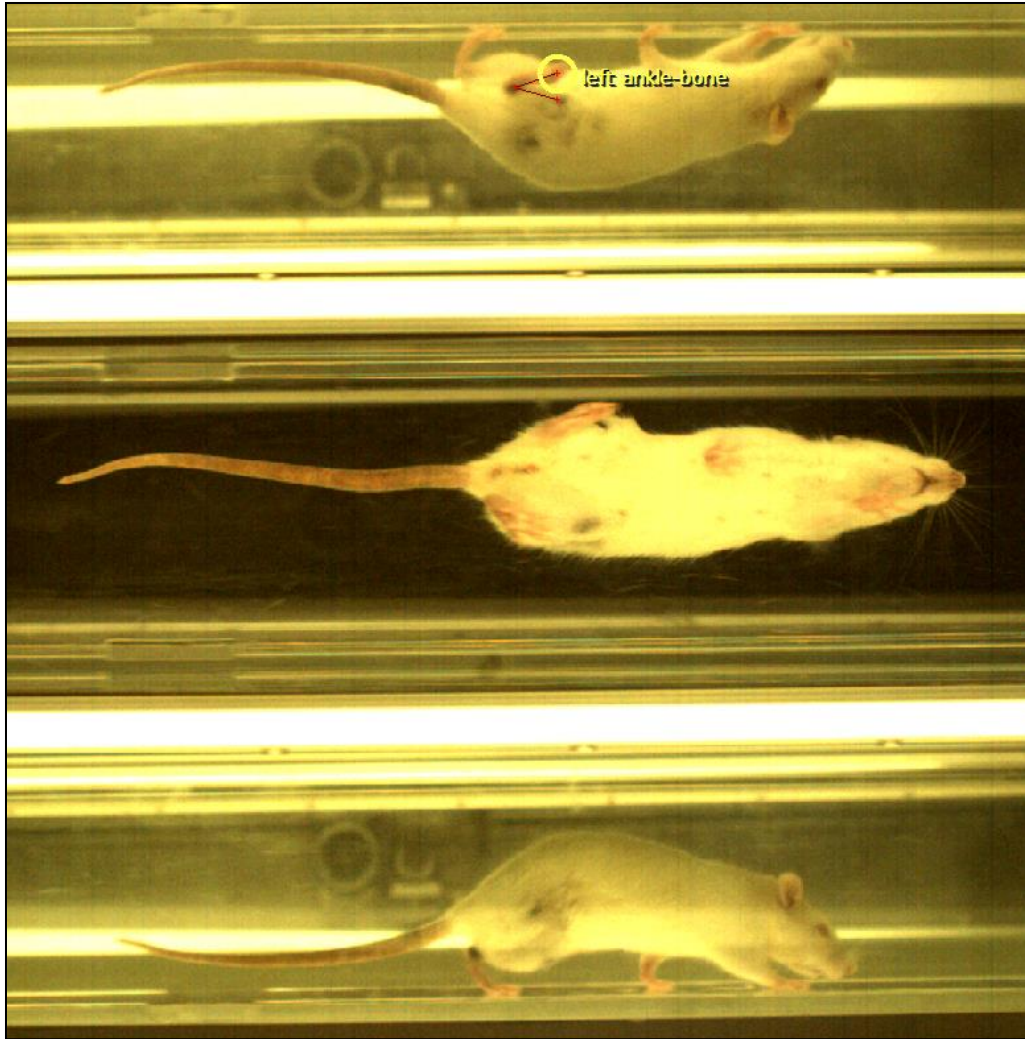


**Figure 24: Representative still of kinematic analysis videos from TSE MotoRater**

#### **4.2.8 Nociception Testing with Von Frey Fibers**

Nociception, or the perception and processing of noxious stimuli was assessed by using a series of von Frey fibers. A custom cage was created with metal mesh screen floor (#14, 1.41 mm). Animals were evaluated at weeks 0, 1, 2, 3, 4, and every even week following out to 24 weeks. Animals were placed into the custom cage and both injured and uninjured rear paws were tested for nociception response. Briefly, starting with a 10 g von Frey fiber the paw was test four times. If the animal responded to at least two of the four tests the next smallest von Frey was used otherwise the next larger fiber was used. The process is repeated until the direction is changed from decreasing size to increasing size three times [208].

#### **4.2.9 Electrophysiologic Analysis of Evoked CMAP**

Electrical conduction of the sciatic nerve was assessed using invoked compound muscle action potential of the tibialis anterior muscle. Briefly, the sciatic nerve was exposed using the same surgical approach as the original intervention. A stimulating probe was hooked around the sciatic nerve proximal to the injury and two recording hook electrodes were embedded into the center body of the tibialis anterior. The sciatic nerve was tested at increasing stimulating amplitudes (0.04, 0.05, 0.06, 0.07, 0.08, 0.09, 0.1, 0.2, 0.3, 0.4, 0.5, 0.6, 0.7, 0.8, 0.9, and 1.0 mA). At each test, the nerve was stimulated twenty times for 200 us and at 10 V. The average root mean square (RMS) value for each stimulating amplitude was calculated using MatLab. The minimal amplitude that achieved motor neuron activation saturation was selected and used for statistical comparisons.

For canine study of the recurrent laryngeal nerve transection a different method was used. Immediately prior to euthanasia, animals were anesthetized, and anesthesia was maintained with isoflurane in O<sub>2</sub> via an endotracheal tube capable of detecting evoked compound motor action potentials (CMAP) from the vocalis muscle following proximal stimulation of the recurrent laryngeal nerve (NIM EMG Endotracheal tube, (inner diameter 7.0 mm, outer diameter 10.5 mm) Medtronic) [209]. Endoscopy was performed during the same anesthetic episode and the degree of arytenoid abduction at peak inspiration determined under light sedation.

The right RLn was exposed by dissection in the mid cervical region and a single monopolar needle (Neuroline monopolar, AMBO Inc.) placed adjacent to the RLn 10 cm caudal to the anterior ring of the cricoid cartilage. A supramaximal pulse (8-14 mA) was applied to the monopolar needle and the corresponding CMAP recorded at the vocalis muscle (Sierra Wave II, Caldwell Laboratories, Kennewick, WA). Presence/absence and peak amplitude of each CMAP was recorded for each of three repetitions. This procedure was repeated on the left side.

Raw CMAP data was exported as a text file and analyzed using custom software written in MATLAB to determine peak amplitude and area of the CMAP. Mean values were determined from the three CMAPs recorded on each side. For each parameter, differences between left and right CMAPs was determined using Wilcoxon-signed rank tests

#### **4.2.10 Staining of NF200 to Analysis Axon Growth Across Injury**

Nerve tissue was subjected to a series of increasing sucrose washes, cut cross-sectionally at the half-way point across the conduit or graft, and then embedded in OCT. For the gap injury, cross sections 10 µm thick were taken every 2mm, collecting samples from the midpoint, and then

$\pm 2$ mm, and  $\pm 4$ mm from the midpoint. Crush injury nerves were only sampled at the distal portion of the sciatic nerve. The slides were then stained for neurofilament heavy chain (NF200) for axons. Consecutive sections were incubated with NF200 antibody (1:300, Sigma) overnight. Corresponding secondary antibodies (1:300, Alexafluor) were given for 1 hour. Sections were then washed with PBS (1X) and cover-slipped. Crush sections were also stained for S-100 for Schwann cells and Fluoromyelin. Consecutive sections were incubated with Fluoromyelin (1:400, Life Technologies) and anti-S-100 antibody (1:200, Sigma) overnight. Corresponding secondary antibodies (1:100, Alexafluor) were given for 1 hour.

#### **4.2.11 Histologic Analysis of Downstream Muscles**

The gastrocnemius muscle collected from both legs at 12 weeks post-surgery was fixed in 10% neutral buffered formalin. The tissue was cut cross sectionally across the thickest region of the muscle. Tissue was paraffin embedded and 8 $\mu$ m thick slides were produced for histology. Hematoxylin and Eosin (H&E) staining was performed to visualize the muscle structure and five 10X images per slide were taken and assessed for fiber diameter. The minor diameter of twenty fibers were measured per image using ImageJ. Macroscopic images of the cross-sectional muscle were also taken, and total cross-sectional area was measured using ImageJ.

For canine study of the recurrent laryngeal nerve transection a different method was used. Posterior cricoarytenoid (PCA) and lateral cricoarytenoid (LCA) muscles were harvested from explanted larynges and weighed. Collagen V immunohistochemistry was performed on mid sections of left and right PCA and LCA muscles and minimum fiber (Feret's) diameters determined using custom semi-automated software written in MatLab. 8  $\mu$ m thick cryosections of

acetone-fixed muscle were used for immunohistochemical analysis. Cryosections were washed with phosphate buffered saline containing 0.05% Tween 20 (PBST) for 3 times (5 min each). Nonspecific staining was blocked with a mixture of 10% rabbit serum and 2% casein for 30 minutes at room temperature. The primary antibody goat anti-*type V collagen* antibody (SouthernBiotech, Birmingham, AL) was diluted to 1:1,000 in PBS containing 1% casein, and the sections were incubated for 1.5 hr at 37° C. Biotinylated rabbit anti-goat IgG (Vector Laboratories, Burlingame, CA) was diluted to 1:200 in PBS and incubated for 30 min at room temperature. Finally, streptavidin-Texas Red (Molecular Probe, Life Technologies, Grand Island, NY) was used to visualize positive staining (used at 1:200 in PBS), and then the sections were mounted in Vectashield containing Dapi (Vector Laboratories). PBST was used for washing throughout the procedure. Goat IgG was diluted to the same final concentration as primary antibody was used as a negative control. IHC results were examined and photographed using Olympus AX 70 compound microscope.

## 4.3 Results

### 4.3.1 Improvement of Function with a Sciatic Nerve Defect Model

SFI from a rat model of critical-length sciatic nerve defect. Groups include a 17 mm silicone conduit with PNM 10 mg/mL lumen filler (PNM10), flipped and replaced nerve section repair (Autograft), and complete resection of the nerve without repair (No Repair, not shown). PNM was used in a critical length defect model test return of function. The equation described by Bain et al. was used (Figure 25A). Abbreviations shown within the equation are E (experimental side), N (contralateral side), PL (print length), TS (outer toe spread), and IT (intermediate toe spread) (Figure 25A). As previously described, this equation uses the paw lengths and the paw widths between the 1<sup>st</sup> and 5<sup>th</sup> digits, and the 2<sup>nd</sup> and 4<sup>th</sup> digits from each paw. Representation of the six measurements taken for SFI as well as representative ink prints from weeks 0, 2, 4, and 6 are shown in (Figure 25B, C). Ink was applied the hind feet of the rat and each rat was subsequently allowed to traverse across a platform with a paper lining, leaving their hind paw prints behind (Figure 25C). The prints were photographed and a MatLab code was written to analyze the images (Appendix B.1.1). SFI from this study showed similar outcomes between a conduit with PNM10 as lumen filler and autograft. Functional outcomes trended towards being better for the PNM10 treatment as well (Figure 26A). A trend towards increasing values was observed for all groups including the negative control. This was controlled for by normalizing to the negative control which was an injury without repair (Figure 26A).

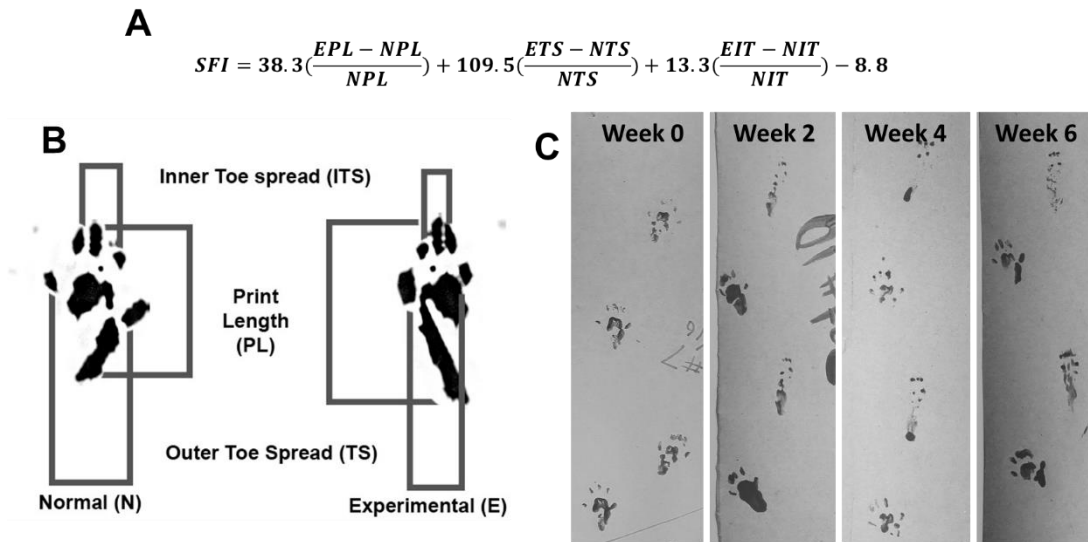


**Figure 25: Representation of SFI walking track analysis using inked paw prints**

(A) Equation used for deriving SFI. Abbreviations used are E (experimental side), N (contralateral side), PL (print length), TS (outer toe spread), and IT (intermediate toe spread). (B) Location of the SFI measurement on a rat paw print. (C) Example of collected prints from a rat sciatic nerve gap defect injury at weeks 0, 2, 4, and 6.

However, a limitation to this comparison is the amount of contracture that formed in the autograft group (Figure 26B). At 20 weeks, all autograft animals had developed some form of contracture. Contracture can signify an imbalance in functional return or the presence of synkinetic innervation. Regardless of cause, paw contracture negatively impacts SFI and is a possible explanation for why the autograft appears to have performed poorly.

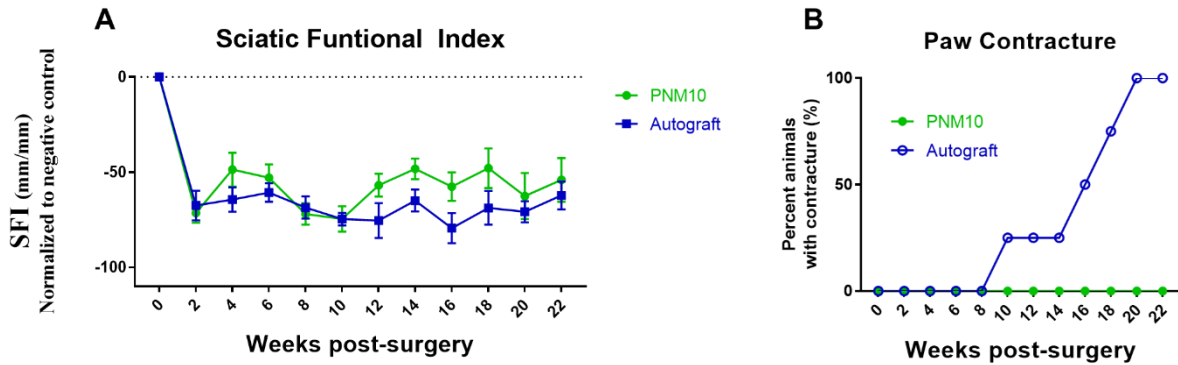


**Figure 26: SFI for PNM in a pilot rat critical length sciatic nerve defect**

(A) SFI collected over 22 weeks and normalized to no repair group to remove variability in collection and analysis or non-recovery related adaptations. (B) Paw contractures that limit the reliability of the SFI measurement was tracked. All autograft animals developed contractures while no PNM treated animals did.

#### 4.3.2 Improvement of Function with a Common Peroneal Defect

As anticipated, modified peroneal functional index decreased significantly after injury in both control and PNM groups ( $p < 0.001$ , 27). Partial recovery was observed in the PNM group with significantly improved PFI 8 and 16 weeks after nerve repair compared to the control group (linear contrasts  $p = 0.004$  and  $p = 0.006$  respectively,  $n = 6$ ). Overall the interaction term (week x group) was significant ( $p = 0.03$ ) as were fixed effects for group ( $p = 0.01$ ) and week ( $p < 0.001$ ). Model fit was good (Adjusted  $R^2 = 0.87$ ) and model assumptions were met. While some autophagy

was observed in the previous study of sciatic nerve transection and gap, autophagy was not observed in any of the rats for this study. The most obvious difference is the severity of the injury involved here was not as great.

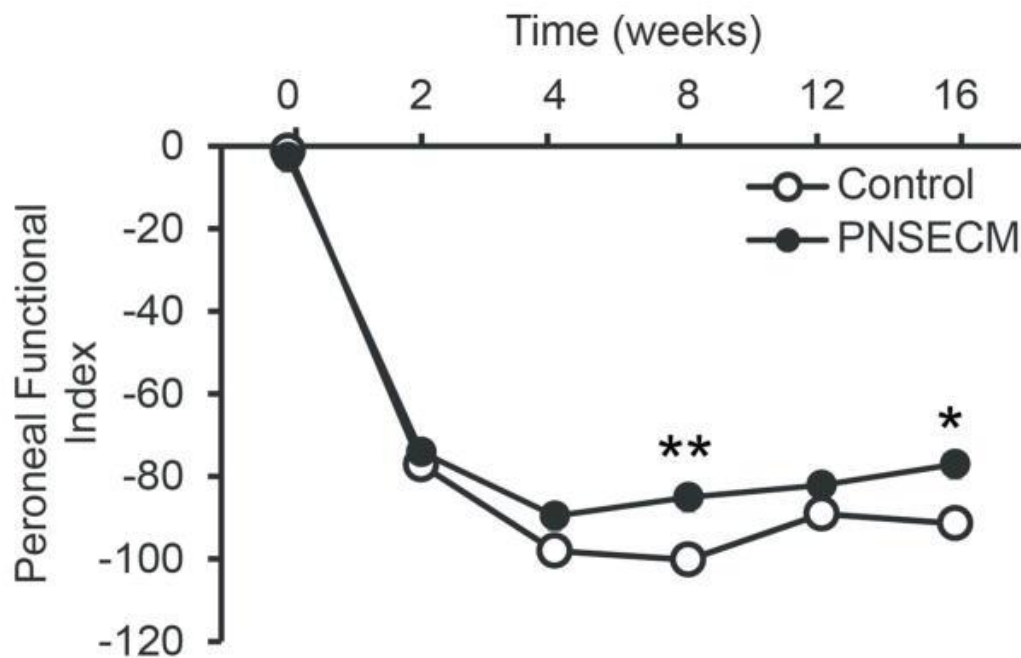


**Figure 27: Common Peroneal Nerve Functional Index (PFI)**

PNM improves hind limb function determined by walking track analysis and modified peroneal functional index. PFI was significantly higher in the PNM group 8 and 16 weeks after nerve repair compared to the control group (linear contrasts  $p=0.004$  and  $p=0.006$  respectively,  $n=6$  / group).

### **4.3.3 Assessment of Functional Recovery in a Rodent Sciatic Nerve Gap Defect Model**

#### **4.3.3.1 Functional Assessment Using Walking Track Analysis**

SFI and ankle angle at toe-off (end of stance phase) were collected from MotoRater (TSE Systems, Chesterfield, MO) videos. PNM had been previously shown to enhance cellular response to peripheral nerve injury including macrophages and Schwann cells. This study focused on electrophysiology and downstream function. Four metrics of regeneration were collected SFI, ankle angle at toe-off, nociception, and compound motor action potential (CMAP) ( 28). Walking track analysis showed an approximately 30-point improvement in SFI after 24 weeks for all three treatment groups (PNM10, PNM20, and PNM40) ( 28A). No dose dependent effect was observed between the three groups. Autograft treated animals recovered by 40-point by the end of the study. The autograft was significantly different (Two-way ANOVA,  $p < 0.01$ ) from all groups except for PNM40 ( $p = 0.057$ ).

Ankle angle was taken at the end of the stance phase during toe-off ( 28B). This is a direct measure of gastrocnemius muscle function during normal locomotion. All treatment groups saw a 200% improvement in ankle angle by the end of study but did not differ from conduit control. By 24 weeks, only autograft is significantly different then conduit control ( $p < 0.001$ ). Ankle angle was the metric most susceptible to the effects of weight change. Over 24 weeks, animals gained weight especially male rats who over doubled in weight.

Nociception, or the response to noxious stimuli was tested using graded von Frey fibers ( 28C). This graph also includes controls from a separate study that followed the same methods including dissection only without injury (DO-NT), no injury or surgery (NI-NT), and transection and ligation to prevent recovery (T-NT). Von Frey testing was expected to be a rigorous test of both sensory and motor function of the affected limb, however controls that were expected not to

recovery (T-NT) began to respond to stimuli. Though the response was not equivalent with dissection only or no injury. This could have been a product of the tester or learned behavior of an unrelated stimulus. Whatever the cause, the controls showed that the experiment did not provide as reliable of testing for sensory recovery.

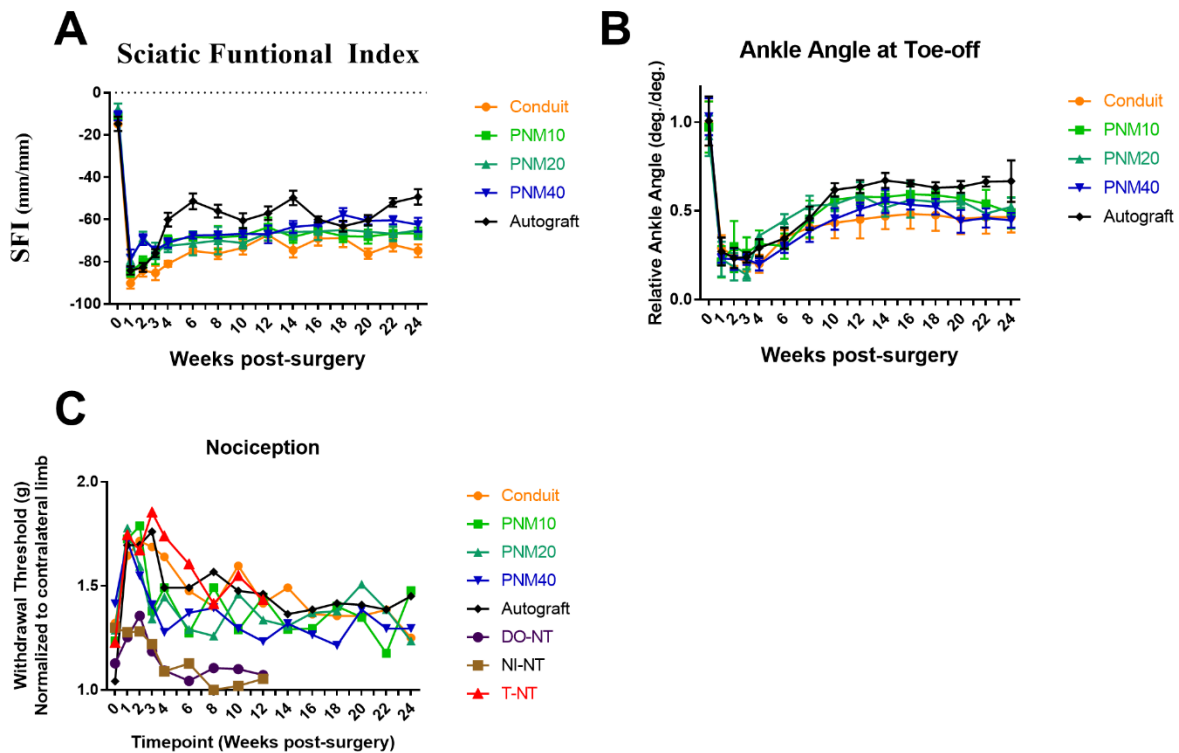


**Figure 28: Functional metrics for a rat model of sciatic nerve defect**

Abbreviations used: PNM10, conduit repair with 10 mg/mL PNM hydrogel as lumen filler; PNM20, conduit repair with 20 mg/mL PNM hydrogel as lumen filler; PNM40, conduit repair with 40 mg/mL PNM hydrogel as lumen filler; DO-NT, dissection down to nerve only with no

nerve injury; NI-NT, no surgery; T-NT, transected and ligated nerve to prevent regrowth (A) SFI and (B) ankle angle at toe-off (end of stance phase) collected from MotoRater (TSE Systems, Chesterfield, MO) videos. (B) Ankle angle is shown as a ratio of injured extremity over uninjured. (C) Nociception tested using von Frey fibers and results show the raw withdrawal thresholds (g).

While differences were not observed at the 24 week timepoint ( 29B), earlier in the study animals showed improvements that resembled more the autograft than the negative control ( 29A, C). SFI at 4 weeks for PNM10 treated animals showed significant differences from negative control (\*,  $p < 0.05$ , 29A). At this timepoint, the autograft was already significantly different from the negative control as well (\*\*\*\*,  $p < 0.0001$ , 29A). Ankle angle also showed early improvements at the 4-week timepoint ( 29C). Both PNM10 and PNM20 were significantly better than the negative control (\*\*,  $p < 0.01$ , \*\*\*,  $p < 0.001$ , 29C). Both were not significantly different from the autograft control.

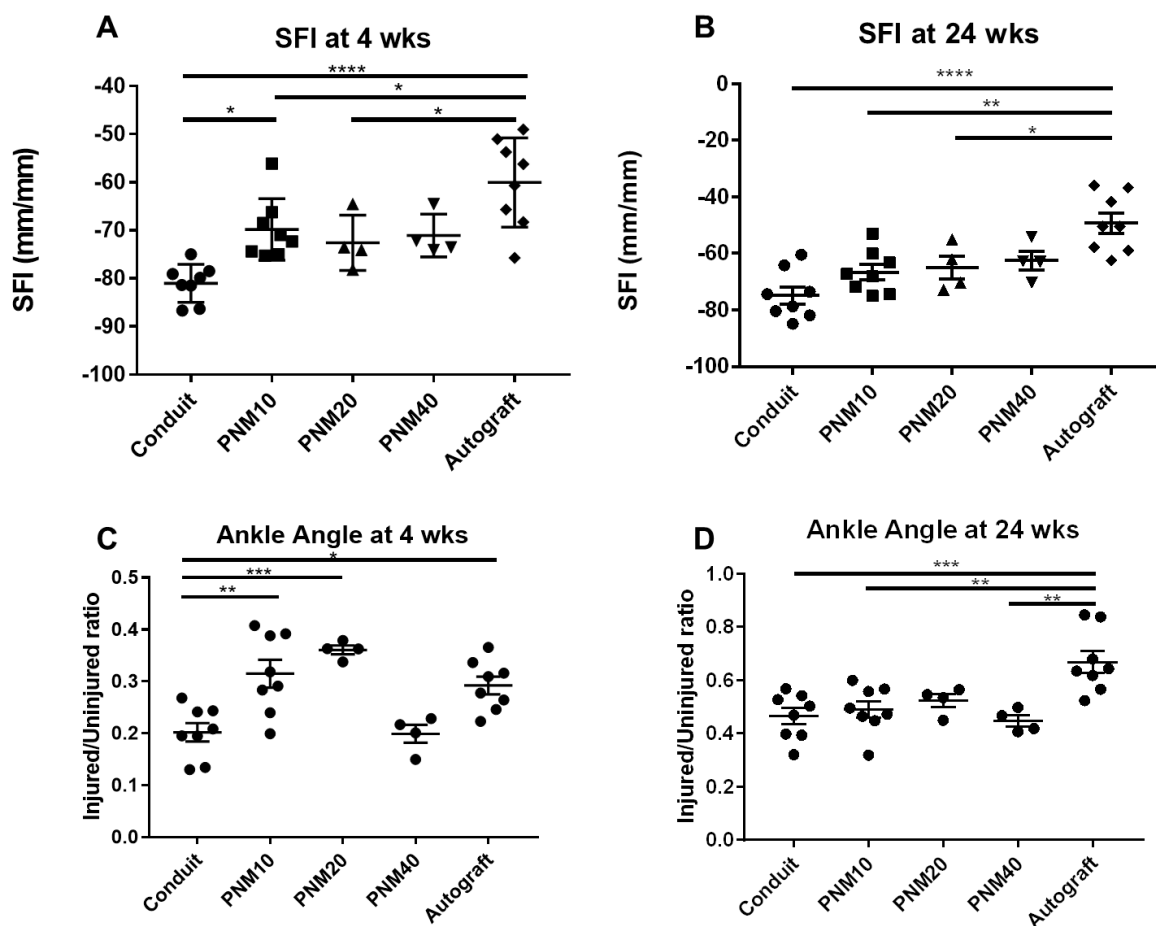


**Figure 29: Assessment of SFI and ankle angle at 4 and 24 weeks**

SFI at 4 weeks (A) and 24 weeks (B) as well as ankle angle at 4 weeks (C) and 24 weeks (D). Difference between conduit and PNM treatment groups are significantly larger after the first month. (\*,  $p < 0.05$ , \*\*,  $p < 0.01$ , \*\*\*,  $p < 0.001$ , \*\*\*\*,  $p < 0.0001$ ,  $n = 4-8$ ).

#### **4.3.3.2 Electrophysiologic Function of Sciatic Nerve at the Tibialis Anterior Muscle**

The sciatic nerve was stimulated above the graft site and the stimulus response was measured at the tibialis anterior muscle by hook electrodes. Stimulus responses were collected across a range of stimulus currents. At each stimulus current, 20 response curves were collected. These were overlaid using MatLab before analyzing ( 30). The 20 response curves for each stimulus current remained consistent and a current. A stimulus current of 0.8 mA was chosen based on stimulus curves ( 31B) to reduce signal clipping at higher intensities. CMAP amplitude analysis was not performed because some clipping was still present and response curves were not simple single peak CMAPs, therefore a different analysis method was used. Analysis was done by taking the root mean square (RMS) of the curves using a MatLab code. Furthermore, response curve complexity was assessed by taking the derivative of the curves. Only conduit differed significantly in the population of stimulus responses at the selected stimulation curve ( 31A). The CMAP RMS after 6 months for the treatment groups were statistically similar to the autograft group and were significantly different than the transection and ligation negative control (T-NT) ( 31C). The autograft was statistically similar to PNM groups but had not returned to a normal CMAP response although was also similar to the dissection only, sham procedure.

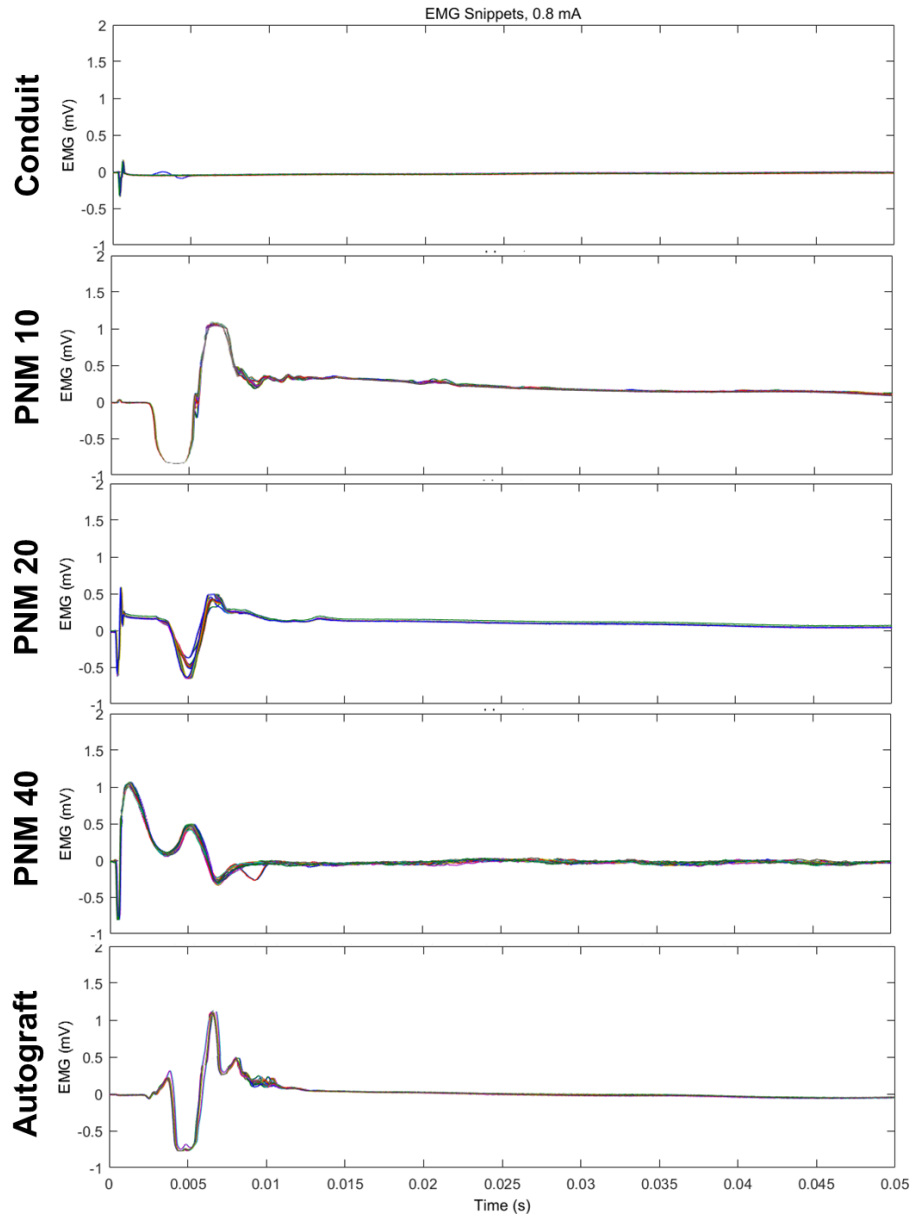


**Figure 30: Representative compound motor action potential traces of the sciatic nerve measured at the tibialis anterior**

Abbreviations used: PNM10, conduit repair with 10 mg/mL PNM hydrogel as lumen filler; PNM20, conduit repair with 20 mg/mL PNM hydrogel as lumen filler; PNM40, conduit repair with 40 mg/mL PNM hydrogel as lumen filler; Sample traces collected at 0.8 mA.

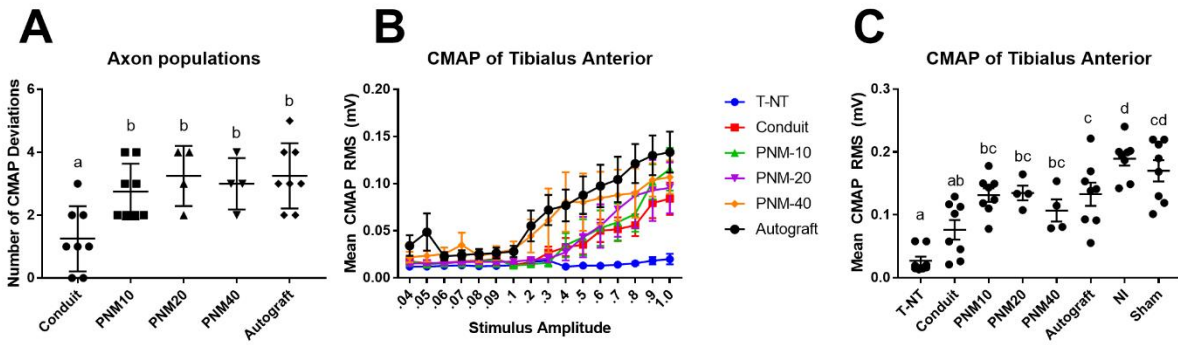


**Figure 31: Compound motor action potential of the sciatic nerve at the tibialis anterior muscle**

(A) Number of unique CMAP responses possibly denoting separate axon populations responding to the stimulus. (B) Response curves were taken from an increasing range of stimulation currents. The mean CMAP RMS is plotted for each stimulation current. Further readings shown at 0.8mA. (C) Mean CMAP RMS of the groups collected at 0.8 mA. Differing letters denote statistical significance ( $p < 0.05$ ) and error bars show standard error.

#### 4.3.3.3 Assessment of Axons Crossing the Nerve Defect Injury

The number of axons across the defect injury was quantified through immunofluorescent imaging and image analysis using Cell Profiler. Representative images show staining of NF200 of the distal (-4mm from midline injury) segment ( 32A). Qualitatively, the bridge formed in the PNM10 treatment group produced was similar to that of the autograft, while the PNM20, PNM40, and conduit were smaller in size ( 32A). All groups except for PNM10 showed a slight decrease

from proximal to distal portions of the defect ( 32B-F). Overall, both PNM10 and PNM20 showed a significantly greater number of axons at the distal portion of the defect than the negative control (conduit) and all three PNM treatment groups were similar to the autograft control ( 32G). Error bars show standard error and different letters denote statistical significance ( $p < 0.05$ ).



#### **4.3.4 Assessing Functional Recovery in a Rat Model of Sciatic Nerve Crush**

The sciatic nerve was crushed using a bulldog clamp with a calibrated force of 500 g. This force deformed 2 mm of nerve tissue, flattening it ( 21B) and causing a complete disruption of signal conduction across the injury. Intraneural injection of the PNM hydrogel caused a slight bulging of the epineurium in the dissection only ( 21A) while the crushed nerve was swelled back to normal dimensions ( 21C).

##### **4.3.4.1 Safety of Direct PNM Hydrogel Injection into Nervous Tissue**

Intraneural injection is generally considered to be safe for anesthesia reasons, with very low risk of peripheral nerve injury complication. However, intraneural injection is not a common practice as a treatment for traumatic nerve injuries. Our test of the safety of PNM injection directly into the nerve (dissection only with PNM injection, DO-PNM), found little to no change in SFI ( 33A) and ankle angle ( 33). Nociception shows no difference between groups whether in withdrawal threshold (g) ( 33C) or normalized to the positive control ( 33D).

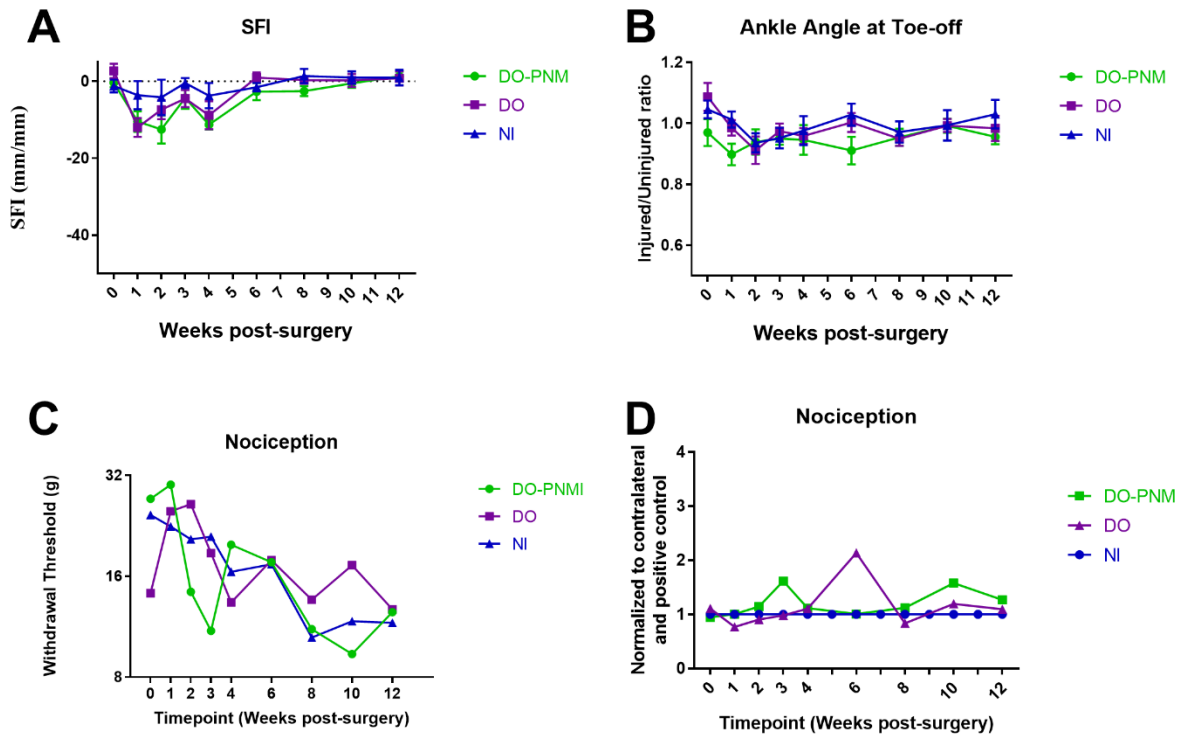


**Figure 33: Safety of PNM hydrogel injection into nervous tissue**

Abbreviations used: NI, no injury or surgery; DO-PNM, dissection down to nerve and PNM injection into healthy nerve; DO, dissection down to nerve without injury. (A) SFI and (B) ankle angle at toe-off (end of stance phase) collected from MotoRater (TSE Systems, Chesterfield, MO) videos. (B) Ankle angle is shown as a ratio of injured extremity over uninjured. (C) Nociception tested using von Frey fibers and results show the raw withdrawal thresholds (g) as well as values normalized to both contralateral side and positive control (D)

#### **4.3.4.2 Intraneural Injection of PNM as a Treatment for Peripheral Nerve Injury**

SFI is a well cited metric for measuring function after sciatic nerve injury. Our controls matched expectations of this metric with the transection and ligation (T-NT) showing no recovery and no injury (NI) remaining at normal. SFI showed that the crush injury returns to normal by 6 to 8 weeks regardless of treatment (Figure 34A). PNM scored significantly higher than crush alone at weeks 2 and 3 ( $p < 0.05$ ). Ankle angle at toe-off is representative of gastrocnemius function during normal gait. This metric also shows a return to normal function of the gastrocnemius by 6-8 weeks (Figure 34B). Function was significantly enhanced for C-PNM over C-NT for weeks 3 and 4. Nociception shows a development of a transient hypersensitivity to noxious stimulus during the first month after the injury (Figure 34C, D). This response is resolved for both crush groups (C-NT, C-PNM) by 6-8 weeks. Transection and ligation group has a steady reduction in sensitivity.

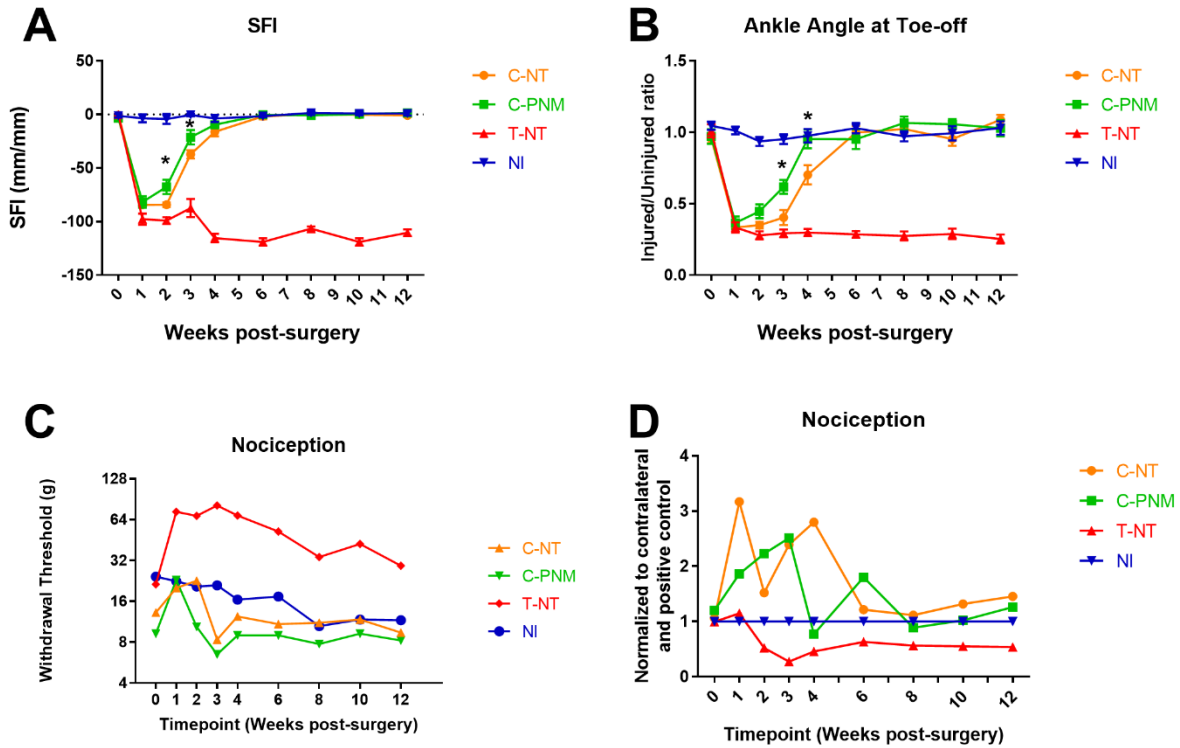


**Figure 34: Intraneural injection of PNM as a treatment for peripheral nerve injury**

Abbreviations used: C-NT, crush with no treatment; C-PNM, crush with PNM injection; T-NT, transection and ligation to prevent regrowth; NI, no injury or surgery. (A) SFI and (B) ankle angle at toe-off (end of stance phase) collected from MotoRater (TSE Systems, Chesterfield, MO) videos. (B) Ankle angle is shown as a ratio of injured extremity over uninjured. (C) Nociception tested using von Frey fibers and results show the raw withdrawal thresholds (g) as well as values normalized to both contralateral side and positive control (D)

#### **4.3.4.3 Axon Growth Across Injury in Sciatic Nerve Crush Injury**

The number of axons distal to the injury was quantified through immunofluorescent imaging and image analysis using Cell Profiler. Representative images show staining of fluoromyelin, NF200, and combined of the tibial, sural, and cutaneous branch portion of the sciatic nerve. Qualitatively, a greater number of large, myelinated axons are present in the crush with PNM similar to the normal sciatic nerve fiber when compared to the crush injury without treatment ( 35A). Myelin appears disrupted in both crush with and without treatment and fewer axons were observed in crush without treatment. All four branches, tibial, sural, cutaneous, and peroneal were imaged and analyzed. Axon counts were normalized to the no injury group. and axon counts of the sciatic nerve distal to the injury show an increased in the number of axons crossing the injury.

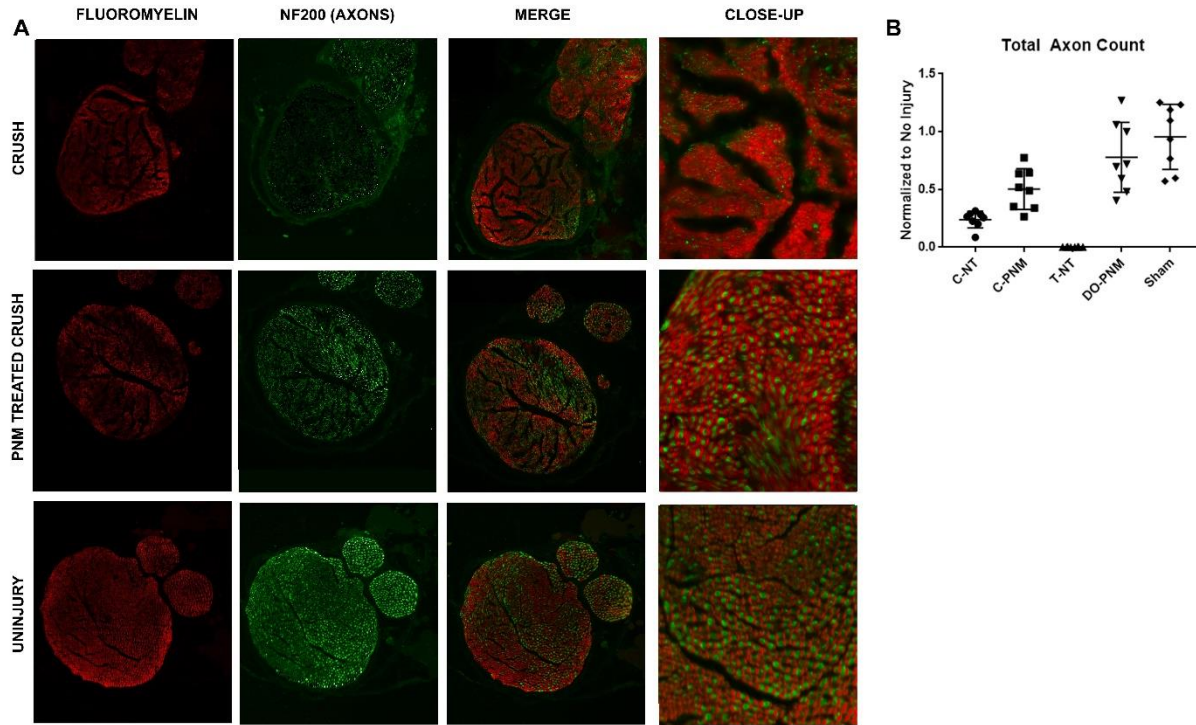


**Figure 35: Axon growth across injury in sciatic nerve crush injury**

(A) Representative cross section immunofluorescent images of NF200 and fluoromyelin staining for axons and myelin for no injury, crush with and without PNM treatment. (B) Axon count taken distal to the crush injury and processed using ImageJ (n=8).

#### 4.3.4.4 Atrophy of Downstream Muscle

The gastrocnemius muscle is a 50:50 mixed fast and slow twitch muscle innervated by tibial branch of the sciatic nerve. Both muscle fiber diameter and total cross-sectioned area was taken for both the injured and uninjured sides. We discovered that this level of nerve injury either

was not sufficient to produce muscle atrophy or that muscle atrophy recovered by the end of the 90-day timepoint. The negative control (T-NT) demonstrated the maximal atrophy possible within the 90-day timepoint. Transection and ligation (T-NT) produced a significant shrinking of both muscle fiber diameter and muscle size by 30% and 60% ( $p < 0.05$ ,  $n=8$ ), respectively (Figure 36A, B). Representative images of the injured side muscle show a slight effect of the crush injury but not a significant difference between crush with and without treatment (Figure 36C).

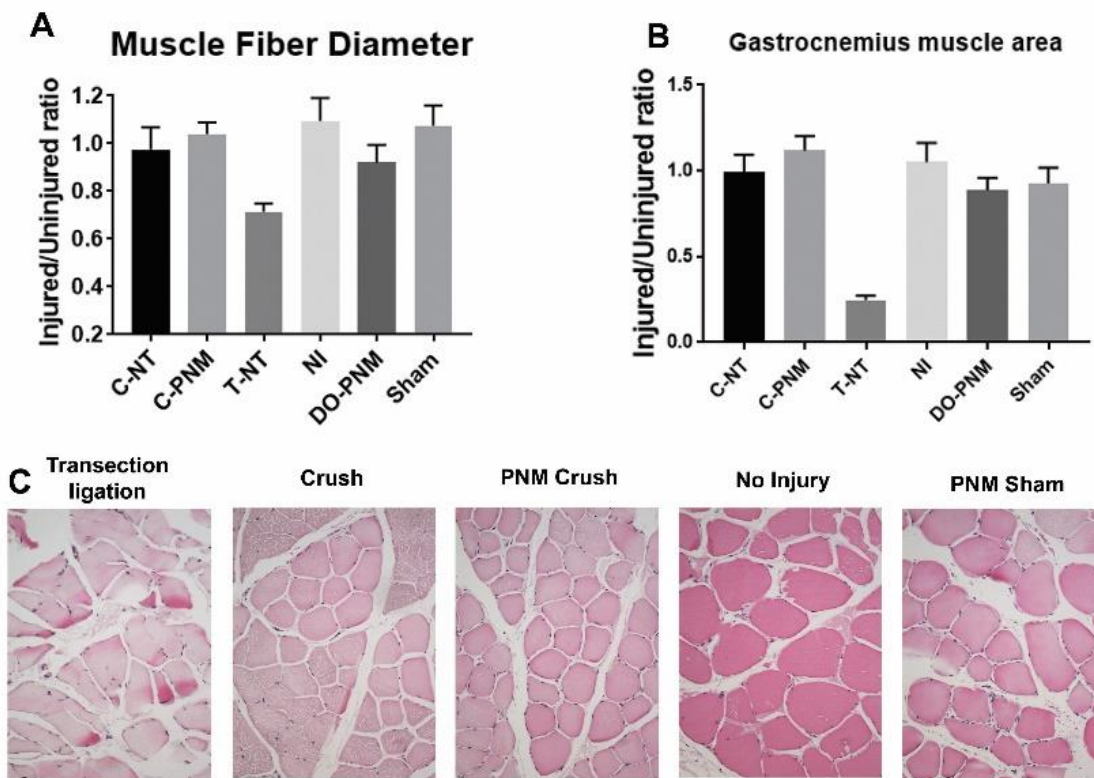


**Figure 36: Atrophy of gastrocnemius muscle after sciatic nerve crush injury**

Abbreviations used: C-NT, crush with no treatment; C-PNM, crush with PNM injection; T-NT, transection and ligation to prevent regrowth; NI, no injury or surgery; DO-PNM, dissection down to nerve and PNM injection into healthy nerve; Sham/DO, dissection down to nerve without injury. (A) Minimum fiber diameter of the gastrocnemius as a ratio of injured over uninjured

muscle. T-NT is significantly different from all other groups ( $p < 0.001$ ). **(B)** Gastrocnemius cross-sectional area as a ratio of injured over uninjured muscle. T-NT is significantly different from all other groups ( $p < 0.001$ ). **(C)** Representative cross-sectional images of injured gastrocnemius muscle stained with H&E.

#### 4.3.5 Electrophysiology of Downstream Muscle

Evoked CMAP of the tibialis anterior performed healthy nerve and immediately after injury shows that the crush model achieves complete disruption in conduction ( 37A). The sciatic nerve proximal to the crush site was excited with an increasing range of stimulation amplitudes. Complete stimulation range included 0.04, 0.05, 0.06, 0.07, 0.08, 0.09, 0.1, 0.2, 0.3, 0.4, 0.5, 0.6, 0.7, 0.8, 0.9, and 1.0 mA and further results shown, and comparisons were made from the 0.8mA reading (Figure 37B).

Average RMS was taken from 20 trances at each stimulation amplitude and overall averages are showed (Figure 37B). Both raw traces and average RMS was assessed for a stimulation amplitude that produced a supramaximal excitation. A stimulation amplitude of 0.8 mA was selected, and those results shown (Figure 37C). Direct injection into nerve did not have a significant impact on electrical conduction (Figure 37C). Application of PNM (C-PNM) significantly increased CMAP over crush alone (C-NT) ( $p < 0.05$ ) and was similar to no injury

(Figure 37D). These results show roughly a 50% increase in conduction for the treatment group over crush alone. PNM injected into a sham control did not significantly affect evoked CMAP and both C-PNM and DO-PNM were not significantly different from no injury or sham groups.

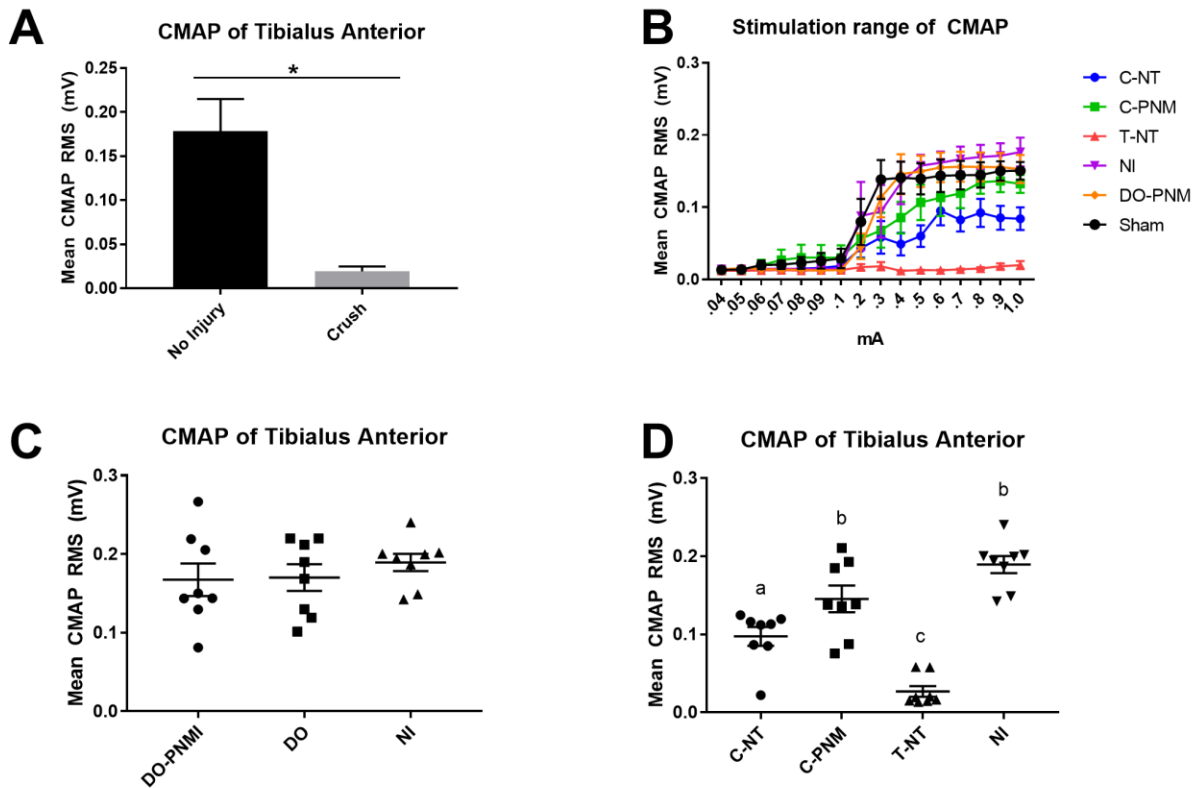


**Figure 37: Electrophysiology of tibialis anterior muscle after sciatic nerve crush injury**

(A) Mean CMAP RMS of normal, no injury and immediately post-crush. Electrophysiologic response shows a complete ablation of signal after crush. (B) Response curves were taken from an increasing range of stimulation currents. The mean CMAP RMS is plotted for each stimulation current. Further readings shown at 0.8mA. (C) Mean CMAP RMS of the groups investigating the safety of intraneural injection of PNM. No significant differences between PNM

injection and controls. (D) PNM enhanced CMAP over crush injury without treatment ( $p < 0.05$ ,  $n=8$ ) and not different than no injury group ( $p=0.08$ ,  $n=8$ ). Differing letters denote statistical significance ( $p < 0.05$ ) and error bars show standard error.

#### **4.3.6 Sex Base Variance in Compound Motor Action Potential Measures of Recovery**

A mix of female and male Lewis rats were used in this study to better represent the normal population. Several groups showed favorable recovery in females over males including the crush with PNM injection (Figure 38). However, these differences were only pronounced in the Compound motor action potential (CMAP) divided by sex for crush study (Figure 38A). No significant differences between sexes were observed in the nerve gap defect study (Figure 38B).

While significance was not found due to small sample size between sexes, the trend still suggests there could be some sex-based variance in peripheral nerve recovery. Earlier studies in the literature have shown that sexually dimorphic hormones and steroids such as testosterone and progesterone, play an active role in nerve regeneration. Concentrations of these neuroactive steroids differ between male and female rats and could lead to this difference seen in this study between male and female rats [210-212].

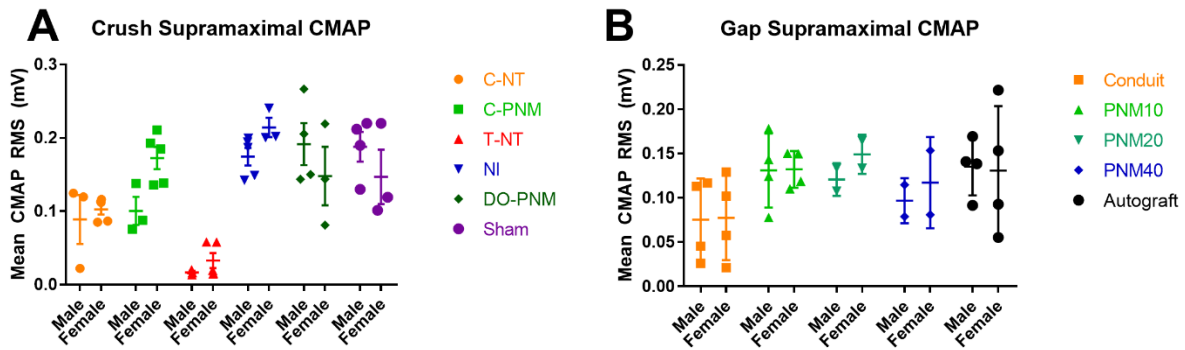


**Figure 38: Sex base variance in compound motor action potential measures of recovery**

(A) Mean CMAP RMS for the crush injury model divided by sex. PNM treated crush injuries show a trend towards more favorable outcomes in females compared to male rodents. (B) The same division shown for the gap defect model. Unlike the crush model, no differences are seen between the male and female animals.

#### 4.3.7 Restoration of Nerve Function Following Reconstruction of the RLn in Canine

##### Model

No laryngeal movement was observed in any animal at 4 weeks. 24 weeks after implantation, laryngeal endoscopy revealed arytenoid movement but ineffective abduction in animals implanted with UBM and PNM but no movement in the animals with coaptation without hydrogel support or transection only CMAP amplitudes for animals at the 24 week time point were

(mean  $\pm$ se) PNM ( $0.68 \pm 0.32$  mV,  $n = 2$ ); UBM ( $0.71 \pm 0.019$  mV,  $n = 2$ ); conduit ( $0.34$  mV,  $n = 1$ ); transection ( $0.09 \pm 0.016$  mV,  $n = 2$ ) with no significant differences between groups ( $p = 0.24$ , ANOVA). CMAP amplitudes at the 4 week time point were all  $0$  mV (conduit only,  $n = 2$ ; UBM,  $n = 2$ ; PNM,  $n = 2$ ) (Figure 39B). Peak CMAP amplitude at the TA complex was strongly and significantly correlated with explanted PCA muscle weight across all animals with a  $0.19 \pm 0.011$  mV increases in CMAP amplitude for every 1-gram increase in PCA weight ( $R^2 = 0.80$ ,  $p = 0.001$ , Figure 33E). The relationship between TA complex peak CMAP amplitude and LCA muscle weight was less strong with a  $0.05 \pm 0.02$  mV increase in CMAP amplitude for every 1 gram increase in LCA weight ( $R^2 = 0.40$ ,  $p = 0.02$ ) (Figure 39E).

Significant differences were observed between the 4- and 24-week time points in right PCA ( $12.6 \pm 2.5$  g,  $20.7 \pm 2.3$  g,  $p = 0.037$ , t-test) and LCA ( $7.9 \pm 1.8$  g,  $12.0 \pm 2.7$  g,  $p = 0.007$ , t-test) muscle weights, although no differences were observed between treatment groups at any time point. Similarly, a significant reduction in right PCA muscle weight (denervated) relative to left PCA (control) at 4 weeks across all groups (right  $12.6 \pm 0.5$  g; left  $19.0 \pm 1.8$  g,  $p = 0.007$ , paired t-test) but not at 24 weeks (right  $23.0 \pm 0.96$  g; left  $20.7 \pm 8$  g,  $p = 0.43$ ). A similar pattern was observed in LCA muscle weights at 4 weeks (right  $7.9 \pm 0.7$  g; left  $12.4 \pm 0.8$  g,  $p = 0.0007$ ) and 24 weeks (right  $12.0 \pm 1.0$  g; left  $14.5 \pm 1.0$  g,  $p = 0.43$ ) after denervation and repair.

No significant differences were observed between PCA or LCA minimum fiber diameters between groups at 24 weeks after repair: PCA-PNM,  $66.9 \pm 4.0$   $\mu$ m; UBM  $72.4 \pm 6.8$   $\mu$ m; conduit only  $58.5$   $\mu$ m; transection  $60.0 \pm 7.6$   $\mu$ m ( $p = 0.54$ ); LCA-PNM,  $57.9 \pm 4.4$   $\mu$ m; UBM  $64.6 \pm 1.67$   $\mu$ m; transection  $62.8 \pm 9.2$   $\mu$ m ( $p = 0.69$ ) (Figure 39D). Similarly, no differences were observed 4

weeks after repair, PCA- PNM,  $49.7 \pm 0.65 \mu\text{m}$ ; UBM  $62.6 \pm 7.4 \mu\text{m}$ ; conduit only  $52.4 \mu\text{m}$  ( $p = 0.24$ ); LCA-PNM,  $54.7 \pm 13.4 \mu\text{m}$ ; UBM  $55.4 \pm 8.67 \mu\text{m}$ ; conduit only  $65.7 \pm 3.1 \mu\text{m}$  ( $p = 0.68$ ) (Figure 39B, E).

Combining treatment groups, right PCA weights were significantly reduced at 4 weeks ( $54.9 \pm 3.2 \mu\text{m}$ ) compared to 24 weeks ( $65.3 \pm 3.3 \mu\text{m}$ ,  $p = 0.04$ ). Right LCA weights were not significantly different at 4 weeks ( $58.6 \pm 4.8 \mu\text{m}$ ) compared to 24 weeks ( $61.8 \pm 2.7 \mu\text{m}$ ,  $p = 0.57$ ) (Figure 39D, E).

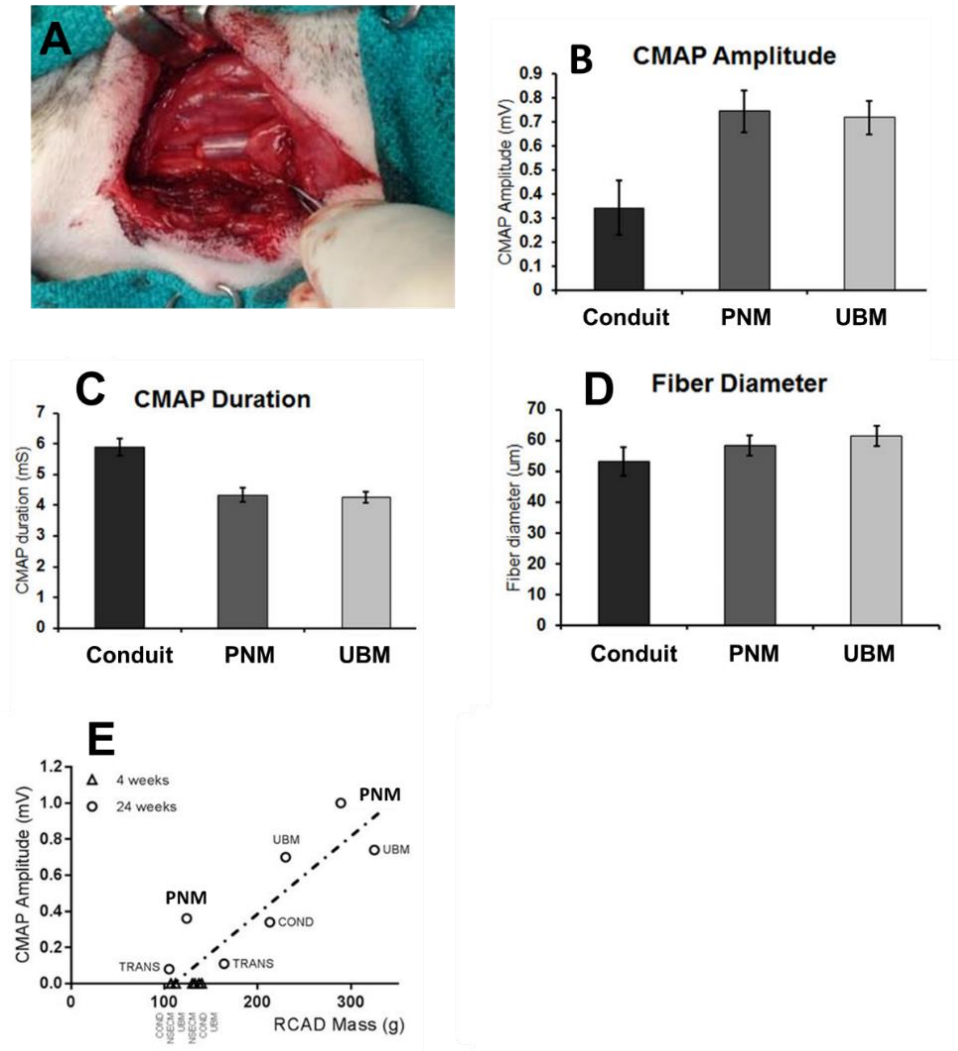


**Figure 39: Functional recovery of RLn in a canine model**

(A) Intraoperative photo of silicone conduit placement after anastomosis of transected RLN. (B) Compound muscle action potential amplitude measured at the vocalis muscle after super-stimulation of the RLN. (C) Duration between stimulation of the RLN and recorded action potential at the vocalis muscle. (D) Muscle fiber diameter of the posterior cricoarytenoid muscle. All three measurements were taken after 6 months of recovery, post-surgery. (E) Relationship between right cricoarytenoid muscle mass and vocalis CMAP amplitude ( $R^2 = 0.80$ ,  $p = 0.001$ )

Statistic are not shown because of the limited group sizes used ( $n = 2$ ).

## 4.4 Discussion

The most prevalent rodent model for testing the functional return of a sciatic nerve injury is the walking track analysis using the sciatic functional index (SFI). In the late 1970s, Hruska, et al. demonstrated that walking tracks made by rats have consistent and reliably quantified characteristics and proposed the measurement of changes in print morphology as a marker of functional recovery [213]. Generally, this method involves the application of some ink-like media to the hind feet of the rat and subsequently allowing them to traverse a substrate upon which they leave their hind paw prints. De Medinaceli et al. developed specific measurements and a formula to provide an index of nerve function between 0 and -100 in 1982 [214]. This first equation incorporated four parameters that were directly measured from the rodent's footprints: distance to opposite foot, print length, outer toe spread, and inner toe spread ( 40A). Later versions of the SFI described by Carlton and Goldberg simplified the equation to just three metrics ( 40B). However, these early SFI formulas weighted parameters equally and were poorly indices of function. Bain et al. drastically improved the SFI by incorporating coefficients derived from multiple linear regression analysis ( 40C).

**A. De Medinaceli, Freed and Wyatt, 1982**

$$SFI = \left( \left( \frac{ETOF - NTOF}{NTOF} \right) + \left( \frac{NPL - EPL}{EPL} \right) + \left( \frac{ETS - NTS}{NTS} \right) + \left( \frac{EIT - NIT}{NIT} \right) \right) \frac{220}{4}$$

**B. Carlton and Goldberg, 1986**

$$SFI = \left( \left( \frac{NPL - EPL}{EPL} \right) + \left( \frac{ETS - NTS}{NTS} \right) + \left( \frac{EIT - NIT}{NIT} \right) \right) \frac{220}{3}$$

**C. Bain, Machinnon, and Hunter, 1989**

$$SFI = -38.3 \left( \frac{EPL - NPL}{NPL} \right) + 109.5 \left( \frac{ETS - NTS}{NTS} \right) + 13.3 \left( \frac{EIT - NIT}{NIT} \right) - 8.8$$

**Figure 40: Equations for calculating Sciatic Functional Index**

(A) SFI equation described by De Medinaceli, Freed and Wyatt in 1982. (B) SFI equation described by Carlton and Goldberg in 1986. (C) SFI equation described by Bain, Machinnon, and Hunter in 1989. Abbreviations are E (experimental side), N (contralateral side), TOF (distance to opposite foot), PL (print length), TS (outer toe spread), and ITS (intermediate toe spread).

The SFI is determined by comparing various geometric parameters of the affected hind paw from an injured rat and comparing it to the contralateral paw. The equation described by Bain et al. produces a value of function, between 0 and -100. There are several equations that are present in the current research community, however each usually provides nearly the same values. The calculations have been most often based on the lengths and widths of the inked impressions of the paws left on a piece of paper during normal locomotion. The simplest equation is based on three

measurements: the paw lengths and the paw widths between the 1<sup>st</sup> and 5<sup>th</sup> digits, and the 2<sup>nd</sup> and 4<sup>th</sup> digits. Paw length is the largest driver of SFI followed by the 1<sup>st</sup>-5<sup>th</sup> toe spread and then the 2<sup>nd</sup>-4<sup>th</sup> toe spread.

SFI is an extremely well published method with a strong correlation with functional recovery when employed correctly but is not immune from issues. Several difficulties can prevent researchers from obtaining usable print marks. Print length is the most influential parameter within the SFI equation but is negatively affected by a static position. If the rodent does not cross the track continuously, SFI can be artificially lowered. This behavior can be avoided by ample conditioning trials. Autotomy presents a permanent problem to gathering SFI data. After transection of the sciatic nerve, rodents may scratch or bite their anaesthetized foot. This behavior can result in autotomy, or the amputation of one or more toes. When this occurs, the rodent can no longer be assessed with SFI. This behavior can be curbed by applying foul-tasting substances upon the foot [215] or starting with a breed, such as Lewis rats that have demonstrated minimal autotomy [216]. Sciatic nerve injuries often cause joint contractures caused by either a faster or more complete reinnervation of the flexor muscles in comparison with the extensor muscle group [217, 218]. While a sign of reinnervation, flexor contracture of the foot can decrease SFI readings and overall make data collection difficult. Physical therapy can mitigate this development [219].

Sciatic nerve transection models have consistently shown a relatively small degree of observable functional recovery when estimated using SFI, limiting its usefulness in peripheral nerve studies [201]. This is the result of two distinct problems: 1) axonal misdirection in the regenerative process and 2) the mixed grouping of fascicles that contribute to the tibial and common peroneal branches of the sciatic nerve. Ultimately, non-selective reinnervation of the distal stump fascicles causing a mixture of tibial and common peroneal tributaries entering the

distal stump results in altered activation patterns of opposing muscle groups during locomotion [49]. One alternative to minimize the effect of synkinetic regrowth in our first look at function recovery is to use a model of common peroneal nerve injury. A peroneal nerve functional index (PFI) equation was described by Bain, Machinnon, and Hunter in 1989 [207]. Using PFI mitigates the limitation imposed on SFI because of non-selective cross-innervation, since the motor units of the common peroneal nerve have related muscular functions, rather than opposing.

The use of PFI is less common than SFI, and SFI and the sciatic nerve injury model still represents a gold standard in current literature. With possible issues that could reduce the power of the standard SFI measurement, it is logical to employ multiple metrics of functional recovery. Further studies that employ sciatic nerve injury models in this chapter include metrics that measure gastrocnemius muscle recovery during walking or score the sensory and pain reflex function. Combining the SFI score with biomechanical measures (kinematics) and measures of sensory and reflex recovery allows for a more holistic picture of functional recovery.

However, for both PFI[220-223] and SFI [129, 220-234], several problems with walking tracks are apparent in the literature, such as contracture, related to loss of function of tarsal flexor/digital extensor muscles[220, 221, 223], or other causes of poor print quality[235, 236]. Other problems have been suggested, but not investigated, such as alteration of contralateral limb prints as a result of compensatory strategies during locomotion[223], and the effect of velocity on walking track analysis [237-239].

One remaining limitation of most metrics used in the chapter is the use of the contralateral limb as a control or normalizing factor. It is very likely that compensatory limb loading would result in altered foot placement or gait in the uninjured contralateral limb. By comparing measurements from all time points for the contralateral limb to pre-injury prints, it has been shown

that there are significant differences in the contralateral limb's SFI post-injury. Therefore, it is possible that results could be muted or exaggerated by compensatory changes in the contralateral limb.

In studies that include both functional metrics (SFI, PFI, ankle angle, etc.) and CMAP, it is observed that electrophysiologic results do not always translate to similar changes in function. For example, PNM10 treatments as lumen fillers in a non-critical sciatic nerve defect significantly increased CMAP amplitude by 70% over conduit control ( $p < 0.05$ ) and provided conduction comparable to the autograft. However, PNM10 did not perform any better than the conduit control in function assays. One possible source for this disparity is the presence of synkinetic growth. For large injuries that disrupt normal axon channels, axonal misdirection in the regenerative process can significantly affect function, particularly in the case of the mixed grouping of fascicles that contribute to the tibial and common peroneal branches of the sciatic nerve. Axonal misdirection, or synkinetic growth can cause a mixture of tibial and common peroneal tributaries entering the distal stump results in altered activation patterns of opposing muscle groups during locomotion [49]. This could lead to positive CMAP readings when evoked in isolation but poor overall function during voluntary locomotion.

CMAP done in the rat gap and crush models experienced signal clipping at higher currents, limiting our confidence that we were accurately comparing groups. This was limited by the equipment used to collect the stimulus curves which was designed for smaller electrophysiologic measurements. Instead of collecting amplitude measurements that would be strongly impacted by recording clipping, the area under the curve was collected by root mean squared (RMS) assessment. The area under of the curve was collected from multiple stimulus curves at different stimulus currents and plotted over stimulus current. The stimulus traces were consulted and a

current that minimized the clipping while still being at a plateau of RMS results. For crush injuries, this current was able to be selected within a response plateau but for the gap injury a plateau was not able to be reached with the protocol being performed. Under normal conditions, CMAP represents a strong test of nerve regeneration. While there are a number of limitations with the current studies using electrophysiology, the CMAP results match closely with axon counts at the distal portion. This could suggest that while the CMAP results for the gap study are not supramaximal, they still represent a relative comparison between groups. In addition to RMS CMAP results, CMAP traces showed multiple peaks at different peak latencies rather than the typical biphasic CMAP response curve at a single peak latency. These multiple waveform components suggest that there were multiple populations of axons with different conduction velocities that were contributing to the overall CMAP recorded from the tibialis anterior muscle. This waveform complexity was scored and compared but no significant differences were found between autograft and treatment groups. Only conduit alone was different and this was possibly because of animals that did not display little to no recovery.

The functional tests, in design also represent a limitation of the present study. SFI is a well described measure [129, 220-234], but conditions that affect the foot can greatly affect the test because the index relies heavily on measures of the toes. These conditions include autophagy (self-amputation of toes) or chronic foot flexion contractures [228, 240]. In our studies, autophagy was extremely rare, with an incidence of <1%. However, we observed a high occurrence of chronic flexion contractures in the sciatic defect injuries, especially in the autograft groups. The prevailing theory is that these flexion contractures symbolize regrowth of the injured nerve but represent either synkinetic reinnervation of opposing muscle groups or a preferential reinnervation of the flexion muscle groups [228, 240].

The von Frey fiber nociception test was added to test the nociceptive sensory component of the sciatic nerve afferent fibers that contribute to the generation of the withdrawal reflex. This was the first sensory test incorporated into the study but was highly variable and limited conclusions were drawn from this experiment. This experiment was also not a pure test of sensory function, instead required a reinnervation of a reflex arc, including the regeneration of both motor and sensory neurons. These limitations combined caused this assay to be a very ineffective test of sensory function return. Future study could use other reflex tests with stimulations generated by heat, cold, or electrical shock that may have less variability. However, this still does not resolve the complexity necessary to recover a full reflex arc. Overall, the reflex test used in this study was a weak measure of functional recovery.

A rat sciatic nerve crush model was used to assess both the safety and efficacy of an intraneural injection of PNM to the site of injury. While both groups returned to full functional recovery by the end of 12 weeks, PNM injection sped return to function by one week, increased the number of axons crossing the injury and evoked CMAP across the injury. The use of PNM injection into the site of injury had a positive impact on peripheral nerve regeneration and could be a potent strategy upon further development.

One limitation to this study is the possible variability of the degree of nerve injury induced. A third degree axonotmesis injury is associated with damage to the axons as well as the endoneurial linings. This can lead to endoneurial scarring, which can impede or misdirect axonal regeneration resulting in a variable functional recovery. Our goal was to achieve this more severe form of the axonotmesis injury. We were interested in an injury without full functional recovery with a more exaggerated inflammatory response. We observed that the crush injury resulted in a decrease in axons at the distal region and a similar decrease in evoked CMAP at the downstream muscle.

However, functional metrics showed a complete recovery after 6-8 weeks. It is possible that the nerve injury achieved was not as severe as intended and therefore provided a narrow window for the PNM to impact recovery. Some studies have highlighted the resistance of rat nerve tissue to higher levels of axonotmesis injury, showing that various methods consistently demonstrated only a second-degree axonotmesis injury with only minor features of third-degree injury.

All intraneural injections were at one point considered to be a portent to nerve injury and were avoided in most medical practices. However, with advances in ultrasound guidance, it is possible to visualize the difference between perineurial space and intrafascular regions allowing for precise delivery of drugs and anesthetics. Current practices show only a 0.5-1.0% occurrence of peripheral nerve injury complication due to anesthesia injections into nerve tissue [241]. Even without advanced visualization techniques to guide injections, we wanted to show that the intraneural injection of our treatment was safe. We saw that PNM injection without nerve crush injury showed no deleterious effect on functional metrics. Small effects on evoked CMAP and axonal count distal to the injury could have been caused by an unintended needle injury to a portion of the nerve.

We hypothesized that PNM would have a positive effect on nerve regeneration of a crush injury through the recruitment of Schwann cells and macrophages, a shift in macrophage polarization, and a reduction in inflammation. We confirmed *in vitro* that PNM degradation products produce an enhanced Schwann cell migratory response and neurite outgrowth. While this study did not investigate these possible mechanisms *in vivo*, previously published work did show that PNM did have an impact on recruitment of Schwann cells and macrophages and a shift in macrophage polarization both *in vitro* and *in vivo*.

For the large animal model of RLn transection, a minimal study design measured evoked CMAP from the laryngeal muscles and compared to muscle size. The approach to detect evoked CMAPs, generated by a supramaximal stimulus proximal to the site of nerve coaptation, was effective and evoked CMAPs were detected in all animals at the 24-week time point. There was a very close correlation between CMAP amplitude and the weight of the intrinsic laryngeal muscles reinnervated by the RLn, although the correlation was stronger for the PCA muscle than the LCA muscle. This difference may be due to the more intricate geometry of the LCA and in its intimate relationship with the TA complex, making precise explanation and subsequent determination of LCA muscle weight difficult. The reduction in PCA (34%) and LCA (37%) weight four weeks after denervation compared to the contralateral innervated muscles is anticipated and reflects the relatively slow atrophy and absence of necrosis found after denervation in other large animal [36-38] rather than rodent models [39, 40].

Taken together, these data suggest that evoked CMAPs detected at the TA complex provide a useful minimally invasive approach to monitor the return of reinnervating axons to the end target organ. In future work, this approach could be combined with an implanted nerve cuff [41, 42] to provide repeated longitudinal assessment of reinnervation. Reinnervation of the thyroarytenoid complex is crucial to the restoration of vocal cord function and voice and this approach would allow ongoing evaluation of the effects of regenerative therapies on RLn reinnervation.

Despite increases in PCA and LCA muscle weights, CMAP amplitudes and minimum fiber diameters at 24 compared to 4 weeks after direct RLn-RLn coaptation, no effective arytenoid movement was observed. This result is anticipated in the case of repair to the common RLn trunk in which abductor and adductor fibers are spatially intermingled [43, 44, 45] due to synkinetic reinnervation [46, 47].

The major limitation of this study was the small number of animals at each time point and within each treatment group in the canine study. The goal of this work was to determine the feasibility of the use of ECM hydrogels in RLn repair. While the results of the study clearly demonstrate the potential for the use of ECM hydrogels in this application, more extensive work is required to determine significant differences between treatment groups and to evaluate the benefits of using a tissue-specific ECM hydrogel for nerve repair [48, 49].

Overall, this work showed that PNM enhanced CMAP conduction across the injury site of both nerve defect and nerve crush and that gross function recovered quicker than conduit control. These results were consistent across the three injury models (crush, transection, and gap defect). The smallest effects on CMAP were observed in the crush group with an increase by about 50%. Both the 1 cm gap defect model and large animal transection model saw large increases in CMAP of about 70% and 100% respectively.

## **5.0 PNM Increases the Effectiveness of an Engineered Nerve Guidance Conduit Containing Cell-secreted Neurotrophic Factors**

### **5.1 Introduction**

To this point, PNM has been investigated for its ability to improve peripheral nerve regeneration in isolation of any other therapies outside of standard surgical repair. For nerve defect models, an inert nerve guidance conduit made from silicone was selected and used. PNM was shown to improve outcomes when combined with this inert silicone conduit but did not exceed the nerve autograft in all studies. One limitation is that silicone conduits are not an accepted material for nerve guidance conduits and does not perform as well as accepted conduit materials such as collagen type 1 or PGA. Current data suggests that PNM can improve the outcomes of all nerve guidance conduits when used as a lumen filler. Studies that compare the autograft repair to the use of PNM as a lumen filler for FDA approved conduits are needed. While not a clinically available conduit, PNM is used as a lumen filler for an engineering conduit that incorporates cell-secreted neurotrophic factors in this last chapter.

In the pursuit of an effective nerve conduit, many physical and biological strategies have been employed during fabrication [193, 242-246]. On the physical side, nanofibers obtained from electrospinning hold great promise due to their ability to be fabricated with aligned arrangements closely resembling native nerve ECM, and they have demonstrated the ability to guide neurite extensions [242, 247-249]. On the biological side, neurotrophic factors (NTFs) such as brain derived neurotrophic factor (BDNF) and vascular endothelial growth factor (VEGF) have been shown to play an important role in facilitating axonal growth, guidance, and survival. In addition,

chemokine gradients are instrumental in driving Schwann cell migration into the regenerating nerve bridge and axon elongation [9, 42, 250-257]. Current methods of sustained delivery of growth factors by microparticles, along with other technologies, have demonstrated utility in experimental models of nerve repair, but these technologies have not yet addressed the dynamic time course of growth factor production, the use of anti-inflammatory cytokines, or the capability to supply a multitude of growth factors simultaneously [243, 244, 258, 259].

A potential route toward addressing these issues lies in the use of stem cells. Mesenchymal stem cells (MSCs) are multipotent cells that have the ability to differentiate into many lineages, including neural-like lineages [260, 261]. Early transplantation experiments involving these stem cells demonstrated that they supported nerve regeneration (originally believed to be due to transdifferentiation to neural lineages but more recently thought to be through production of NTFs), and they have also been shown to possess immunoregulatory functions, which could potentially decrease scar tissue infiltration into conduits and neuroma formation [193, 253, 262, 263]. Indeed, studies utilizing nerve conduits seeded with MSCs reported both larger axons as well as greater amounts of myelination per axon [193].

This chapter investigates the combination of PNM with an engineered nerve conduit as well as the addition of a cell-secreted neurotrophic gradient. The effect of the regenerative response of peripheral nerve was examined through a 1 cm sciatic nerve transection model in rats. Basic histologic and function metrics were used to examine the effect that each component had on nerve regeneration.

## 5.2 Materials and Methods

All chemicals were purchased from Sigma Aldrich (St. Louis, MO, USA) unless otherwise specified. All procedures were performed according to the guidelines of the Institutional Animal Care and Use Committee at the University of Pittsburgh, protocol number 16036308.

### 5.2.1 Fabrication of Cell-seeded PCL/GelMA Nerve Conduits

The composite PCL/GelMA scaffold was produced as previously described [264]. Briefly, a dual spinning setup with 14.0% w/v PCL (80 kDa) in 2,2,2-trifluoroethanol and 18% methacrylated-gelatin (GelMA) in 95% 2,2,2-trifluoroethanol in water was used to produce random and aligned scaffolds. A 2.0 x 5.5 cm sheet of aligned scaffold and a 2.2 x 5.5 cm sheet of random scaffold was cut for each group and subsequently exposed to UV irradiation for 30 minutes to sterilize. The aligned scaffold was then overlapped on top of the random scaffold by 2 mm, and approximately 20  $\mu$ L of photoinitiator solution (8% methacrylated gelatin, 0.3% photoinitiator lithium phenyl-2,4,6-trimethylbenzoylphosphinate (LAP) in HBSS (Gibco, Waltham, MA, USA) was applied to the overlapped region. This area was then irradiated with a visible light source supplying wavelength of 395 nm (7202UV395, LEDWholesalers) for 40 seconds to cure the gelatin and bond the two sheets together. Following this, approximately 300  $\mu$ L of photoinitiator solution was used to wet both scaffolds. 50  $\mu$ L of photoinitiator solution was then used to resuspend 6 million cells, which were then pipetted in three vertical stripes 1.2 cm apart equidistant from the horizontal edges of the scaffold. This completed sheet was then rolled up around a hypodermic needle of 1.5 mm diameter, and subsequently photopolymerized with visible light for 2 minutes while rotating on the needle. The construct was then removed, and 0.95 cm was removed from

each end of the tube followed by cutting the remaining 3.6 cm into three 1.2 cm tubes such that the cell stripes fell into the central third of each conduit (2 million cells/conduit). These wall-encapsulated cellular conduits were then placed in culture medium (10% fetal bovine serum (FBS) [Invitrogen, Carlsbad, CA, USA], 1x PSF [Gibco] in Dulbecco's Minimal Essential Medium (DMEM) [ThermoFisher, Waltham, MA, USA]) until surgical implantation.

### **5.2.2 ECM Hydrogel Preparation**

Peripheral nerve ECM was prepared from sciatic nerves collected from market-weight pigs (Tissue Source; LLC, Lafayette, IN, USA). The tissue was then frozen for at least 16 h at -80° C. The tissue was quartered longitudinally and cut into sections of less than 5 cm. Decellularization is performed as previously described [162]. Enzymatic degradation products were produced from solid ECM scaffold material as previously described [162]. Enzymatic degradation products were aliquoted and lyophilized. Immediately before use, lyophilized degradation products were rehydrated using sterile water. Gelation was then initiated by adjusting the pH of the digest to 7.4 and 0.5X PBS concentration through the addition of 0.2 M NaOH and 10X PBS. A concentration of 20 mg/mL was tested in this study.

### **5.2.3 Scaffold Implantation**

Nerve conduits with wall-encapsulated rat ASCs (DiI-labeled with Vibrant CM solution (Invitrogen) for 1 to 6 week experiments according to manufacturer's protocol) or cell-free conduits were prepared for implantation. The sciatic nerves in Lewis rats were exposed and a 10

mm segment was removed using microscissors. Nerve stumps were sutured 1 mm into each end of the 12 mm conduit (for a gap of 10 mm) using 8-0 nylon suture. The conduit was either unseeded and left empty (Figure 41A), unseeded and filled with PNM20 (Figure 41B), seeded with MSCs and left empty (Figure 41C), or seeded with MSCs and filled with PNM20 as a lumen filler (Figure 41D). A total of  $n = 6$  rats was used for each group at each timepoint.

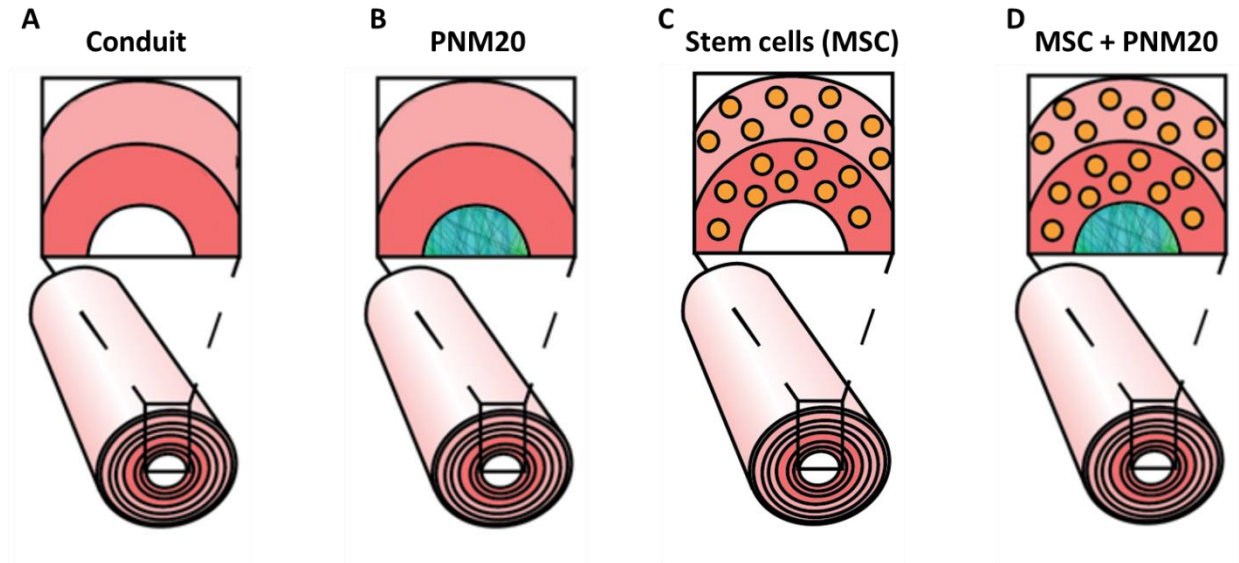


**Figure 41: Diagram of groups used to test engineered conduit with PNM as lumen filler**

#### **5.2.4 Explanation and Immunohistochemical Analysis**

Scaffolds were explanted at their specified timepoints (either 1, 2, 4, 6, or 16 weeks). Scaffolds were then fixed in 10% buffered formalin phosphate for 2 days at 4° C. These were then passed through a series of solutions: 10% sucrose for 4h at room temperature, 20% sucrose overnight at 4° C, and lastly 30% sucrose overnight at 4° C. Samples were then placed in optimal cutting temperature gel (OCT) (Sakura Finetek USA, Torrance, CA, USA) for 2 h to equilibrate. Following this, 3 samples were transversely cut through the middle of the conduit and frozen in new OCT cut side down. Sections were collected at every millimeter with a thickness of 16 µm starting from the center to study cellular distributions. The other 3 samples were embedded longitudinally in fresh OCT for longitudinal sections to assess continuity of nerve growth. Samples were subsequently stored at -80° C until sectioning.

#### **5.2.5 Rat Sciatic Functional Index Testing**

Rats were placed in the MotoRater System (TSE GmbH, Chesterfield, MO, USA) and acclimated for two days prior to testing. Videos were then recorded for rats walking across the length of the MotoRater System. Simi Motion 9.2.1 software (Simi Reality Motion Systems GmbH, Unterschleissheim, Germany) was used to measure toe spread distances from acquired videos. SFI measurements from 4 steps were averaged for each rat.

### **5.2.6 Statistical Analysis**

All data were expressed as mean  $\pm$  standard error of measurement (SEM). Statistical analysis was performed in Prism 7. Statistical analysis was performed using ANOVA with Tukey's HSD post-hoc testing unless specified otherwise. One-tailed Mann-Whitney testing was used to determine differences in distributions, and non-linear fitting was used to determine Gaussian and quadratic fitting. One-way ANOVA followed by Fishers LSD post-hoc testing against wall or control was used for Week 6 Schwann and myelin thickness/ratio, respectively. A threshold of  $p < 0.05$  was used to determine statistical significance.

### **5.2.7 Immunohistochemistry of Nerve Conduit Sections and Analysis**

Sections were equilibrated in PBS for 10 minutes to remove OCT compound. They were then blocked for one 1 h at room temperature with 0.1% Tween-20, 4% Goat Serum (Gibco) in Tris buffered saline (TBS). Following this, primary antibody was applied in block solution and left on overnight. Slides were subsequently washed 3x with 0.1% Tween-20 in TBS wash buffer, and secondary was applied in 0.5% Triton X-100 in TBS for 1h at room temperature. Slides were then washed 3x with wash buffer. Lastly, DAPI stain mixed in 0.5% Triton X-100 in TBS was applied for 10 minutes. After drying, slides were mounted and coverslipped with Vectashield hardset aqueous mounting medium (Vector Laboratories, Burlingame, CA, USA). The following primary antibodies were used: NF160 (1:250, mouse IgG1; Sigma), S100 (1:250, rabbit IgG; DakoCytomation), and Fluoromyelin Red (1:300, Invitrogen). The following secondary antibodies were used: goat anti-rabbit IgG Alexa 488/594/647 (1:220; Invitrogen) and goat anti-mouse IgG1 Alexa 488/594/647 (1:220; Invitrogen). Slides were imaged with an Olympus inverted microscope

(IX81). To quantify Schwann cells and ASCs within cross-sections, aggregate fluorescent intensity or area was used as a surrogate. Within and between groups, exposure times and thresholding were kept consistent. Fluorescent channels were then analyzed using Fiji (ImageJ) applying over/under thresholding to limit analysis to the positive-staining areas. Myelin thickness and percent myelination was calculated using custom python code reported by Mokarram et al (56). Briefly, the algorithm designates myelination status if 40% or more of an axon is encircled by Fluoromyelin positive tissue. Myelin thickness is computed using a rotating vector that measures the thickness of the Fluoromyelin positive tissue.

In addition to immunohistochemical analysis, 6-week explants were also analyzed qualitatively for cell infiltration and collagen production using Masson Trichrome stain (American Master Tech, Lodi, CA, USA) following the manufacturer protocols. Collagen stains blue and nuclei stains red.

## 5.3 Results

### 5.3.1 Multilayered Nanofibrous Nerve Conduits Possess Suitable Physical Properties for *in Vivo* Implantation

A nerve guidance conduit had been previously engineered to possess suitable physical and biological properties for *in vivo* implantation [265]. The conduit had showed physical suitability for surgical manipulation and implantation. This included the ability to flex around physiologically relevant curvatures, retain patency after full compression, and adequate tensile suture retention strength. Lastly, as expected, conduits have a faster degrading GelMA component and slower-

degrading PCL component to avoid conduit collapse during the regeneration process [265]. The conduit was also previously tested for biocompatibility. Cells implanted into the conduit increase metabolic activity over the course of 28 days, indicating proliferation and biocompatibility [265]. Given the importance of neurotrophic factors in nerve regeneration, it was found that the 3D scaffold design increased gene expression levels of BDNF and VEGF (two NTFs known to be produced by MSCs in abundance [247, 264]) and seeded cells produced neurotrophic factors that permeated through the scaffold.

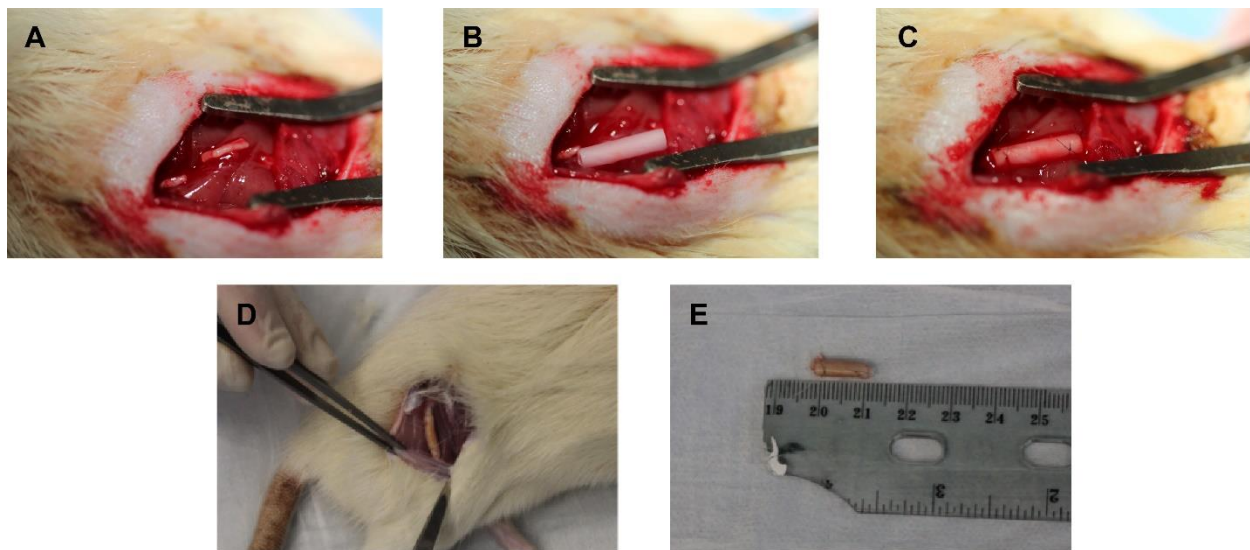


**Figure 42: Implant and explant of nerve conduits**

(A) 1 cm of sciatic nerve was removed and (B) a 1.2 cm long nerve conduit was placed in the gap. (C) Proximal and distal ends of the nerve were sutured 1 mm into each end of the tube. (D) Gross morphology of conduit attached to nerve at 6 weeks. (E) Gross morphology of nerve conduit explant at 6 weeks.

### **5.3.2 Conduits with Wall-encapsulated Cells Improve Peripheral Nerve Regeneration**

The ability of the nerve conduit with PNM to effect functional recovery in sciatic nerve defect model was analyzed. Conduits were implanted allogeneically into Lewis rats in a 1 cm sciatic nerve defect model (Figure 42). Briefly, 1 cm of sciatic nerve was removed ( 42A) and a 1.2 cm long nerve conduit was placed in the gap ( 42B) Proximal and distal ends of the nerve were sutured 1 mm into each end of the tube ( 42C). Gross morphology of conduit attached to nerve at 6 weeks (42D). Gross morphology of nerve conduit explant at 6 weeks ( 42E).

Four groups were tested: conduits with or without wall-encapsulated cells in the central third of the conduit and with or without PNM10 hydrogel filler. Implanted conduits did not elicit a foreign body reaction, and at 6 weeks PNM10 plus cells produced a robust connective tissue bridge (Figure 43).

Longitudinal and transverse sections of conduits at the center, respectively. Blue stains for collagen while red stains nuclei. Note: the conduit itself also stains lightly blue. Control groups display a thin regenerating bridge through the conduit while cell and hydrogel + cell (combo) groups demonstrate much thicker regenerating bridges. Control and hydrogel conduits possess much less collagen production in their walls when compared to cell-containing groups, and it can be seen that cells do not infiltrate into the inner aligned layers of the conduit (evidenced by red staining only in the outer portion of the conduit walls) ( 43).

At 16 weeks post-surgery, the wall-encapsulated cell group (cell) and combination of wall-encapsulated cells with PNM10 (combo) both presented with significantly higher sciatic functional index (SFI) when compared to control ( $p < 0.001$ ) (Figure 44). In addition, the cell group also significantly increased SFI compared to the no-cell with hydrogel filler group (hydrogel) ( $p < 0.05$ ). The hydrogel vs. control and combo vs. hydrogel were both at the border of significance ( $p = 0.0627$  and  $p = 0.0505$ , respectively).

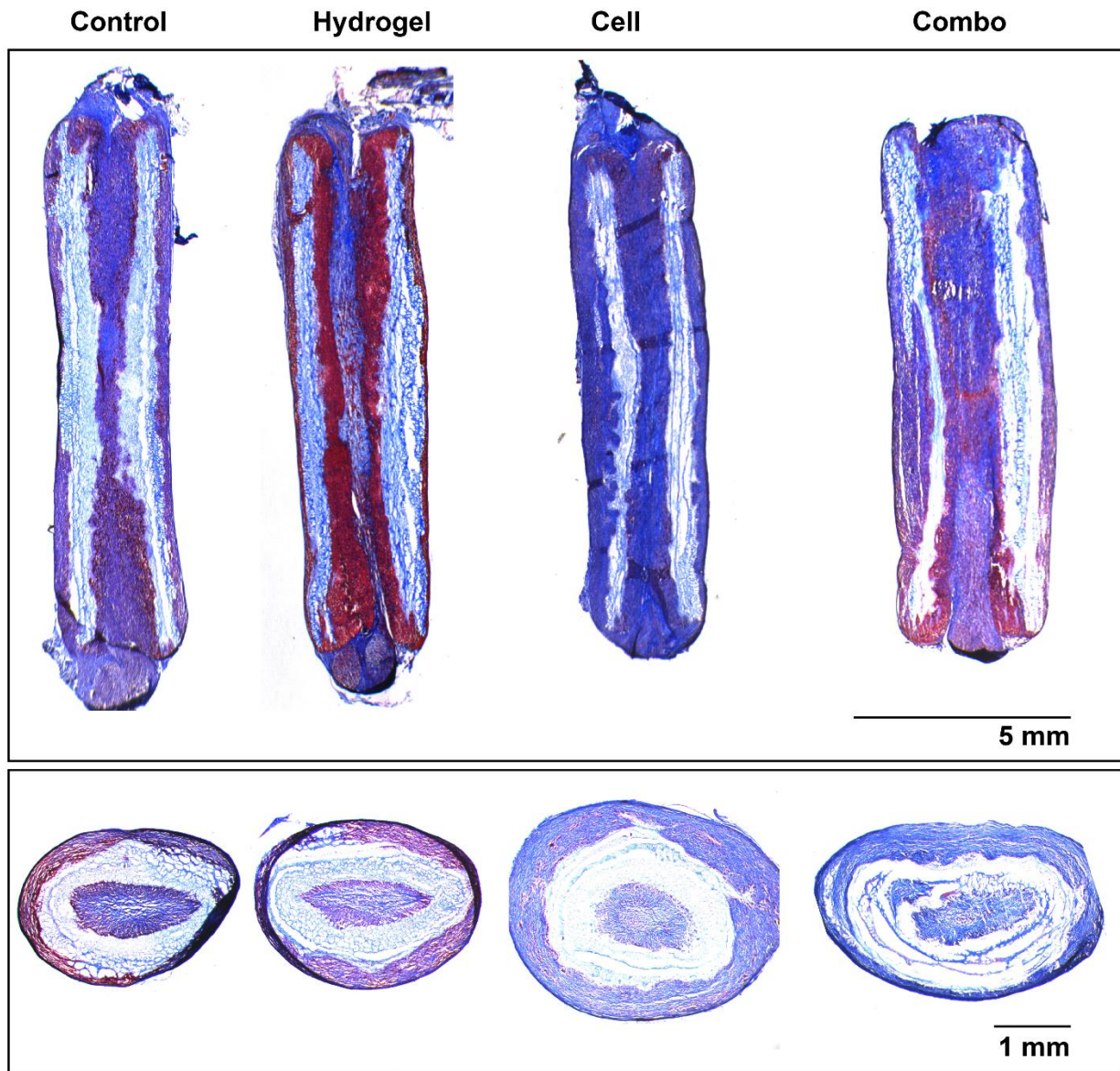


**Figure 43: Masson Trichrome staining of 6-week nerve conduit explants. (Top, Bottom)**

Longitudinal and transverse sections of conduits at the center, respectively. Blue stains for collagen while red stains nuclei. Note: the conduit itself also stains lightly blue. Control groups display a thin regenerating bridge through the conduit while cell and PNM + cell (combo) groups demonstrate much thicker regenerating bridges. Control and PNM conduits possess much less

collagen production in their walls when compared to cell-containing groups, and it can be seen that cells do not infiltrate into the inner aligned layers of the conduit (evidenced by red staining only in the outer portion of the conduit walls).

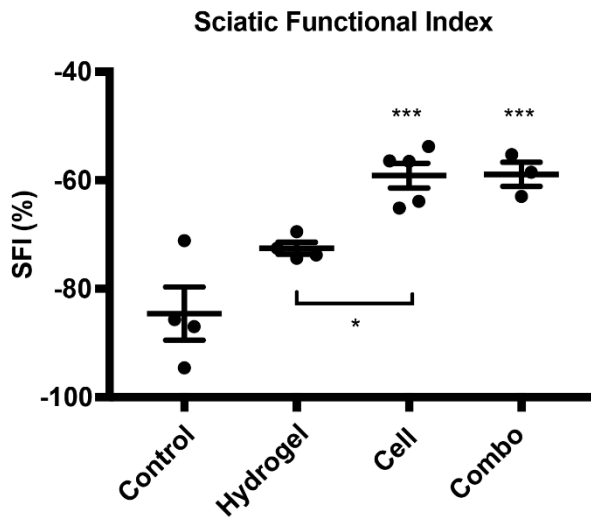


**Figure 44: Combination of centrally located wall-encapsulated ASCs and PNM improve functional return**

Sciatic functional index at 16 weeks for cell-free control (control), nerve conduits with ECM hydrogel lumen filler (hydrogel), nerve conduit with wall-encapsulated cells (cell), or nerve conduit with wall-encapsulated cells plus PNM hydrogel lumen filler groups (combo). \*,  $p < 0.05$ .

\*\*\*,  $p < 0.001$  compared to Control.

Lastly, axon myelination at 16 weeks was also assessed to correlate with functional outcomes (Figure 45). MSCs have been shown to increase myelination when applied in nerve conduits [193]. Figure 45A depicts representative images of neurofilament, myelin, and DAPI staining while Figure 45B displays the same images with only the myelin channel for better visualization (Scale: bar = 15  $\mu$ m). Representative images of nuclear, axon, and myelin staining at distal end of conduit for cell-free control (control), nerve conduit with ECM hydrogel lumen filler (hydrogel), nerve conduit with wall-encapsulated cells (cell), or nerve conduit with wall-encapsulated cells plus ECM hydrogel lumen filler groups (combo) are shown with NF-160 stain (green), Fluoromyelin (red), and DAPI (blue). At both the center of the conduit and 2 mm from the distal end of the transected nerve (Wallerian degeneration mainly affects the distal end of the nerve), the cell group possessed thicker axon myelination compared to control ( $p < 0.05$ ) (Figure 45C, D). The hydrogel group also exhibited increased myelination compared to control (\*,  $p < 0.05$  compared to Control) (Figure 45C, D). Looking at percentage of myelinated axons, the hydrogel group displayed a significantly higher percentage over control ( $p < 0.05$ ) (Figure 45E). The cell and combo group both had higher average myelination than control, but failed to reach statistical significance likely due to lack of power ( $p = 0.1361$  and  $p = 0.0896$ , respectively) (Figure 45E). Overall, nerve conduits with wall-encapsulated cells significantly enhance functional return and axon myelination in rats 16 weeks post-repair.

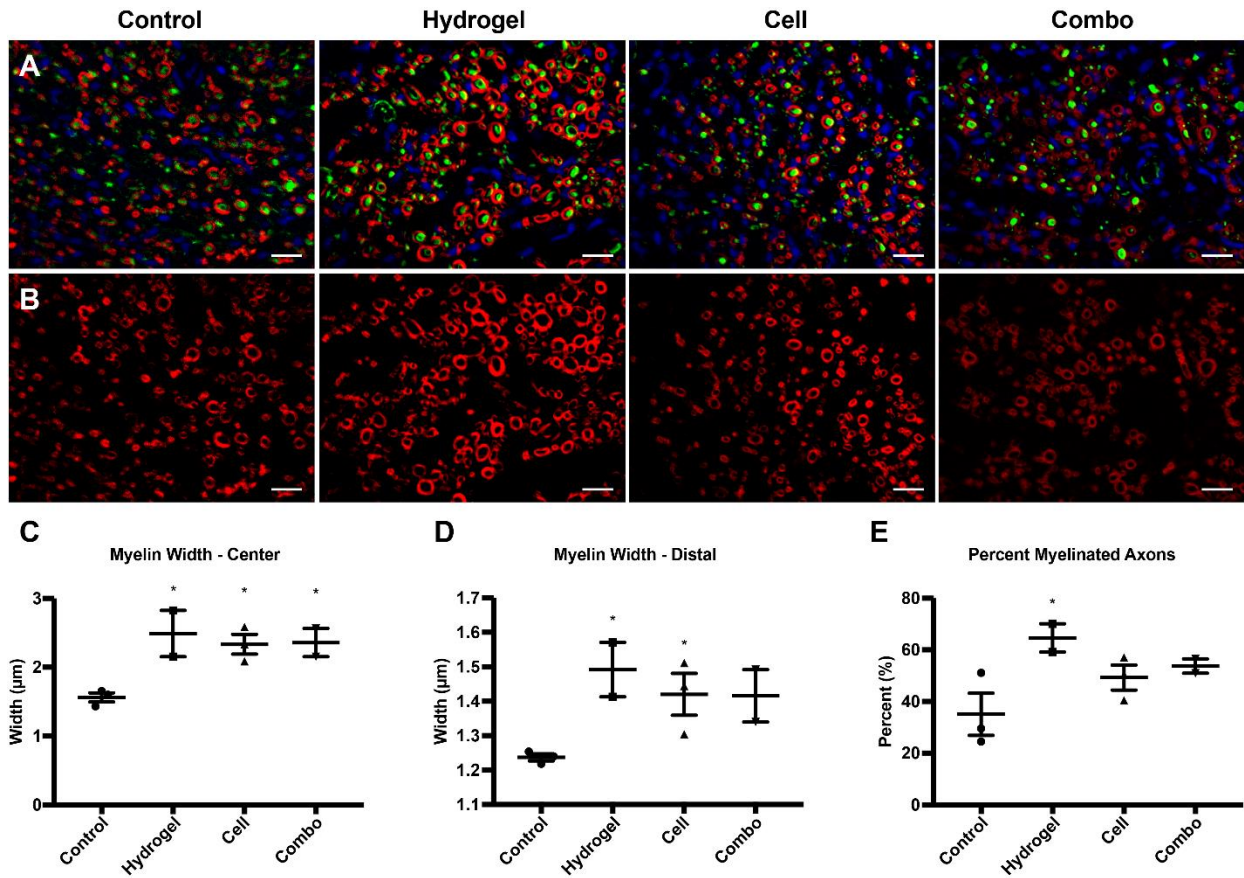


**Figure 45: Conduits with centrally located wall-encapsulated ASCs improve axon myelination**

Representative images of nuclear, axon, and myelin staining at distal end of conduit for cell-free control (control), nerve conduit with ECM hydrogel lumen filler (hydrogel), nerve conduit with wall-encapsulated cells (cell), or nerve conduit with wall-encapsulated cells plus ECM hydrogel lumen filler groups (combo). Green channel is NF-160 stain, red is Fluoromyelin, and blue is DAPI. (B) Myelin staining from images in A for better visualization of myelin. (C) Myelin width at center of conduit. (D) Myelin width at distal end of conduit. (E) Percent myelinated axons in distal end of conduit. \*,  $p < 0.05$  compared to Control. Scale bar = 15  $\mu\text{m}$ .

## 5.4 Discussion

In this study, PNM was combined with a nerve conduit harnessing cell-secreted neurotrophic gradient and its effect on the regenerative response of peripheral nerves was examined. A 1 cm sciatic nerve transection model in rats, implants with cells wall-encapsulated along the central third of the conduit length directed a stronger migration of Schwann cells into the center of the conduit compared to their counterparts with lumen-injected cells. This led to complete bridging of the conduit at 6 weeks by Schwann cells, and a significantly higher Schwann cell area in the center of the conduit compared to both cell-free conduits and conduits with lumen-injected cells. At 16 weeks, rats with these wall-encapsulated cellular conduits presented with significantly increased sciatic functional index and axon myelination over controls. Furthermore, PNM increased the robustness of the connective tissue bridge and increased myelination over cell-alone groups. Thus, the use of spatially controlled cell seeding to produce neurotrophic gradients presents a powerful strategy to maximize the potential of cell application in improving peripheral nerve regeneration.

There have been many descriptions of neurotrophic factors in the MSC secretome that enhance nerve growth [193, 266]. This is further supported by observations that VEGF and BDNF, two growth factors found in high levels with these cell types, have been shown to significantly aid axonal extension [11, 192, 247, 264, 267]. In addition, our observations are in accordance with previous findings and suggest that wall-encapsulated cells exert their effects through neurotrophic

factor secretion rather than other processes such as transdifferentiation [268]. Utilizing a cell-seeded conduit with cells located only in the walls along only the central third of the conduit, we sought to create a biomolecular gradient [250] of cell-secreted NTFs with the highest concentration in the center that decreased towards the ends of the conduit due to diffusion of NTFs (Figure 5). This pattern of cellular seeding led to a Gaussian distribution instead of the quadratic distribution observed with cell injection (Figure 5D, E). This gradient was enough to drive Schwann cells into the center of the regenerating nerve bridge.

At week 16, conduits with both PNM alone and wall-encapsulated cells displayed enhanced functional return and axon myelination (Figure 45C). This increase in myelination is in accordance with observations that injected or seeded MSCs promote axon myelination [193]. Surprisingly, the presence of PNM lumen filler derived from decellularized peripheral nerve did not synergistically add to the capabilities of the cellular conduit. We hypothesize that this is because the hydrogel and cells both act through neurotrophic factor enhancement of nerve regeneration, such that the cell-secretome induced migration of Schwann cells is not further augmented by the NTFs found in PNM.

Through this study, we sought to examine the use of PNM hydrogel as a lumen filler for a nerve guidance conduit that was engineered for peripheral nerve repair. Results matched previous studies where PNM hydrogel was able to support the use of a conduit. Again, PNM enhanced morphologic, histologic, and functional aspects of peripheral nerve regeneration. In this study, PNM hydrogel alone did not outperform the conduit with seeded MSCs. However, the combination of the MSC-seeded conduits and PNM hydrogel produced interesting results and could be worth investigating further. Furthermore, PNM still represents an accessible and off-the-shelf augmentation to peripheral nerve repair.

## 6.0 Overall Summary and Conclusions

Macrophages and Schwann cells play a key role in the conducting the early events after peripheral nerve injury. Throughout this dissertation we have investigated one strategy for improved functional improvement by utilizing the PNM to manipulate the microenvironment at the site of nerve repair to promote modulation of the host inflammatory response and promote Schwann cell (SC) migration and axon extension across the repair site (Figure 46). We have shown that this is an effective approach. Here we determined the effects of the PNM hydrogel on macrophage gene expression, phenotype and migration using a combination of Nanostring technology and immunohistochemistry. We also evaluate effects on SC migration, numbers of motor neurons reaching their target and axon extension using rat models of sciatic and common peroneal nerve injuries. Finally, functional recovery was determined after both sciatic crush injury and common peroneal and sciatic nerve transection associated with a short gap. Control groups including uninjured animals, exposure of the nerve without injury, transection and ligation without repair and injection of hydrogel in uninjured nerves were also performed (n = 8/group). Animals were followed for 12 weeks and assessed longitudinally using multiple measures of sensory and functional recovery. Metrics included von Frey nociception assay, sciatic functional index, and kinematic analysis. At 12 weeks animals were subjected to electrophysiologic assessment of evoked compound motor action potential prior to euthanasia for tissue collection and subsequent histologic analysis.

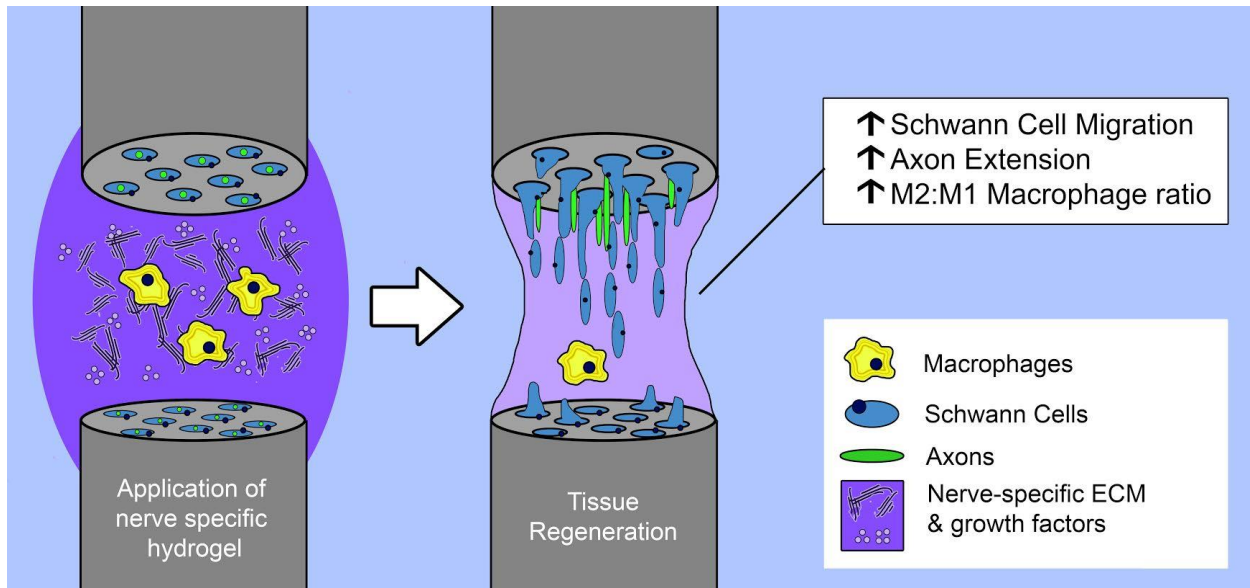


**Figure 46: Graphical abstract of the use of PNM in augmenting peripheral nerve injury response**

PNM promoted expression of Platelet Derived Growth Factor and M2 (regenerative) genes including *Chi313*, *Retnla* and *IL4ra*. Macrophage, particularly M2, recruitment to the injury site was increased in rats ( $p < 0.05$ ). PMN promoted SC migration both *in vitro* and *in vivo* ( $p < 0.05$ ). Axon extension determined by extension of axons in a crush model and across an 8mm gap was increased in the presence of PNM compared with an empty conduit ( $p < 0.05$ ).

The amplitude of CMAP across the sciatic crush injury site, demonstrating axonal regrowth to the terminal muscle was increased by 50% compared to control following intraneural injection of PNM 12 weeks after nerve crush. Furthermore, CMAP amplitude was increased by 70% in an 8 mm gap in the presence of PNM compared with an empty conduit ( $p < 0.05$ ).

These results demonstrate that an injectable, peripheral nerve matrix hydrogel derived from porcine sciatic nerve can modulate the response of two key cell types which conduct the early response to nerve injury. The present dissertation does not attempt to investigate the mechanisms by which the injectable ECM promote these phenomena; however, a recent study has described M2 macrophage mediated angiogenesis as a mechanism leading to Schwann cell chemotaxis and downstream regeneration [181]. However, though the exact mechanisms are not clear, these results link these phenomena to functional improvements downstream and suggest that PNM has the possibility to be used as a tool for improving nerve repair.

However, this dissertation was not without limitations, including the limited comparison to non-nerve specific ECM, several underpowered animal studies, and weakness of functional metrics assessed. In composition and in vitro assays, PNM was compared to UBM and SIS. Differences were observed in many of these experiments and these differences suggested that PNM would perform better in an animal model of peripheral nerve injury. However, this dissertation did not include either SIS or UBM in the majority of subsequent animal studies. UBM was only included with a large animal pilot study of recurrent laryngeal nerve transection and re-anastomosis repair. In this study, both PNM and UBM showed a similar trend towards improved recovery but little to no difference was observed between the two ECM sources. Future work could examine the use of non-nerve specific ECM hydrogels in nerve defect repair further. This work could elucidate the effect of nerve specific components from the general effect of having any extracellular matrix present. Furthermore, the inclusion of a simple collagen type I hydrogel as a control would further provide evidence that PNM provides a specific benefit.

Chapter 4 of this dissertation focused on measuring return to function after peripheral nerve injuries. The studies incorporated several different measures of function including functional indexes, nociceptive withdrawal reflex testing, gait kinematics, and electrophysiology. This was meant to capture a full picture of nerve function while covering for limitations of single measurements. While we were able to make some conclusions from these experiments, we found that the indexes, nociceptive withdrawal reflex testing, gait kinematic measures of function were limited by a number of factors that limited the utility of these tests. We still found the motor function test valuable to understand the impact that the PNM treatment had on downstream function but do not believe that these tests were indicative of the full effect that PNM had on the regeneration after injury. The most accurate measures of regeneration are the histology and axon counts of the regenerating axons and secondly the electrical conduction of the nerve axons to the downstream muscles measured through CMAP electrophysiology.

To this point, PNM has yet to be combined with an FDA approved conduit and has only been investigated minimally in combination with other regeneration strategies. For the majority of nerve defect models, an inert nerve guidance conduit made from silicone was used. PNM was shown to improve outcomes when combined with this inert silicone conduit but did not exceed the nerve autograft in all studies. Current data suggests that PNM can improve the outcomes of all nerve guidance conduits when used as a lumen filler. Studies that compare the autograft repair to the use of PNM as a lumen filler for FDA approved conduits are needed. Furthermore, present studies showed an increased rate of regeneration during the first month after crush and transection injuries. Evidence suggests that this ECM hydrogel might only remain within the conduit for the first 1-2 weeks [97, 162, 269]. One possible future direction could be the additional supplementation of PNM to the injury site after the first month to boost regeneration. This process

would use already established techniques as well as developing new practices for using image-guided injection of the PNM hydrogel through the skin to refill the nerve guidance conduit. In addition, these techniques could be used to further investigate the injection of PNM directly into the nerve tissue to lead the nature regeneration as it regrows back through the distal end of the nerve.

## Appendix A. Abbreviations Used

<b>A</b>	FDA (Food and Drug Administration)
<b>B</b>	<b>G</b>
BDNF (brain derived neurotrophic factor)	GAG (glycosaminoglycans)
bFGF (basic fibroblast growth factor)	GDNF (Glial derived neurotrophic factor)
BM (Bone Marrow)	GFAP (Glial Fibrillary Acidic Protein)
BMSC (Bone Marrow Stromal Cells)	<b>H</b>
BSA (Bovine serum albumin)	h (Hours)
<b>C</b>	HCT/P (Human Cellular and Tissue-based Product)
cm (Centimeter)	<b>I</b>
CNS (Central Nervous System)	IL-1 (Protein)
C-NT (crush without treatment)	<b>K</b>
C-PNM (crush with PNM injection)	kg (Kilograms)
<b>D</b>	<b>L</b>
DNA (Deoxyribonucleic acid)	<b>M</b>
DNase (Deoxyribonuclease)	mg (Milligram)
DO-PNM (dissection down to nerve and PNM injection into healthy nerve)	min (Minute)
DRG (Dorsal Root Ganglion)	mm (Millimeter)
<b>E</b>	MMP (metalloproteinases)
ECM (Extra Cellular Matrix)	MSC (Mesenchymal Stem Cells)
EMG (Electromyography)	<b>N</b>
EVA (Ethylene-vinyl acetate)	NFs (Neurotrophic Factors)
<b>F</b>	NGF (Nerve Growth Factor)

NI (No injury or surgery)	PNS (Peripheral Nervous System)
NIH (National Institutes of Health)	<b>R</b>
NT-3 (Neurotrophin-3)	R&D (Research and Development)
NT-4 (Neurotrophin-4)	RNA (Ribonucleic acid)
<b>P</b>	<b>S</b>
p (P-Value)	s (Second)
PCL (Poly(DL-Lactide-E-Caprolactone))	S-100 (low molecular weight Protein)
PDGF- $\beta$ (Platelet derive growth factor $\beta$ )	SC (Schwann Cells)
PGA (Polyglycolic Acid)	SD (Sodium deoxycholate)
PHB (polyhydroxybutyrate)	SDS (sodiumdodecyle sulfate)
PhD (Doctorate)	Sham/DO (dissection down to nerve without injury)
PHEMA-MMA (Polyhydroxyethylmethacrylate)	SIS (Porcine Small Intestinal Submucosa)
PI (Principle Investigator)	<b>T</b>
PLGA (Polylactic-co-glycolic acid)	T-NT (transection and ligation)
PNM (Peripheral nerve matrix)	TS (Toe-spread Test)
PNM10 (PNM hydrogel at 10 mg/mL concentration)	<b>U</b>
PNM20 (PNM hydrogel at 20 mg/mL concentration)	UBM (Urinary bladder matrix)
PNM40 (PNM hydrogel at 40 mg/mL concentration)	<b>V</b>
	VEGF (Vascular Endothelial Growth Factor)
	$\mu$ m (Micrometer)

## Appendix B. Programing Code

### B.1 Matlab Code

#### B.1.1 MatLab Code Used to Process SFI from Photographs of Ink Footprint Impressions.

```
cont=1;
    if exist('sciaticfunctionalindex')==0
        sciaticfunctionalindex=zeros(40,9);
        sciaticfunctionalindex=double(sciaticfunctionalindex);
        count=1;
    end
r=0;
timepoint=input('Please input timepoint week: ','s');
filename= strcat('SFI_rodentfunction_wk',timepoint)
timepoint=str2num(timepoint);
while cont==1;

imagenam = uigetfile('.jpg');

A = imread(imagenam);

image(A)
    number=input('Please input animal number: ');
    standardlength=1;

disp('Please measure experimental 3rd toe to heel');
EPL=imdistline();
pause;
centertoheeldistance = getDistance(EPL);
centertoheeldistance = centertoheeldistance/standardlength;

disp('Please measure normal 3rd toe to heel');
NPL=imdistline();
pause;
```

```
ncentertoheeldistance = getDistance(NPL);
ncentertoheeldistance = ncentertoheeldistance/standardlength;
delete(EPL);
delete(NPL);
```

```
disp('Please measure experimental first to 5th toe');
ETS=imdistline();
pause;
outertoedistance = getDistance(ETS);
outertoedistance = outertoedistance/standardlength;
```

```
disp('Please measure normal first to 5th toe');
NTS=imdistline();
pause;
```

```
noutertoedistance = getDistance(NTS);
noutertoedistance = noutertoedistance/standardlength;
delete(ETS);
delete(NTS);
```

```
disp('Please measure experimental 2nd to 4th toe');
EIT=imdistline();
pause;
innertoedistance = getDistance(EIT);
innertoedistance = innertoedistance/standardlength;
```

```
disp('Please measure normal 2nd to 4th toe');
NIT=imdistline();
pause;
ninnertoedistance = getDistance(NIT);
ninnertoedistance = ninnertoedistance/standardlength;
delete(EIT);
delete(NIT);
```

```
% disp('Please measure direction of travel (first heel to last heel of one foot)');
% wa=imdistline();
% pause;
% walkingangle=getAngleFromHorizontal(wa);
%
% disp('Please measure experimental deviation angle');
% efa = imdistline();
% pause;
% EDA=getAngleFromHorizontal(efa)
% EDA=abs(abs(walkingangle)-abs(EDA))
```

```

%
%
% disp('Please measure normal deviation angle');
% nfa = imdistline();
% pause;
% NDA=getAngleFromHorizontal(nfa)
% NDA=abs(abs(walkingangle)-abs(NDA))
%     if NDA>90
%         NDA=180-NDA
%     end
%     if EDA>90
%         EDA=180-EDA
%     end
%
%     EDA=EDA*0.0174533
%     NDA=NDA*0.0174533
SFI=38.3*((centertoeheldistance-
ncentertoeheldistance)/ncentertoeheldistance)+109.5*((outertoedistance-
noutertoedistance)/noutertoedistance)+13.3*((innertoedistance-
ninnertoedistance)/ninnertoedistance)-8.8
% PFI=-
63.58*(centertoeheldistance)+88.98*outertoedistance+26.55*ncentertoeheldistance+(328.34*(
EDA)-265.02*NDA)-7.95
question=input('Do you want to continue (y/n): ','s');
if strcmp(question,'n');
    cont=0;
end

sciaticfunctionalindex(count,:)=
[number,timepoint,SFI,centertoeheldistance,ncentertoeheldistance,outertoedistance,noutertoedi
stance,innertoedistance,ninnertoedistance]
count=count+1;
end

save (filename,'sciaticfunctionalindex');

```

### B.1.2 MS Amplitude from CMAP Analysis RMS Amplitude from CMAP Analysis

```

addpath 'C:\TDT\OpenEx\Examples\TTankX_Example\Matlab\';

tank = 'C:\TDTData\Travis';
block_prefix = '2017_09_12_R6';
blocks = {'-1', '-2', '-3', '-4', '-5', '-6', '-7', '-8', '-9', '-10', '-11', '-12', '-13', '-14', '-15', '-16', '-17', '-18', '-19'};

```

```

stim_amp = [0.04 0.05 0.06 0.07 0.08 0.09 0.1 0.5 0.6 0.7 0.8 0.9 1 0.2 0.3 0.4];

emg_blocks = [];
for j=1:length(blocks)
    block = [block_prefix blocks{j}];

    data = TDT2mat(tank,block);

    estim = data.streams.EWav.data;
    emg_wav = data.streams.EMG_.data(1,:)*1000/20;

    fs = data.streams.EMG_.fs;
    t = (0:length(estim)-1)/fs;

    stimon = diff(estim)>1;
    stiminds = find(stimon);

    pre_t = 0;
    post_t = 5000;

    emg_snip = [];
    emg_rms = [];
    for i=1:length(stiminds)
        emg_snip(i,:) = emg_wav(1,stiminds(i)-pre_t:stiminds(i)+post_t);
        emg_rms(i) = sqrt(mean(emg_wav(1,stiminds(i)-pre_t:stiminds(i)+post_t).^2));
    end
    emg_blocks(j).emg_snip = emg_snip;
    emg_blocks(j).emg_rms = emg_rms;
    emg_blocks(j).emg_wav = emg_wav;
    emg_blocks(j).estim = estim;
    emg_blocks(j).fs = fs;
    emg_blocks(j).t = t;
    emg_blocks(j).mean_emg_rms = mean(emg_rms);

    snip_t = (-pre_t:post_t)/fs;
    figure;plot(snip_t,emg_snip')
    title(['EMG Snippets, ' num2str(stim_amp(j)) ' mA'])
    xlabel('Time (s)')
    ylabel('EMG (mV)')
end
Figure;plot(stim_amp,[emg_blocks.mean_emg_rms],'bo')
title('Mean EMG RMS vs. Stim Amplitude')
xlabel('Stim Amp (mA)')
ylabel('EMG RMS (mV)');

save([block_prefix '.mat'], 'emg_blocks')

```

## Bibliography

- [1] D.M. Faulk, S.F. Badylak, Chapter 8 - Natural Biomaterials for Regenerative Medicine Applications, in: G. Orlando, J. Lerut, S. Soker, R.J. Stratta (Eds.), *Regenerative Medicine Applications in Organ Transplantation*, Academic Press, Boston, 2014, pp. 101-112.
- [2] D.M. Faulk, S.A. Johnson, S.F. Badylak, 7 - Decellularized biological scaffolds for cardiac repair and regeneration, in: R.-K. Li, R.D. Weisel (Eds.), *Cardiac Regeneration and Repair*, Woodhead Publishing 2014, pp. 180-200.
- [3] J.R. Miner, P.M. Paris, D.M. Yealy, e.a. Marx, *Mark: Rosen's Emergency Medicine, Pain Management* (2010).
- [4] B.M. Reuss, Glial Growth Factors, in: L.R. Squire (Ed.), *Encyclopedia of Neuroscience*, Academic Press, Oxford, 2009, pp. 819-825.
- [5] R.M.G. Menorca, T.S. Fussell, J.C. Elfar, Nerve physiology: mechanisms of injury and recovery, *Hand clinics* 29(3) (2013) 317-330.
- [6] S. Sunderland, A classification of peripheral nerve injuries producing loss of function, *Brain : a journal of neurology* 74(4) (1951) 491-516.
- [7] M. Caillaud, L. Richard, J.M. Vallat, A. Desmouliere, F. Billet, Peripheral nerve regeneration and intraneural revascularization, *Neural Regen Res* 14(1) (2019) 24-33.
- [8] D. Grinsell, C.P. Keating, Peripheral nerve reconstruction after injury: a review of clinical and experimental therapies, *Biomed Res Int* 2014 (2014) 698256.
- [9] M.P. Clements, E. Byrne, L.F. Camarillo Guerrero, A.L. Cattin, L. Zakka, A. Ashraf, J.J. Burden, S. Khadayate, A.C. Lloyd, S. Marguerat, S. Parrinello, The Wound Microenvironment Reprograms Schwann Cells to Invasive Mesenchymal-like Cells to Drive Peripheral Nerve Regeneration, *Neuron* 96(1) (2017) 98-114.e7.
- [10] S.K. Lee, S.W. Wolfe, Peripheral nerve injury and repair, *The Journal of the American Academy of Orthopaedic Surgeons* 8(4) (2000) 243-52.

- [11] I. Allodi, E. Udina, X. Navarro, Specificity of peripheral nerve regeneration: interactions at the axon level, *Prog Neurobiol* 98(1) (2012) 16-37.
- [12] D. Gonzalez-Forero, B. Moreno-Lopez, Retrograde response in axotomized motoneurons: nitric oxide as a key player in triggering reversion toward a dedifferentiated phenotype, *Neuroscience* 283 (2014) 138-65.
- [13] K.R. Jessen, R. Mirsky, The repair Schwann cell and its function in regenerating nerves, *The Journal of physiology* 594(13) (2016) 3521-31.
- [14] J. Scheib, A. Hoke, Advances in peripheral nerve regeneration, *Nature reviews. Neurology* 9(12) (2013) 668-76.
- [15] A.D. Gaudet, P.G. Popovich, Extracellular matrix regulation of inflammation in the healthy and injured spinal cord, *Exp Neurol* 258 (2014) 24-34.
- [16] A.L. Cattin, A.C. Lloyd, The multicellular complexity of peripheral nerve regeneration, *Current opinion in neurobiology* 39 (2016) 38-46.
- [17] K.C.S. Roballo, J. Bushman, Evaluation of the host immune response and functional recovery in peripheral nerve autografts and allografts, *Transplant immunology* (2019).
- [18] C.R. Cashman, A. Hoke, Deficiency of adaptive immunity does not interfere with Wallerian degeneration, *PLoS One* 12(5) (2017) e0177070.
- [19] P. Chen, X. Piao, P. Bonaldo, Role of macrophages in Wallerian degeneration and axonal regeneration after peripheral nerve injury, *Acta Neuropathol* 130(5) (2015) 605-18.
- [20] M. Eder, W. Schulte-Mattler, P. Poschl, Neurographic course Of Wallerian degeneration after human peripheral nerve injury, *Muscle Nerve* 56(2) (2017) 247-252.
- [21] A.-L. Cattin, J.J. Burden, L. Van Emmenis, F.E. Mackenzie, J.J.A. Hoving, N. Garcia Calavia, Y. Guo, M. McLaughlin, L.H. Rosenberg, V. Quereda, D. Jamecna, I. Napoli, S. Parrinello, T. Enver, C. Ruhrberg, A.C. Lloyd, Macrophage-Induced Blood Vessels Guide Schwann Cell-Mediated Regeneration of Peripheral Nerves, *Cell* 162(5) (2015) 1127-1139.
- [22] N. Mokarram, A. Merchant, V. Mukhatyar, G. Patel, R.V. Bellamkonda, Effect of modulating macrophage phenotype on peripheral nerve repair, *Biomaterials* 33(34) (2012) 8793-801.

- [23] B.M. Reuss, Glial Growth Factors, (2009) 819-825.
- [24] J.W. Griffin, R. George, T. Ho, Macrophage systems in peripheral nerves. A review, Journal of neuropathology and experimental neurology 52(6) (1993) 553-60.
- [25] X. Navarro, Functional evaluation of peripheral nerve regeneration and target reinnervation in animal models: a critical overview, Eur J Neurosci 43(3) (2016) 271-86.
- [26] W. Sulaiman, T. Gordon, Neurobiology of peripheral nerve injury, regeneration, and functional recovery: from bench top research to bedside application, The Ochsner journal 13(1) (2013) 100-8.
- [27] A. Chemnitz, A. Bjorkman, L.B. Dahlin, B. Rosen, Functional outcome thirty years after median and ulnar nerve repair in childhood and adolescence, J Bone Joint Surg Am 95(4) (2013) 329-37.
- [28] S.P. Galanakos, A.B. Zoubos, I. Ignatiadis, I. Papakostas, N.E. Gerostathopoulos, P.N. Soucacos, Repair of complete nerve lacerations at the forearm: an outcome study using Rosen-Lundborg protocol, Microsurgery 31(4) (2011) 253-62.
- [29] K.E. LeBlanc, W. Cestia, Carpal tunnel syndrome, American family physician 83(8) (2011) 952-8.
- [30] F.W. Drislane, M. Benatar, B. Chang, J. Acosta, A. Tarulli, L. Caplan, Blueprints Neurology, Fourth ed., Wolers Kluwer Health, Philadelphia, PA, 2014.
- [31] K. Brattain, Analysis of the peripheral nerve repair market in the United States, Magellan Medical Technology Consultants, Inc., Minneapolis, Minnesota, 2013, pp. 1-11.
- [32] D. Grinsell, C. P Keating, Peripheral Nerve Reconstruction after Injury: A Review of Clinical and Experimental Therapies, 2014.
- [33] L.H. Poppler, K. Davidge, J.C.Y. Lu, J. Armstrong, I.K. Fox, S.E. Mackinnon, Alternatives to sural nerve grafts in the upper extremity, Hand (New York, N.Y.) 10(1) (2015) 68-75.
- [34] C.C. Chen, J. Yu, H.Y. Ng, A.K. Lee, C.C. Chen, Y.S. Chen, M.Y. Shie, The Physicochemical Properties of Decellularized Extracellular Matrix-Coated 3D Printed Poly(epsilon-caprolactone)

Nerve Conduits for Promoting Schwann Cells Proliferation and Differentiation, *Materials (Basel)* 11(9) (2018).

[35] F.E. Karabekmez, A. Duymaz, S.L. Moran, Early clinical outcomes with the use of decellularized nerve allograft for repair of sensory defects within the hand, *Hand (N Y)* 4(3) (2009) 245-9.

[36] S.W. Kemp, S.K. Walsh, R. Midha, Growth factor and stem cell enhanced conduits in peripheral nerve regeneration and repair, *Neurol Res* 30(10) (2008) 1030-8.

[37] F.G. M, M. M, H. S, W.S. Khan, Peripheral nerve injury: principles for repair and regeneration, *The open orthopaedics journal* 8 (2014) 199-203.

[38] B. Rinker, J. Zoldos, R.V. Weber, J. Ko, W. Thayer, J. Greenberg, F.J. Leversedge, B. Safa, G. Buncke, Use of Processed Nerve Allografts to Repair Nerve Injuries Greater Than 25 mm in the Hand, *Ann Plast Surg* 78(6S Suppl 5) (2017) S292-S295.

[39] J. Isaacs, B. Safa, A Preliminary Assessment of the Utility of Large-Caliber Processed Nerve Allografts for the Repair of Upper Extremity Nerve Injuries, *Hand (N Y)* 12(1) (2017) 55-59.

[40] A. Yampolsky, V. Ziccardi, S.K. Chuang, Efficacy of Acellular Nerve Allografts in Trigeminal Nerve Reconstruction, *J Oral Maxillofac Surg* 75(10) (2017) 2230-2234.

[41] P.J. Apel, J.P. Garrett, P. Sierpinski, J. Ma, A. Atala, T.L. Smith, L.A. Koman, M.E. Van Dyke, Peripheral nerve regeneration using a keratin-based scaffold: long-term functional and histological outcomes in a mouse model, *The Journal of hand surgery* 33(9) (2008) 1541-7.

[42] M.C. Dodla, R.V. Bellamkonda, Differences between the effect of anisotropic and isotropic laminin and nerve growth factor presenting scaffolds on nerve regeneration across long peripheral nerve gaps, *Biomaterials* 29(1) (2008) 33-46.

[43] E.G. Fine, I. Decosterd, M. Papaloizos, A.D. Zurn, P. Aebischer, GDNF and NGF released by synthetic guidance channels support sciatic nerve regeneration across a long gap, *The European journal of neuroscience* 15(4) (2002) 589-601.

[44] A.C. Lee, V.M. Yu, J.B. Lowe, 3rd, M.J. Brenner, D.A. Hunter, S.E. Mackinnon, S.E. Sakiyama-Elbert, Controlled release of nerve growth factor enhances sciatic nerve regeneration, *Exp Neurol* 184(1) (2003) 295-303.

- [45] R. Midha, C.A. Munro, P.D. Dalton, C.H. Tator, M.S. Shoichet, Growth factor enhancement of peripheral nerve regeneration through a novel synthetic hydrogel tube, *J Neurosurg* 99(3) (2003) 555-65.
- [46] A.M. Moore, M.D. Wood, K. Chenard, D.A. Hunter, S.E. Mackinnon, S.E. Sakiyama-Elbert, G.H. Borschel, Controlled delivery of glial cell line-derived neurotrophic factor enhances motor nerve regeneration, *The Journal of hand surgery* 35(12) (2010) 2008-17.
- [47] A. Mosahebi, M. Wiberg, G. Terenghi, Addition of fibronectin to alginate matrix improves peripheral nerve regeneration in tissue-engineered conduits, *Tissue Eng* 9(2) (2003) 209-18.
- [48] P. Sierpinski, J. Garrett, J. Ma, P. Apel, D. Klorig, T. Smith, L.A. Koman, A. Atala, M. Van Dyke, The use of keratin biomaterials derived from human hair for the promotion of rapid regeneration of peripheral nerves, *Biomaterials* 29(1) (2008) 118-28.
- [49] E. Udina, F.J. Rodriguez, E. Verdu, M. Espejo, B.G. Gold, X. Navarro, FK506 enhances regeneration of axons across long peripheral nerve gaps repaired with collagen guides seeded with allogeneic Schwann cells, *Glia* 47(2) (2004) 120-9.
- [50] M.D. Wood, A.M. Moore, D.A. Hunter, S. Tuffaha, G.H. Borschel, S.E. Mackinnon, S.E. Sakiyama-Elbert, Affinity-based release of glial-derived neurotrophic factor from fibrin matrices enhances sciatic nerve regeneration, *Acta biomaterialia* 5(4) (2009) 959-68.
- [51] M.D. Wood, S.W. Kemp, C. Weber, G.H. Borschel, T. Gordon, Outcome measures of peripheral nerve regeneration, *Ann Anat* 193(4) (2011) 321-33.
- [52] T.A. Prest, E. Yeager, S.T. LoPresti, E. Zygelyte, M.J. Martin, L. Dong, A. Gibson, O.O. Olutoye, B.N. Brown, J. Cheetham, Nerve-specific, xenogeneic extracellular matrix hydrogel promotes recovery following peripheral nerve injury, *J Biomed Mater Res A* 106(2) (2018) 450-459.
- [53] D.J. Terris, K.M. Toft, M. Moir, J. Lum, M. Wang, Brain-derived neurotrophic factor-enriched collagen tubule as a substitute for autologous nerve grafts, *Archives of otolaryngology--head & neck surgery* 127(3) (2001) 294-8.
- [54] M.A. Wood MD, Hunter DA, et al., Affinity-based release of glial-derived neurotrophic factor from fibrin matrices enhances sciatic nerve regeneration, *Acta Biomaterials* 5(4) (2009) 589-601.

- [55] T. Mimura, M. Dezawa, H. Kanno, H. Sawada, I. Yamamoto, Peripheral nerve regeneration by transplantation of bone marrow stromal cell-derived Schwann cells in adult rats, *J Neurosurg* 101(5) (2004) 806-12.
- [56] S.H. Hsu, C.J. Chang, C.M. Tang, F.T. Lin, In vitro and in vivo effects of Ginkgo biloba extract EGb 761 on seeded Schwann cells within poly(DL-lactic acid-co-glycolic acid) conduits for peripheral nerve regeneration, *Journal of biomaterials applications* 19(2) (2004) 163-82.
- [57] L. Schaefer, R.M. Schaefer, Proteoglycans: from structural compounds to signaling molecules, *Cell and tissue research* 339(1) (2010) 237-46.
- [58] H. Järveläinen, A. Sainio, M. Koulu, T.N. Wight, R. Penttinen, Extracellular Matrix Molecules: Potential Targets in Pharmacotherapy, *Pharmacological Reviews* 61(2) (2009) 198-223.
- [59] C. Frantz, K.M. Stewart, V.M. Weaver, The extracellular matrix at a glance, *Journal of Cell Science* 123(24) (2010) 4195-4200.
- [60] S. Ricard-Blum, F. Ruggiero, The collagen superfamily: from the extracellular matrix to the cell membrane, *Pathologie-biologie* 53(7) (2005) 430-42.
- [61] J. Myllyharju, K.I. Kivirikko, Collagens, modifying enzymes and their mutations in humans, flies and worms, *Trends in genetics : TIG* 20(1) (2004) 33-43.
- [62] S. Koochekpour, A. Merzak, G.J. Pilkington, Extracellular matrix proteins inhibit proliferation, upregulate migration and induce morphological changes in human glioma cell lines, *European journal of cancer (Oxford, England : 1990)* 31a(3) (1995) 375-80.
- [63] C.M. Williams, A.J. Engler, R.D. Slone, L.L. Galante, J.E. Schwarzbauer, Fibronectin expression modulates mammary epithelial cell proliferation during acinar differentiation, *Cancer research* 68(9) (2008) 3185-92.
- [64] D. Bosnakovski, M. Mizuno, G. Kim, S. Takagi, M. Okumura, T. Fujinaga, Chondrogenic differentiation of bovine bone marrow mesenchymal stem cells (MSCs) in different hydrogels: influence of collagen type II extracellular matrix on MSC chondrogenesis, *Biotechnology and bioengineering* 93(6) (2006) 1152-63.

- [65] S.R. Chastain, A.K. Kundu, S. Dhar, J.W. Calvert, A.J. Putnam, Adhesion of mesenchymal stem cells to polymer scaffolds occurs via distinct ECM ligands and controls their osteogenic differentiation, *Journal of biomedical materials research. Part A* 78(1) (2006) 73-85.
- [66] P. Simon-Assmann, M. Kedinger, A. De Arcangelis, V. Rousseau, P. Simo, Extracellular matrix components in intestinal development, *Experientia* 51(9-10) (1995) 883-900.
- [67] J.A. DeQuach, V. Mezzano, A. Miglani, S. Lange, G.M. Keller, F. Sheikh, K.L. Christman, Simple and high yielding method for preparing tissue specific extracellular matrix coatings for cell culture, *PLoS One* 5(9) (2010) e13039.
- [68] M.J. Bissell, J. Aggeler, Dynamic reciprocity: how do extracellular matrix and hormones direct gene expression?, *Progress in clinical and biological research* 249 (1987) 251-62.
- [69] P. Bornstein, E.H. Sage, Matricellular proteins: extracellular modulators of cell function, *Current opinion in cell biology* 14(5) (2002) 608-16.
- [70] T.R. Kyriakides, P. Bornstein, Matricellular proteins as modulators of wound healing and the foreign body response, *Thrombosis and haemostasis* 90(6) (2003) 986-92.
- [71] X. Gao, Y. Wang, J. Chen, J. Peng, The role of peripheral nerve ECM components in the tissue engineering nerve construction, *Rev Neurosci* 24(4) (2013) 443-53.
- [72] S.N. Masand, I.J. Perron, M. Schachner, D.I. Shreiber, Neural cell type-specific responses to glycomimetic functionalized collagen, *Biomaterials* 33(3) (2012) 790-7.
- [73] L. Zilic, P.E. Garner, T. Yu, S. Roman, J.W. Haycock, S.-P. Wilshaw, An anatomical study of porcine peripheral nerve and its potential use in nerve tissue engineering, *Journal of Anatomy* 227(3) (2015) 302-314.
- [74] J.P. Hodde, R.D. Record, H.A. Liang, S.F. Badylak, Vascular endothelial growth factor in porcine-derived extracellular matrix, *Endothelium : journal of endothelial cell research* 8(1) (2001) 11-24.
- [75] S.L. Voytik-Harbin, A.O. Brightman, M.R. Kraine, B. Waisner, S.F. Badylak, Identification of extractable growth factors from small intestinal submucosa, *Journal of cellular biochemistry* 67(4) (1997) 478-91.

- [76] H. Marcal, T. Ahmed, S.F. Badylak, S. Tottey, L.J. Foster, A comprehensive protein expression profile of extracellular matrix biomaterial derived from porcine urinary bladder, *Regen Med* 7(2) (2012) 159-66.
- [77] R.W. Bonvillain, S. Danchuk, D.E. Sullivan, A.M. Betancourt, J.A. Semon, M.E. Eagle, J.P. Mayeux, A.N. Gregory, G. Wang, I.K. Townley, Z.D. Borg, D.J. Weiss, B.A. Bunnell, A nonhuman primate model of lung regeneration: detergent-mediated decellularization and initial in vitro recellularization with mesenchymal stem cells, *Tissue engineering. Part A* 18(23-24) (2012) 2437-52.
- [78] D.A. Taylor, L.C. Sampaio, Z. Ferdous, A.S. Gobin, L.J. Taite, Decellularized matrices in regenerative medicine, *Acta biomaterialia* (2018).
- [79] S.F. Badylak, D.O. Freytes, T.W. Gilbert, Extracellular matrix as a biological scaffold material: Structure and function, *Acta Biomater* 5(1) (2009) 1-13.
- [80] P.M. Crapo, T.W. Gilbert, S.F. Badylak, An overview of tissue and whole organ decellularization processes, *Biomaterials* 32(12) (2011) 3233-43.
- [81] S.F. Badylak, D.J. Weiss, A. Caplan, P. Macchiarini, Engineered whole organs and complex tissues, *Lancet (London, England)* 379(9819) (2012) 943-952.
- [82] I.T. Swinehart, S.F. Badylak, Extracellular matrix bioscaffolds in tissue remodeling and morphogenesis, *Developmental dynamics : an official publication of the American Association of Anatomists* 245(3) (2016) 351-360.
- [83] T.L. Adair-Kirk, R.M. Senior, Fragments of extracellular matrix as mediators of inflammation, *The international journal of biochemistry & cell biology* 40(6-7) (2008) 1101-10.
- [84] G.E. Davis, K.J. Bayless, M.J. Davis, G.A. Meininger, Regulation of tissue injury responses by the exposure of matricryptic sites within extracellular matrix molecules, *The American journal of pathology* 156(5) (2000) 1489-98.
- [85] Z.L. Shen, F. Lassner, A. Bader, M. Becker, G.F. Walter, A. Berger, Cellular activity of resident macrophages during Wallerian degeneration, *Microsurgery* 20(5) (2000) 255-61.
- [86] D. Lindholm, R. Heumann, M. Meyer, H. Thoenen, Interleukin-1 regulates synthesis of nerve growth factor in non-neuronal cells of rat sciatic nerve, *Nature* 330(6149) (1987) 658-9.

- [87] S. Gordon, F.O. Martinez, Alternative activation of macrophages: mechanism and functions, *Immunity* 32(5) (2010) 593-604.
- [88] M. Mueller, C. Leonhard, K. Wacker, E.B. Ringelstein, M. Okabe, W.F. Hickey, R. Kiefer, Macrophage response to peripheral nerve injury: the quantitative contribution of resident and hematogenous macrophages, *Laboratory investigation; a journal of technical methods and pathology* 83(2) (2003) 175-85.
- [89] N. Mokarram, A. Merchant, V. Mukhatyar, G. Patel, R.V. Bellamkonda, Effect of modulating macrophage phenotype on peripheral nerve repair, *Biomaterials* 33(34) (2012) 8793-8801.
- [90] M.P. Lutolf, J.A. Hubbell, Synthetic biomaterials as instructive extracellular microenvironments for morphogenesis in tissue engineering, *Nature biotechnology* 23(1) (2005) 47-55.
- [91] S. Uriel, E. Labay, M. Francis-Sedlak, M.L. Moya, R.R. Weichselbaum, N. Ervin, Z. Cankova, E.M. Brey, Extraction and assembly of tissue-derived gels for cell culture and tissue engineering, *Tissue engineering. Part C, Methods* 15(3) (2009) 309-21.
- [92] M.M. Stern, R.L. Myers, N. Hammam, K.A. Stern, D. Eberli, S.B. Kritchevsky, S. Soker, M. Van Dyke, The influence of extracellular matrix derived from skeletal muscle tissue on the proliferation and differentiation of myogenic progenitor cells ex vivo, *Biomaterials* 30(12) (2009) 2393-9.
- [93] Y. Zhang, Y. He, S. Bharadwaj, N. Hammam, K. Carnagey, R. Myers, A. Atala, M. Van Dyke, Tissue-specific extracellular matrix coatings for the promotion of cell proliferation and maintenance of cell phenotype, *Biomaterials* 30(23-24) (2009) 4021-8.
- [94] D.A. Young, D.O. Ibrahim, D. Hu, K.L. Christman, Injectable hydrogel scaffold from decellularized human lipoaspirate, *Acta biomaterialia* 7(3) (2011) 1040-9.
- [95] S.B. Seif-Naraghi, M.A. Salvatore, P.J. Schup-Magoffin, D.P. Hu, K.L. Christman, Design and characterization of an injectable pericardial matrix gel: a potentially autologous scaffold for cardiac tissue engineering, *Tissue Eng Part A* 16(6) (2010) 2017-27.
- [96] D.O. Freytes, J. Martin, S.S. Velankar, A.S. Lee, S.F. Badylak, Preparation and rheological characterization of a gel form of the porcine urinary bladder matrix, *Biomaterials* 29(11) (2008) 1630-7.

[97] C.J. Medberry, P.M. Crapo, B.F. Siu, C.A. Carruthers, M.T. Wolf, S.P. Nagarkar, V. Agrawal, K.E. Jones, J. Kelly, S.A. Johnson, S.S. Velankar, S.C. Watkins, M. Modo, S.F. Badylak, Hydrogels derived from central nervous system extracellular matrix, *Biomaterials* 34(4) (2013) 1033-40.

[98] E.P. Brennan, X.H. Tang, A.M. Stewart-Akers, L.J. Gudas, S.F. Badylak, Chemoattractant activity of degradation products of fetal and adult skin extracellular matrix for keratinocyte progenitor cells, *Journal of tissue engineering and regenerative medicine* 2(8) (2008) 491-8.

[99] R.A. Allen, L.M. Seltz, H. Jiang, R.T. Kasick, T.L. Sellaro, S.F. Badylak, J.B. Ogilvie, Adrenal extracellular matrix scaffolds support adrenocortical cell proliferation and function in vitro, *Tissue engineering. Part A* 16(11) (2010) 3363-74.

[100] T.L. Sellaro, A. Ranade, D.M. Faulk, G.P. McCabe, K. Dorko, S.F. Badylak, S.C. Strom, Maintenance of human hepatocyte function in vitro by liver-derived extracellular matrix gels, *Tissue engineering. Part A* 16(3) (2010) 1075-82.

[101] T.L. Sellaro, A.K. Ravindra, D.B. Stolz, S.F. Badylak, Maintenance of hepatic sinusoidal endothelial cell phenotype in vitro using organ-specific extracellular matrix scaffolds, *Tissue Eng* 13(9) (2007) 2301-10.

[102] M.T. Wolf, K.A. Daly, J.E. Reing, S.F. Badylak, Biologic scaffold composed of skeletal muscle extracellular matrix, *Biomaterials* 33(10) (2012) 2916-25.

[103] A.J. Beattie, T.W. Gilbert, J.P. Guyot, A.J. Yates, S.F. Badylak, Chemoattraction of progenitor cells by remodeling extracellular matrix scaffolds, *Tissue engineering. Part A* 15(5) (2009) 1119-25.

[104] S.F. Badylak, R. Tullius, K. Kokini, K.D. Shelbourne, T. Klootwyk, S.L. Voytik, M.R. Kraine, C. Simmons, The use of xenogeneic small intestinal submucosa as a biomaterial for Achilles tendon repair in a dog model, *Journal of biomedical materials research* 29(8) (1995) 977-85.

[105] S.F. Badylak, T. Hoppo, A. Nieponice, T.W. Gilbert, J.M. Davison, B.A. Jobe, Esophageal preservation in five male patients after endoscopic inner-layer circumferential resection in the setting of superficial cancer: a regenerative medicine approach with a biologic scaffold, *Tissue engineering. Part A* 17(11-12) (2011) 1643-50.

[106] P.M. Crapo, S. Tottey, P.F. Slivka, S.F. Badylak, Effects of biologic scaffolds on human stem cells and implications for CNS tissue engineering, *Tissue Eng Part A* 20(1-2) (2014) 313-23.

- [107] P.M. Crapo, C.J. Medberry, J.E. Reing, S. Tottey, Y. van der Merwe, K.E. Jones, S.F. Badylak, Biologic scaffolds composed of central nervous system extracellular matrix, *Biomaterials* 33(13) (2012) 3539-47.
- [108] S.J. Armstrong, M. Wiberg, G. Terenghi, P.J. Kingham, ECM molecules mediate both Schwann cell proliferation and activation to enhance neurite outgrowth, *Tissue Eng* 13(12) (2007) 2863-70.
- [109] B.N. Brown, J.E. Valentin, A.M. Stewart-Akers, G.P. McCabe, S.F. Badylak, Macrophage phenotype and remodeling outcomes in response to biologic scaffolds with and without a cellular component, *Biomaterials* 30(8) (2009) 1482-91.
- [110] B.N. Brown, R. Londono, S. Tottey, L. Zhang, K.A. Kukla, M.T. Wolf, K.A. Daly, J.E. Reing, S.F. Badylak, Macrophage phenotype as a predictor of constructive remodeling following the implantation of biologically derived surgical mesh materials, *Acta Biomater* 8(3) (2012) 978-87.
- [111] X. Navarro, M. Vivo, A. Valero-Cabre, Neural plasticity after peripheral nerve injury and regeneration, *Prog Neurobiol* 82(4) (2007) 163-201.
- [112] R.D. Madison, G.A. Robinson, S.R. Chadaram, The specificity of motor neurone regeneration (preferential reinnervation), *Acta physiologica (Oxford, England)* 189(2) (2007) 201-6.
- [113] B.N. Brown, S.F. Badylak, Extracellular matrix as an inductive scaffold for functional tissue reconstruction, *Transl Res* 163(4) (2014) 268-85.
- [114] F. Meng, M. Modo, S.F. Badylak, Biologic scaffold for CNS repair, *Regen Med* 9(3) (2014) 367-83.
- [115] A.C. Pollins, R.B. Boyer, M. Nussenbaum, W.P. Thayer, Comparing Processed Nerve Allografts and Assessing Their Capacity to Retain and Release Nerve Growth Factor, *Ann Plast Surg* 81(2) (2018) 198-202.
- [116] T.W. Hudson, S. Zawko, C. Deister, S. Lundy, C.Y. Hu, K. Lee, C.E. Schmidt, Optimized acellular nerve graft is immunologically tolerated and supports regeneration, *Tissue engineering* 10(11-12) (2004) 1641-51.

- [117] S. Gao, Y. Zheng, Q. Cai, W. Yao, J. Wang, P. Zhang, X. Wang, Comparison of morphology and biocompatibility of acellular nerve scaffolds processed by different chemical methods, *J Mater Sci Mater Med* 25(5) (2014) 1283-91.
- [118] D. Neubauer, J.B. Graham, D. Muir, Chondroitinase treatment increases the effective length of acellular nerve grafts, *Exp Neurol* 207(1) (2007) 163-70.
- [119] M. Sondell, G. Lundborg, M. Kanje, Vascular endothelial growth factor stimulates Schwann cell invasion and neovascularization of acellular nerve grafts, *Brain Res* 846(2) (1999) 219-28.
- [120] M. Cai, T. Huang, B. Hou, Y. Guo, Role of Demyelination Efficiency within Acellular Nerve Scaffolds during Nerve Regeneration across Peripheral Defects, *Biomed Res Int* 2017 (2017) 4606387.
- [121] M. Sondell, G. Lundborg, M. Kanje, Regeneration of the rat sciatic nerve into allografts made acellular through chemical extraction, *Brain Res* 795(1-2) (1998) 44-54.
- [122] G. Giusti, W.F. Willems, T. Kremer, P.F. Friedrich, A.T. Bishop, A.Y. Shin, Return of motor function after segmental nerve loss in a rat model: comparison of autogenous nerve graft, collagen conduit, and processed allograft (AxoGen), *J Bone Joint Surg Am* 94(5) (2012) 410-7.
- [123] C.A. Hundepool, T.H. Nijhuis, D. Kotsougiani, P.F. Friedrich, A.T. Bishop, A.Y. Shin, Optimizing decellularization techniques to create a new nerve allograft: an in vitro study using rodent nerve segments, *Neurosurg Focus* 42(3) (2017) E4.
- [124] M.M. Garcia-Perez, H.G. Martinez-Rodriguez, G.G. Lopez-Guerra, A. Soto-Dominguez, S.L. Said-Fernandez, R. Morales-Avalos, R.E. Elizondo-Omana, R. Montes-de-Oca-Luna, S. Guzman-Lopez, M.L. Castillo-Galvan, O.F. Mendoza-Lemus, F. Vilchez-Cavazos, A modified chemical protocol of decellularization of rat sciatic nerve and its recellularization with mesenchymal differentiated schwann-like cells: morphological and functional assessments, *Histol Histopathol* 32(8) (2017) 779-792.
- [125] A.C. Pollins, J.S. Kim, R.B. Boyer, W.P. Thayer, Mass spectrometry comparison of nerve allograft decellularization processes, *J Mater Sci Mater Med* 28(1) (2017) 20.
- [126] Z. Zhao, Y. Wang, J. Peng, Z. Ren, L. Zhang, Q. Guo, W. Xu, S. Lu, Improvement in nerve regeneration through a decellularized nerve graft by supplementation with bone marrow stromal cells in fibrin, *Cell Transplant* 23(1) (2014) 97-110.

- [127] T. Lin, S. Liu, S. Chen, S. Qiu, Z. Rao, J. Liu, S. Zhu, L. Yan, H. Mao, Q. Zhu, D. Quan, X. Liu, Hydrogel derived from porcine decellularized nerve tissue as a promising biomaterial for repairing peripheral nerve defects, *Acta Biomater* 73 (2018) 326-338.
- [128] N. Mligiliche, M. Kitada, C. Ide, Grafting of detergent-denatured skeletal muscles provides effective conduits for extension of regenerating axons in the rat sciatic nerve, *Archives of histology and cytology* 64(1) (2001) 29-36.
- [129] R.J. Nagao, S. Lundy, Z.Z. Khaing, C.E. Schmidt, Functional characterization of optimized acellular peripheral nerve graft in a rat sciatic nerve injury model, *Neurol Res* 33(6) (2011) 600-8.
- [130] J.K. Kim, Y.D. Koh, J.O. Kim, D.H. Seo, Development of a decellularization method to produce nerve allografts using less invasive detergents and hyper/hypotonic solutions, *J Plast Reconstr Aesthet Surg* 69(12) (2016) 1690-1696.
- [131] S. Vasudevan, J. Huang, B. Botterman, H.S. Matloub, E. Keefer, J. Cheng, Detergent-free Decellularized Nerve Grafts for Long-gap Peripheral Nerve Reconstruction, *Plast Reconstr Surg Glob Open* 2(8) (2014) e201.
- [132] R. Sridharan, R.B. Reilly, C.T. Buckley, Decellularized grafts with axially aligned channels for peripheral nerve regeneration, *J Mech Behav Biomed Mater* 41 (2015) 124-35.
- [133] W. Wang, S. Itoh, K. Takakuda, Comparative study of the efficacy of decellularization treatment of allogenic and xenogenic nerves as nerve conduits, *J Biomed Mater Res A* 104(2) (2016) 445-54.
- [134] Y. Gu, J. Zhu, C. Xue, Z. Li, F. Ding, Y. Yang, X. Gu, Chitosan/silk fibroin-based, Schwann cell-derived extracellular matrix-modified scaffolds for bridging rat sciatic nerve gaps, *Biomaterials* 35(7) (2014) 2253-63.
- [135] Z.T. Kokkalis, C. Pu, G.A. Small, R.W. Weiser, A.I. Venouziou, D.G. Sotereanos, Assessment of processed porcine extracellular matrix as a protective barrier in a rabbit nerve wrap model, *J Reconstr Microsurg* 27(1) (2011) 19-28.
- [136] Y. Wakimura, W. Wang, S. Itoh, M. Okazaki, K. Takakuda, An Experimental Study to Bridge a Nerve Gap with a Decellularized Allogeneic Nerve, *Plast Reconstr Surg* 136(3) (2015) 319e-327e.

- [137] R.B. Boyer, K.W. Sexton, C.L. Rodriguez-Feo, R. Nookala, A.C. Pollins, N.L. Cardwell, K.Y. Tisdale, L.B. Nanney, R.B. Shack, W.P. Thayer, Adjuvant neurotrophic factors in peripheral nerve repair with chondroitin sulfate proteoglycan-reduced acellular nerve allografts, *J Surg Res* 193(2) (2015) 969-77.
- [138] A.M. Moore, M. MacEwan, K.B. Santosa, K.E. Chenard, W.Z. Ray, D.A. Hunter, S.E. Mackinnon, P.J. Johnson, Acellular nerve allografts in peripheral nerve regeneration: a comparative study, *Muscle Nerve* 44(2) (2011) 221-34.
- [139] X. Sun, Y. Wang, Z. Guo, B. Xiao, Z. Sun, H. Yin, H. Meng, X. Sui, Q. Zhao, Q. Guo, A. Wang, W. Xu, S. Liu, Y. Li, S. Lu, J. Peng, Acellular Cauda Equina Allograft as Main Material Combined with Biodegradable Chitin Conduit for Regeneration of Long-Distance Sciatic Nerve Defect in Rats, *Adv Healthc Mater* 7(17) (2018) e1800276.
- [140] Y. Zhang, H. Luo, Z. Zhang, Y. Lu, X. Huang, L. Yang, J. Xu, W. Yang, X. Fan, B. Du, P. Gao, G. Hu, Y. Jin, A nerve graft constructed with xenogeneic acellular nerve matrix and autologous adipose-derived mesenchymal stem cells, *Biomaterials* 31(20) (2010) 5312-24.
- [141] A. Gilpin, Y. Yang, Decellularization Strategies for Regenerative Medicine: From Processing Techniques to Applications, *BioMed research international* 2017 (2017) 9831534-9831534.
- [142] O. Syed, N.J. Walters, R.M. Day, H.W. Kim, J.C. Knowles, Evaluation of decellularization protocols for production of tubular small intestine submucosa scaffolds for use in oesophageal tissue engineering, *Acta Biomater* 10(12) (2014) 5043-5054.
- [143] J.D. O'Neill, R. Anfang, A. Anandappa, J. Costa, J. Javidfar, H.M. Wobma, G. Singh, D.O. Freytes, M.D. Bacchetta, J.R. Sonett, G. Vunjak-Novakovic, Decellularization of human and porcine lung tissues for pulmonary tissue engineering, *The Annals of thoracic surgery* 96(3) (2013) 1046-55; discussion 1055-6.
- [144] F. Boriani, N. Fazio, C. Fotia, L. Savarino, N. Nicoli Aldini, L. Martini, N. Zini, M. Bernardini, N. Baldini, A novel technique for decellularization of allogenic nerves and in vivo study of their use for peripheral nerve reconstruction, *J Biomed Mater Res A* 105(8) (2017) 2228-2240.
- [145] L. Zilic, S.P. Wilshaw, J.W. Haycock, Decellularisation and histological characterisation of porcine peripheral nerves, *Biotechnol Bioeng* 113(9) (2016) 2041-53.

- [146] E. Meezan, J.T. Hjelle, K. Brendel, E.C. Carlson, A simple, versatile, nondisruptive method for the isolation of morphologically and chemically pure basement membranes from several tissues, *Life sciences* 17(11) (1975) 1721-32.
- [147] J.Y. Wang, A. Liou, Z.H. Ren, L. Zhang, B.N. Brown, X.T. Cui, S.F. Badylak, Y.N. Cai, Y.Q. Guan, R.K. Leak, J. Chen, X. Ji, L. Chen, Neurorestorative effect of urinary bladder matrix-mediated neural stem cell transplantation following traumatic brain injury in rats, *CNS & neurological disorders drug targets* 12(3) (2013) 413-425.
- [148] X. Wen, Y. Wang, Z. Guo, H. Meng, J. Huang, L. Zhang, B. Zhao, Q. Zhao, Y. Zheng, J. Peng, Cauda equina-derived extracellular matrix for fabrication of nanostructured hybrid scaffolds applied to neural tissue engineering, *Tissue Eng Part A* 21(5-6) (2015) 1095-105.
- [149] T.W. Hudson, S.Y. Liu, C.E. Schmidt, Engineering an improved acellular nerve graft via optimized chemical processing, *Tissue engineering* 10(9-10) (2004) 1346-58.
- [150] R. Junka, X. Yu, Novel Acellular Scaffold Made from Decellularized Schwann Cell Sheets for Peripheral Nerve Regeneration, *Regen Eng Transl Med* 1(1) (2015) 22-31.
- [151] T. Ren, A. Faust, Y. van der Merwe, B. Xiao, S. Johnson, A. Kandakatla, V.S. Gorantla, S.F. Badylak, K.M. Washington, M.B. Steketee, Fetal extracellular matrix nerve wraps locally improve peripheral nerve remodeling after complete transection and direct repair in rat, *Sci Rep* 8(1) (2018) 4474.
- [152] H. Wang, X.F. Lin, L.R. Wang, Y.Q. Lin, J.T. Wang, W.Y. Liu, G.Q. Zhu, M. Braddock, M. Zhong, M.H. Zheng, Decellularization technology in CNS tissue repair, *Expert Rev Neurother* 15(5) (2015) 493-500.
- [153] S.E. Gilpin, J.P. Guyette, G. Gonzalez, X. Ren, J.M. Asara, D.J. Mathisen, J.P. Vacanti, H.C. Ott, Perfusion decellularization of human and porcine lungs: bringing the matrix to clinical scale, *The Journal of heart and lung transplantation : the official publication of the International Society for Heart Transplantation* 33(3) (2014) 298-308.
- [154] T.W. Gilbert, S. Gilbert, M. Madden, S.D. Reynolds, S.F. Badylak, Morphologic assessment of extracellular matrix scaffolds for patch tracheoplasty in a canine model, *The Annals of thoracic surgery* 86(3) (2008) 967-74; discussion 967-74.
- [155] L.K. Papatheodorou, B.G. Williams, D.G. Sotereanos, Preliminary results of recurrent cubital tunnel syndrome treated with neurolysis and porcine extracellular matrix nerve wrap, *J Hand Surg Am* 40(5) (2015) 987-92.

- [156] K. Sawada, D. Terada, T. Yamaoka, S. Kitamura, T. Fujisato, Cell removal with supercritical carbon dioxide for acellular artificial tissue, *Journal of Chemical Technology & Biotechnology* 83(6) (2008) 943-949.
- [157] C. Philips, F. Campos, A. Roosens, M.D.C. Sanchez-Quevedo, H. Declercq, V. Carriel, Qualitative and Quantitative Evaluation of a Novel Detergent-Based Method for Decellularization of Peripheral Nerves, *Ann Biomed Eng* 46(11) (2018) 1921-1937.
- [158] C. Philips, M. Cornelissen, V. Carriel, Evaluation methods as quality control in the generation of decellularized peripheral nerve allografts, *J Neural Eng* 15(2) (2018) 021003.
- [159] R.C. Cornelison, S.M. Wellman, J.H. Park, S.L. Porvasnik, Y.H. Song, R.A. Wachs, C.E. Schmidt, Development of an apoptosis-assisted decellularization method for maximal preservation of nerve tissue structure, *Acta Biomater* 77 (2018) 116-126.
- [160] H.L. Xu, F.R. Tian, C.T. Lu, J. Xu, Z.L. Fan, J.J. Yang, P.P. Chen, Y.D. Huang, J. Xiao, Y.Z. Zhao, Thermo-sensitive hydrogels combined with decellularised matrix deliver bFGF for the functional recovery of rats after a spinal cord injury, *Sci Rep* 6 (2016) 38332.
- [161] I.J.-P. J, K. Jansen, A. Gramsbergen, M.F. Meek, Transection of peripheral nerves, bridging strategies and effect evaluation, *Biomaterials* 25(9) (2004) 1583-92.
- [162] T.A. Prest, E. Yeager, S.T. LoPresti, E. Zygelyte, M.J. Martin, L. Dong, A. Gibson, O.O. Olutoye, B.N. Brown, J. Cheetham, Nerve-Specific, Xenogeneic Extracellular Matrix Hydrogel Promotes Recovery Following Peripheral Nerve Injury, *Journal of biomedical materials research. Part A* (2017).
- [163] B. Brown, K. Lindberg, J. Reing, D.B. Stolz, S.F. Badylak, The basement membrane component of biologic scaffolds derived from extracellular matrix, *Tissue Eng* 12(3) (2006) 519-26.
- [164] B.N. Brown, K. Lindberg, J.E. Reing, D.B. Stolz, S.F. Badylak, The basement membrane component of biologic scaffolds derived from extracellular matrix, *Tissue Eng* 12(519) (2006).
- [165] D.O. Freytes, J. Martin, S.S. Velankar, A.S. Lee, S.F. Badylak, Preparation and rheological characterization of a gel form of the porcine urinary bladder matrix, *Biomaterials* 29(1630) (2008).
- [166] J.F.J. Woessner, The determination of hydroxyproline in tissue and protein samples containing small proportions of this amino acid, *Biochem Biophys* 93(440) (1961).

- [167] T. GrandPre, S. Li, S.M. Strittmatter, Nogo-66 receptor antagonist peptide promotes axonal regeneration, *Nature* 417(547) (2002).
- [168] T.W. Gilbert, J.M. Freund, S.F. Badylak, Quantification of DNA in biologic scaffold materials, *J Surg Res* 152(135) (2009).
- [169] X. Li, E. Katsanevakis, X. Liu, N. Zhang, X. Wen, Engineering neural stem cell fates with hydrogel design for central nervous system regeneration, *Progress in Polymer Science* 37(8) (2012) 1105-1129.
- [170] T.D. Johnson, S.Y. Lin, K.L. Christman, Tailoring material properties of a nanofibrous extracellular matrix derived hydrogel, *Nanotechnology* 22(49) (2011) 494015-494015.
- [171] S.F. Badylak, B.N. Brown, T.W. Gilbert, K.A. Daly, A. Huber, N.J. Turner, Biologic scaffolds for constructive tissue remodeling, *Biomaterials* 32(316) (2011).
- [172] B.N. Brown, S.F. Badylak, Extracellular matrix as an inductive scaffold for functi, *Transl Res* 163(268) (2014).
- [173] F. Meng, M. Modo, S.F. Badylak, Biologic scaffold for CNS repair, *Regen Med* 9(367) (2014).
- [174] J. Rosenblatt, B. Devereux, D.G. Wallace, Injectable collagen as a pH-sensitive hydrogel, *Biomaterials* 15(12) (1994) 985-95.
- [175] F.H. Silver, J.W. Freeman, G.P. Seehra, Collagen self-assembly and the development of tendon mechanical properties, *Journal of biomechanics* 36(10) (2003) 1529-53.
- [176] F.W. Meng, P.F. Slivka, C.L. Dearth, S.F. Badylak, Solubilized extracellular matrix from brain and urinary bladder elicits distinct functional and phenotypic responses in macrophages, *Biomaterials* 46 (2015) 131-40.
- [177] H. Ghuman, A.R. Massensini, J. Donnelly, S.M. Kim, C.J. Medberry, S.F. Badylak, M. Modo, ECM hydrogel for the treatment of stroke: Characterization of the host cell infiltrate, *Biomaterials* 91 (2016) 166-181.

- [178] M. Achilli, D. Mantovani, Tailoring Mechanical Properties of Collagen-Based Scaffolds for Vascular Tissue Engineering: The Effects of pH, Temperature and Ionic Strength on Gelation, *Polymers* 2(4) (2010).
- [179] A. Pabari, S.Y. Yang, A. Mosahebi, A.M. Seifalian, Recent advances in artificial nerve conduit design: strategies for the delivery of luminal fillers, *Journal of controlled release : official journal of the Controlled Release Society* 156(1) (2011) 2-10.
- [180] Y.Y. Chen, D. McDonald, C. Cheng, B. Magnowski, J. Durand, D.W. Zochodne, Axon and Schwann cell partnership during nerve regrowth, *J Neuropathol Exp Neurol* 64(613) (2005).
- [181] A.L. Cattin, J.J. Burden, L. Van Emmenis, F.E. Mackenzie, J.J. Hoving, N. Garcia Calavia, Y. Guo, M. McLaughlin, L.H. Rosenberg, V. Quereda, D. Jamecna, I. Napoli, S. Parrinello, T. Enver, C. Ruhrberg, A.C. Lloyd, Macrophage-Induced Blood Vessels Guide Schwann Cell-Mediated Regeneration of Peripheral Nerves, *Cell* 162(5) (2015) 1127-39.
- [182] N. Ghalib, L. Haoust'ava, P. Haninec, P. Dubovy, Morphometric analysis of early regeneration of motor axons through motor and cutaneous nerve grafts, *Ann Anat* 183(363) (2001).
- [183] S.M. Hall, Regeneration in cellular and acellular autografts in the peripheral nervous system, *Neuropathol Appl Neurobiol* 12(27) (1986).
- [184] S.M. Hall, The effect of inhibiting Schwann cell mitosis on the re-innervation of acellular autografts in the peripheral nervous system of the mouse, *Neuropathol Appl Neurobiol* 12(401) (1986).
- [185] S.M. Hall, Regeneration in the peripheral nervous system, *Neuropathol Appl Neurobiol* 15(513) (1989).
- [186] V. Agrawal, B.N. Brown, A.J. Beattie, T.W. Gilbert, S.F. Badylak, Evidence of innervation following extracellular matrix scaffold-mediated remodelling of muscular tissues, *Journal of tissue engineering and regenerative medicine* 3(8) (2009) 590-600.
- [187] J.E. Valentin, N.J. Turner, T.W. Gilbert, S.F. Badylak, Functional skeletal muscle formation with a biologic scaffold, *Biomaterials* 31(29) (2010) 7475-84.
- [188] H.L. Cheng, M. Shy, E.L. Feldman, Regulation of insulin-like growth factor-binding protein-5 expression during Schwann cell differentiation, *Endocrinology* 140(10) (1999) 4478-85.

- [189] A. Golzadeh, R. Mohammadi, Effect of local administration of platelet-derived growth factor B on functional recovery of peripheral nerve regeneration: A sciatic nerve transection model, *Dental research journal* 13(3) (2016) 225-232.
- [190] J.B. Davis, P. Stroobant, Platelet-derived growth factors and fibroblast growth factors are mitogens for rat Schwann cells, *J Cell Biol* 110(4) (1990) 1353-60.
- [191] G. Lundborg, L.B. Dahlin, N. Danielsen, R.H. Gelberman, F.M. Longo, H.C. Powell, e. al., Nerve regeneration in silicone chambers: influence of gap length and of distal stump components, *Exp Neurol* 76(361) (1982).
- [192] A.J. Man, G. Kujawski, T.S. Burns, E.N. Miller, F.A. Fierro, J.K. Leach, P. Bannerman, Neurogenic potential of engineered mesenchymal stem cells overexpressing VEGF, *Cellular and molecular bioengineering* 9(1) (2016) 96-106.
- [193] N.G. Fairbairn, A.M. Meppelink, J. Ng-Glazier, M.A. Randolph, J.M. Winograd, Augmenting peripheral nerve regeneration using stem cells: A review of current opinion, *World journal of stem cells* 7(1) (2015) 11-26.
- [194] A.L. Dellon, S.E. Mackinnon, Selection of the appropriate parameter to measure neural regeneration, *Annals of plastic surgery* 23(3) (1989) 197-202.
- [195] F. Kanaya, J.C. Firrell, W.C. Breidenbach, Sciatic function index, nerve conduction tests, muscle contraction, and axon morphometry as indicators of regeneration, *Plast Reconstr Surg* 98(7) (1996) 1264-71, discussion 1272-4.
- [196] S.E. Mackinnon, A.L. Dellon, J.P. O'Brien, Changes in nerve fiber numbers distal to a nerve repair in the rat sciatic nerve model, *Muscle & nerve* 14(11) (1991) 1116-22.
- [197] P.C. Belafsky, Bilateral vocal fold immobility, *Current opinions in otolaryngology and head and neck surgery* 19(415) (2011).
- [198] M.B. Marina, J.P. Mare, M.A. Birchall, Laryngeal reinnervation for bilateral vocal fold paralysis, *Current opinions in otolaryngology and head and neck surgery* 19(434) (2011).
- [199] B.B. Avnehchi, E.D. McCoul, K. Sundaram, Systematic review of laryngeal reinnervation techniques, *Otolaryngology Head Neck Surgery* 143 (2010) 749.

- [200] F.Y. Chiang, L.F. Wang, Y.F. Huang, K.W. Lee, W.R. Kuo, Recurrent laryngeal nerve palsy after thyroidectomy with routine identification of the recurrent laryngeal nerve, *Surgery* 137(342) (2005).
- [201] W. G.E., Spontaneous laryngeal reinnervation after recurrent laryngeal or vagus nerve injury, *Ann Otol Rhinol Laryngol* 116(57) (2007).
- [202] D. Chen, S. Chen, W. Wang, C. Zhang, H. Zheng, Spontaneous regeneration of recurrent laryngeal nerve following long-term vocal fold paralysis in humans: Histologic evidence, *Laryngoscope* 121(1035) (2011).
- [203] H. Daya, A. Hosni, I. Bejar-Solar, J.N. Evans, C.M. Bailey, Pediatric vocal fold paralysis: a long-term retrospective study, *Archives of otolaryngology--head & neck surgery* 126(21) (2000).
- [204] G.E. Woodson, L.F. Hughes, R. Helfert, Quantitative assessment of laryngeal muscle morphology after recurrent laryngeal nerve injury: right vs. left differences, *Laryngoscope* 118(10) (2008) 1768-70.
- [205] N.G. Ducharme, J. Cheetham, I. Sanders, J.W. Hermanson, R.P. Hackett, L.V. Soderholm, L.M. Mitchell, Considerations for pacing of the cricoarytenoid dorsalis muscle by neuroprosthesis in horses, *Equine Vet J* 42(6) (2010) 534-40.
- [206] N. Jansson, N.G. Ducharme, R.P. Hackett, H.O. Mohammed, An in vitro comparison of cordopexy, cordopexy and laryngoplasty, and laryngoplasty for treatment of equine laryngeal hemiplegia, *Veterinary surgery : VS* 29(4) (2000) 326-34.
- [207] J.R. Bain, S.E. Mackinnon, D.A. Hunter, Functional evaluation of complete sciatic, peroneal, and posterior tibial nerve lesions in the rat, *Plast Reconstr Surg* 83(1) (1989) 129-38.
- [208] J.R. Deuis, L.S. Dvorakova, I. Vetter, Methods Used to Evaluate Pain Behaviors in Rodents, *Frontiers in molecular neuroscience* 10 (2017) 284-284.
- [209] H. Dralle, C. Sekulla, K. Lorenz, M. Brauckhoff, A. Machens, German IONM Study Group, Intraoperative monitoring of the recurrent laryngeal nerve in thyroid surgery, *World J Surg* 32(1358) (2008).
- [210] R.C. Melcangi, S. Giatti, M. Pesaresi, D. Calabrese, N. Mitro, D. Caruso, L.M. Garcia-Segura, Role of neuroactive steroids in the peripheral nervous system, *Frontiers in endocrinology* 2 (2011) 104-104.

- [211] N. Sharma, S.J. Marzo, K.J. Jones, E.M. Foecking, Electrical stimulation and testosterone differentially enhance expression of regeneration-associated genes, *Exp Neurol* 223(1) (2010) 183-91.
- [212] M. Pesaresi, O. Maschi, S. Giatti, L.M. Garcia-Segura, D. Caruso, R.C. Melcangi, Sex differences in neuroactive steroid levels in the nervous system of diabetic and non-diabetic rats, *Hormones and behavior* 57(1) (2010) 46-55.
- [213] R.E. Hruska, S. Kennedy, E.K. Silbergeld, Quantitative aspects of normal locomotion in rats, *Life sciences* 25(2) (1979) 171-9.
- [214] L. de Medinaceli, W.J. Freed, R.J. Wyatt, An index of the functional condition of rat sciatic nerve based on measurements made from walking tracks, *Exp Neurol* 77(3) (1982) 634-43.
- [215] R.E. Sporel-Ozakat, P.M. Edwards, K.T. Hepgul, A. Savas, W.H. Gispen, A simple method for reducing autotomy in rats after peripheral nerve lesions, *Journal of neuroscience methods* 36(2-3) (1991) 263-5.
- [216] M.M. Carr, T.J. Best, S.E. Mackinnon, P.J. Evans, Strain differences in autotomy in rats undergoing sciatic nerve transection or repair, *Annals of plastic surgery* 28 (1992) 538-544.
- [217] J.M. Carlton, N.H. Goldberg, Quantitating integrated muscle function following reinnervation, *Surg Forum* 37 (1986) 611-614.
- [218] L.J. Chamberlain, I.V. Yannas, H.P. Hsu, G.R. Strichartz, M. Spector, Near-terminus axonal structure and function following rat sciatic nerve regeneration through a collagen-GAG matrix in a ten-millimeter gap, *Journal of neuroscience research* 60(5) (2000) 666-77.
- [219] J. Kobayashi, S.E. Mackinnon, O. Watanabe, D.J. Ball, X.M. Gu, D.A. Hunter, W.M. Kuzon, Jr., The effect of duration of muscle denervation on functional recovery in the rat model, *Muscle & nerve* 20(7) (1997) 858-66.
- [220] K.H. Wong, M. Naidu, P. David, M.A. Abdulla, N. Abdullah, U.R. Kuppusamy, V. Sabaratnam, Peripheral Nerve Regeneration Following Crush Injury to Rat Peroneal Nerve by Aqueous Extract of Medicinal Mushroom *Hericium erinaceus* (Bull.: Fr) Pers. (Aphylophoromycetidae), *Evidence-based complementary and alternative medicine : eCAM* 2011 (2011) 580752.

- [221] B. Chen, Y. Song, Z. Liu, Promotion of nerve regeneration in peripheral nerve by short-course FK506 after end-to-side neurorrhaphy, *J Surg Res* 152(2) (2009) 303-10.
- [222] G.C. de Rooter, R.J. Spinner, A.O. Alaid, A.J. Koch, H. Wang, M.J. Malessy, B.L. Currier, M.J. Yaszemski, K.R. Kaufman, A.J. Windebank, Two-dimensional digital video ankle motion analysis for assessment of function in the rat sciatic nerve model, *Journal of the peripheral nervous system : JPNS* 12(3) (2007) 216-22.
- [223] G.M. Hare, P.J. Evans, S.E. Mackinnon, T.J. Best, J.R. Bain, J.P. Szalai, D.A. Hunter, Walking track analysis: a long-term assessment of peripheral nerve recovery, *Plast Reconstr Surg* 89(2) (1992) 251-8.
- [224] V.V. Monte-Raso, C.H. Barbieri, N. Mazzer, A.C. Yamasita, G. Barbieri, Is the Sciatic Functional Index always reliable and reproducible?, *Journal of neuroscience methods* 170(2) (2008) 255-61.
- [225] P. Dinh, A. Hazel, W. Palispis, S. Suryadevara, R. Gupta, Functional assessment after sciatic nerve injury in a rat model, *Microsurgery* 29(8) (2009) 644-9.
- [226] S.M. Kim, S.K. Lee, J.H. Lee, Peripheral nerve regeneration using a three dimensionally cultured schwann cell conduit, *The Journal of craniofacial surgery* 18(3) (2007) 475-88.
- [227] J.A. Clavijo-Alvarez, V.T. Nguyen, L.Y. Santiago, J.S. Doctor, W.P. Lee, K.G. Marra, Comparison of biodegradable conduits within aged rat sciatic nerve defects, *Plast Reconstr Surg* 119(6) (2007) 1839-51.
- [228] J.Y. Lee, G. Giusti, H. Wang, P.F. Friedrich, A.T. Bishop, A.Y. Shin, Functional evaluation in the rat sciatic nerve defect model: a comparison of the sciatic functional index, ankle angles, and isometric tetanic force, *Plast Reconstr Surg* 132(5) (2013) 1173-80.
- [229] L. Xu, S. Zhou, G.Y. Feng, L.P. Zhang, D.M. Zhao, Y. Sun, Q. Liu, F. Huang, Neural stem cells enhance nerve regeneration after sciatic nerve injury in rats, *Molecular neurobiology* 46(2) (2012) 265-74.
- [230] V. Penna, K. Wewetzer, B. Munder, G.B. Stark, E.M. Lang, The long-term functional recovery of repair of sciatic nerve transection with biogenic conduits, *Microsurgery* 32(5) (2012) 377-82.

- [231] G.D. Bittner, C.P. Keating, J.R. Kane, J.M. Britt, C.S. Spaeth, J.D. Fan, A. Zuzek, R.W. Wilcott, W.P. Thayer, J.M. Winograd, F. Gonzalez-Lima, T. Schallert, Rapid, effective, and long-lasting behavioral recovery produced by microsutures, methylene blue, and polyethylene glycol after completely cutting rat sciatic nerves, *Journal of neuroscience research* 90(5) (2012) 967-80.
- [232] K. Matsuda, H.X. Wang, C. Suo, D. McCombe, M.K. Horne, W.A. Morrison, G.F. Egan, Retrograde axonal tracing using manganese enhanced magnetic resonance imaging, *NeuroImage* 50(2) (2010) 366-74.
- [233] M.D. Wood, M.R. MacEwan, A.R. French, A.M. Moore, D.A. Hunter, S.E. Mackinnon, D.W. Moran, G.H. Borschel, S.E. Sakiyama-Elbert, Fibrin matrices with affinity-based delivery systems and neurotrophic factors promote functional nerve regeneration, *Biotechnology and bioengineering* 106(6) (2010) 970-9.
- [234] X. Nie, Y.J. Zhang, W.D. Tian, M. Jiang, R. Dong, J.W. Chen, Y. Jin, Improvement of peripheral nerve regeneration by a tissue-engineered nerve filled with ectomesenchymal stem cells, *International journal of oral and maxillofacial surgery* 36(1) (2007) 32-8.
- [235] M.F. Meek, W.F. den Dunnen, P.H. Robinson, A.J. Pennings, J.M. Schakenraad, Evaluation of functional nerve recovery after reconstruction with a new biodegradable poly (DL-lactide-epsilon-caprolactone) nerve guide, *The International journal of artificial organs* 20(8) (1997) 463-8.
- [236] T. Maeda, S.E. Mackinnon, T.J. Best, P.J. Evans, D.A. Hunter, R.T. Midha, Regeneration across 'stepping-stone' nerve grafts, *Brain research* 618(2) (1993) 196-202.
- [237] J.L. Walker, J.M. Evans, P. Meade, P. Resig, B.F. Siskin, Gait-stance duration as a measure of injury and recovery in the rat sciatic nerve model, *Journal of neuroscience methods* 52(1) (1994) 47-52.
- [238] A.S. Varejao, M.F. Meek, A.J. Ferreira, J.A. Patricio, A.M. Cabrita, Functional evaluation of peripheral nerve regeneration in the rat: walking track analysis, *Journal of neuroscience methods* 108(1) (2001) 1-9.
- [239] J.M. Shenaq, S.M. Shenaq, M. Spira, Reliability of sciatic function index in assessing nerve regeneration across a 1 cm gap, *Microsurgery* 10(3) (1989) 214-9.
- [240] A.L. Dellon, S.E. Mackinnon, Sciatic nerve regeneration in the rat. Validity of walking track assessment in the presence of chronic contractures, *Microsurgery* 10(3) (1989) 220-5.

- [241] C.L. Jeng, T.M. Torrillo, M.A. Rosenblatt, Complications of peripheral nerve blocks, *British Journal of Anaesthesia* 105 (2010) i97-i107.
- [242] V. Chiono, C. Tonda-Turo, Trends in the design of nerve guidance channels in peripheral nerve tissue engineering, *Prog Neurobiol* 131 (2015) 87-104.
- [243] S. Madduri, B. Gander, Growth factor delivery systems and repair strategies for damaged peripheral nerves, *Journal of controlled release : official journal of the Controlled Release Society* 161(2) (2012) 274-82.
- [244] R.D. Price, S.A. Milne, J. Sharkey, N. Matsuoka, Advances in small molecules promoting neurotrophic function, *Pharmacology & therapeutics* 115(2) (2007) 292-306.
- [245] A.C. Pinho, A.C. Fonseca, A.C. Serra, J.D. Santos, J.F. Coelho, Peripheral Nerve Regeneration: Current Status and New Strategies Using Polymeric Materials, *Advanced healthcare materials* 5(21) (2016) 2732-2744.
- [246] A.D. Widgerow, A.A. Salibian, S. Lalezari, G.R. Evans, Neuromodulatory nerve regeneration: adipose tissue-derived stem cells and neurotrophic mediation in peripheral nerve regeneration, *Journal of neuroscience research* 91(12) (2013) 1517-24.
- [247] H.R.H. Zupanc, P.G. Alexander, R.S. Tuan, Neurotrophic support by traumatized muscle-derived multipotent progenitor cells: Role of endothelial cells and Vascular Endothelial Growth Factor-A, *Stem cell research & therapy* 8(1) (2017) 226.
- [248] Y.T. Kim, V.K. Haftel, S. Kumar, R.V. Bellamkonda, The role of aligned polymer fiber-based constructs in the bridging of long peripheral nerve gaps, *Biomaterials* 29(21) (2008) 3117-27.
- [249] I.P. Clements, Y.T. Kim, A.W. English, X. Lu, A. Chung, R.V. Bellamkonda, Thin-film enhanced nerve guidance channels for peripheral nerve repair, *Biomaterials* 30(23-24) (2009) 3834-46.
- [250] T.M. Keenan, A. Folch, Biomolecular gradients in cell culture systems, *Lab on a chip* 8(1) (2008) 34-57.
- [251] S. Tang, J. Zhu, Y. Xu, A.P. Xiang, M.H. Jiang, D. Quan, The effects of gradients of nerve growth factor immobilized PCLA scaffolds on neurite outgrowth in vitro and peripheral nerve regeneration in rats, *Biomaterials* 34(29) (2013) 7086-96.

- [252] B.J. Dickson, Molecular mechanisms of axon guidance, *Science (New York, N.Y.)* 298(5600) (2002) 1959-64.
- [253] D. Mortimer, T. Fothergill, Z. Pujic, L.J. Richards, G.J. Goodhill, Growth cone chemotaxis, *Trends in neurosciences* 31(2) (2008) 90-8.
- [254] K. Moore, M. MacSween, M. Shoichet, Immobilized concentration gradients of neurotrophic factors guide neurite outgrowth of primary neurons in macroporous scaffolds, *Tissue Eng* 12(2) (2006) 267-78.
- [255] L.M. Yu, F.D. Miller, M.S. Shoichet, The use of immobilized neurotrophins to support neuron survival and guide nerve fiber growth in compartmentalized chambers, *Biomaterials* 31(27) (2010) 6987-99.
- [256] Y.C. Lin, M. Ramadan, M. Hronik-Tupaj, D.L. Kaplan, B.J. Philips, W. Sivak, J.P. Rubin, K.G. Marra, Spatially controlled delivery of neurotrophic factors in silk fibroin-based nerve conduits for peripheral nerve repair, *Annals of plastic surgery* 67(2) (2011) 147-55.
- [257] Y.C. Chang, M.H. Chen, S.Y. Liao, H.C. Wu, C.H. Kuan, J.S. Sun, T.W. Wang, Multichanneled Nerve Guidance Conduit with Spatial Gradients of Neurotrophic Factors and Oriented Nanotopography for Repairing the Peripheral Nervous System, *ACS applied materials & interfaces* 9(43) (2017) 37623-37636.
- [258] L.E. Kokai, A.M. Ghaznavi, K.G. Marra, Incorporation of double-walled microspheres into polymer nerve guides for the sustained delivery of glial cell line-derived neurotrophic factor, *Biomaterials* 31(8) (2010) 2313-22.
- [259] L.E. Kokai, D. Bourbeau, D. Weber, J. McAtee, K.G. Marra, Sustained growth factor delivery promotes axonal regeneration in long gap peripheral nerve repair, *Tissue engineering. Part A* 17(9-10) (2011) 1263-75.
- [260] S. Suon, H. Jin, A.E. Donaldson, E.J. Caterson, R.S. Tuan, G. Deschennes, C. Marshall, L. Iacovitti, Transient differentiation of adult human bone marrow cells into neuron-like cells in culture: development of morphological and biochemical traits is mediated by different molecular mechanisms, *Stem cells and development* 13(6) (2004) 625-35.
- [261] M.F. Pittenger, A.M. Mackay, S.C. Beck, R.K. Jaiswal, R. Douglas, J.D. Mosca, M.A. Moorman, D.W. Simonetti, S. Craig, D.R. Marshak, Multilineage potential of adult human mesenchymal stem cells, *Science (New York, N.Y.)* 284(5411) (1999) 143-7.

- [262] W.M. Jackson, L.J. Nesti, R.S. Tuan, Concise review: clinical translation of wound healing therapies based on mesenchymal stem cells, *Stem cells translational medicine* 1(1) (2012) 44-50.
- [263] L.Y. Santiago, J. Clavijo-Alvarez, C. Brayfield, J.P. Rubin, K.G. Marra, Delivery of adipose-derived precursor cells for peripheral nerve repair, *Cell transplantation* 18(2) (2009) 145-58.
- [264] R.M. Brick, A.X. Sun, R.S. Tuan, Neurotrophically Induced Mesenchymal Progenitor Cells Derived from Induced Pluripotent Stem Cells Enhance Neuritogenesis via Neurotrophin and Cytokine Production, 7(1) (2018) 45-58.
- [265] A.X. Sun, T.A. Prest, J.R. Fowler, R.M. Brick, K.M. Gloss, X. Li, M. DeHar, H. Shen, G. Yang, B.N. Brown, P.G. Alexander, R.S. Tuan, Conduits Harnessing Spatially Controlled Cell-Secreted Neurotrophic Factors Improve Peripheral Nerve Regeneration., *Biomaterials* (2018).
- [266] Y. Sowa, T. Imura, T. Numajiri, K. Nishino, S. Fushiki, Adipose-derived stem cells produce factors enhancing peripheral nerve regeneration: influence of age and anatomic site of origin, *Stem cells and development* 21(11) (2012) 1852-62.
- [267] Y. Cho, J.E. Shin, E.E. Ewan, Y.M. Oh, W. Pita-Thomas, V. Cavalli, Activating Injury-Responsive Genes with Hypoxia Enhances Axon Regeneration through Neuronal HIF-1alpha, *Neuron* 88(4) (2015) 720-34.
- [268] Y. Sowa, T. Kishida, T. Imura, T. Numajiri, K. Nishino, Y. Tabata, O. Mazda, Adipose-Derived Stem Cells Promote Peripheral Nerve Regeneration In Vivo without Differentiation into Schwann-Like Lineage, *Plast Reconstr Surg* 137(2) (2016) 318e-330e.
- [269] M.T. Wolf, K.A. Daly, E.P. Brennan-Pierce, S.A. Johnson, C.A. Carruthers, A. D'Amore, S.P. Nagarkar, S.S. Velankar, S.F. Badylak, A hydrogel derived from decellularized dermal extracellular matrix, *Biomaterials* 33(29) (2012) 7028-38.